University of Liège - School of Engineering and Computer Science

Integrated Geochemical and Mineralogical Characterization of Thalanga Mine Waste, Assessment of AMD, and Critical Element Potential

Presented by Joseph Kamara

Submitted in partial fulfilment of the requirements for the EMerald Tripple Degree of:

Master of Mining and Geological Engineering from University of Liège

Master of Sciences de la Terre et des Planètes Environnement from L'École Nationale Supérieure de Géologie, Université de Lorraine, Nancy

Master of Science- Major: Geosciences from Luleå University of Technology

Academic Supervisor:

PIRARD Eric

BOUZAHZAH Hassan

(*University of Liège*)

Academic Supervisor

PARBHAKAR-FOX Anita

(*University of Queensland*)

Academic Year 2023-2024

Co-funded by
the European Union

Erasmus+

EMERALD
ERASMUS MUNDUS MASTER
IN GEORESOURCES ENGINEERING

LIÈGE
université

UNIVERSITÉ
DE LORRAINE

LULEÅ
UNIVERSITY
OF TECHNOLOGY

TU BERGAKADEMIE
FREIBERG

eit | European Institute of
Innovation & Technology

eit RawMaterials

THE UNIVERSITY
OF QUEENSLAND
AUSTRALIA

Abstract

This thesis assesses the potential for secondary sourcing of critical and high-tech elements from the Thalanga mine waste in Northern Queensland and investigates the associated environmental risk of Acid Mine Drainage (AMD). Comprehensive sampling and subsequent geochemical analyses, mineralogical characterisation, and Acid Base Accounting (ABA) tests identified considerable concentrations of Bi, Sb and As in the mine waste. Although ICP-MS geochemical data identified Se, and Te, these were not identified during the mineralogical characterisation. Some important elements that were identified but was not within the scope of this project is W and Sn in the form of scheelite and cassiterite respectively. The findings show significant secondary resource potential for Bi, As, and Sb which are important for the green energy transition and circular economy through numerous applications. An attempt to determine the exact mineralogical hosts of these elements was made, mineral names proposed are those as close as possible to the stoichiometry of the identified phases. The ABA tests returned results that indicate a high acid-generating potential in the waste necessitating continuous monitoring and management to mitigate/prevent AMD risks. The research emphasizes the dual opportunity for environmental management and economic potential benefit through resource recovery, encouraging geometallurgical approaches in optimizing resource utilisation and waste management. This study provides a contribution to the existing framework for sustainable mining practices, enhancing both resource utilisation and environmental protection.

Acknowledgement

First and foremost, I thank God for the opportunity and the grace to complete what I started. In every step of the way of EMerald master programme He never left me alone.

I express my most sincere gratitude to my supervisors, Prof. Eric Pirard for allowing me to take this project on, A. Prof. Anita Parbhakar-Fox for making the collaborative research and internship with the Sustainable Minerals Institute of the University of Queensland possible. My co-supervisor, Dr. Hassan Bouzahzah for the unfailing support throughout the entire project. My peer reviewer, Prof. Bertil Pålsson for the constructive critiques. Together, you made a strong team to show me how real-world research work looks like and what is expected of me as an engineer and geoscientist.

I would like to thank the Staff of SMI: Dr. Kam Bhowany, Dr. Allan Silva Gomes, Dr. Rosie Blannin, and Dipanshu Shama for sample collection from Thalanga site. Through this, my appreciation goes to Dr. Geoff Fraser and Allison Britt from Geoscience Australia, Cindy Sesak and Mitchell Thompson from the Queensland Department of Resources for facilitating site access and for helping the SMI/UQ team onsite. Not forgetting Dr. Sibele Nascimento, Dr. Francesco Colombi, and Gabriele Baldassarre for your assistance during the initial stages at Brisbane.

I would like to thank my family- both in Ghana and diaspora for the unparalleled love demonstrated throughout these years, I was never left alone. Especially, the woman who never stepped foot into classroom but found the relevance of education and sacrificed her all to push me this far. Doris I heart you so much, you are the reason I cannot give up when I feel to.

To my EMeraldhinos, you are amazing, and I cannot tell how these years would have been without you guys, the ski trips, dinners, karaoke and all makes us unique. In unity we started, and in unity we won- “Ubuntu”. Special thanks to Giuseppe, Precious and Javier for the support. The sarcasms, arguments, academic discussions, the sports and time together were great moments. We made it guys!

“Ubuntu “I am because we are!

Table of Contents

List of Figures

List of Tables

Chapter One Introduction

1.1 Introduction

Processed rocks that are barren of specific minerals of interest are classified as waste materials in mining operations. Similarly, the residues of processed ore (tailings and metallurgical slags) are considered waste. Rocks often comprise several minerals, and the extraction of one or two target minerals does not necessarily render the residue completely barren of other minerals, contrary to common perception in mining operations. Due to unsuitable technologies, unfavourable economics, and the lack of criticality for certain metal commodities, these materials are often classified as waste. Waste is a human construct, and many older mining operations, conducted before the advent of advanced geometallurgy and mineral processing, may have secondary potential, particularly for critical elements. The increase in population and the corresponding demand for metals for global sustainability and urbanization have driven the mining industry to develop strategies to process low-grade ores and re-mine waste as secondary sources of critical and other base metals, thereby enhancing the circular economy.

Globally, the use of smart technologies is increasing in fields such as medicine, aviation, automotive, defence, and communications. Critical elements and rare earth elements (REEs) are crucial to this industrial shift. However, REEs and critical elements often exist as trace or minor elements in mineralisation or as by-products of their extraction. Consequently, many of these metalloids/metals may end up in mining, processing, and metallurgical residues, making these residues potential secondary sources of critical elements and REEs.

While mine waste can be an important secondary source of critical and base metals, it also poses a potential environmental threat, such as Acid Mine Drainage (AMD), if not responsibly managed. Therefore, assessing the mineralogical and metallogenic potential of mine waste requires comprehensive Acid Base Accounting (ABA) analysis to document environmental impacts and mitigation strategies.

More than ever, mine waste characterization and transformation are crucial to meeting the future demand for critical elements and REEs, mitigating the environmental impacts of mine wastes, and closing the circular economy loop of the green transition. Geometallurgical characterization of mine waste aims to determine quantifiable geological, mineralogical, and geochemical information and explore how the synergy of geology, mining, processing,

metallurgy, and economic variables can be applied to derive value from mining wastes while effectively managing them to prevent AMD.

This study is part of the broader research program of Sustainable Minerals Institute's Mine Waste Transformation through Characterization (MIWATCH) in University of Queensland. The program aims to characterize and determine the potential of critical elements in Australian mining wastes, develop novel technologies for their extraction and valorisation, and address the environmental issues associated with mine waste. Given the similarity in critical mineral lists between the European Union and Australia, this thesis is conducted in close collaboration between SMI-MIWATCH at the University of Queensland and the University of Liège under the Emerald Master program. The focus is to determine the concentration of critical elements (Bi, As, Se, Sb, and Te) in Thalanga mining waste in Northern Queensland. The results will be used to decide on further detailed research on the feasibility of re-mining critical elements and mitigation of acid metalliferous drainage if the mine waste classify as acid generating.

1.2 State of the Art

Geochemical and mineralogical characterization of mine waste has been extensively studied by many authors worldwide, assessing both the economic potential and environmental impact of mining wastes. Numerous new process technologies for recovering valuable elements from mining and processing waste have been highlighted over the past few years. These methods include geochemical analysis, mineral liberation analysis, phytomining, extractive metallurgy, and recently, vapor metallurgy (Parbhakar-Fox et al., 2022; Whitworth et al., 2022; Moyo et al., 2023; Glen & Raimondo, 2018; Valenta et al., 2021). Butcher et al. (2023) discuss various techniques available for primary and secondary ore characterization (including wastes). Parbhakar-Fox and Baumgartner (2023) explains how the geometallurgical approach applied to total deposit characterization can be crucial for understanding the composition and environmental impact of various residues along the mining value chain.

The mining industry is a major producer of acidic, sulfur-rich wastewaters that may originate from active mines and legacy mine wastes (Johnson & Hallberg, 2004). Acid Mine Drainage (AMD), also known as Acid Metalliferous Drainage, has been extensively studied and documented by various authors worldwide to understand its occurrence, impacts, and remediation (Lottermoser, 2017; Lottermoser & Parbhakar-Fox, 2017; Bouzahzah et al., 2020; Simate & Ndlovu, 2014; Mafra et al., 2022; Jackson & Parbhakar-Fox, 2016). Despite the available scientific knowledge on AMD, the mining industry continues to face closure liabilities and the development of Acid Metalliferous Drainage (Lottermoser, 2010), which may be

related to factors such as the reliability of prediction and the lack of effective execution of geometallurgical approach that considers the whole mine value chain. Proper application of geometallurgical characterisation from the onset of a mine operation presents a robust aproach to manage all types of waste thereby mininmizing AMD during and post mining activities.

These previous studies provide valuable information on the characterization of mine waste, the potential recovery of critical and rare earth metals from the residues, and environmental impact assessment and remediation solutions. However, they are often specific to particular locations and geological contexts. Additionally, reliably quantifying or estimating the amount of critical elements in a given volume of waste is more challenging compared to primary resource estimation. This is because once the material is moved from insitu there is no more a natural pattern to explaining the inherent variability, alteration and historical uncertainties associated with it, especially tailings. Tailings therefore, will require a more rigorous and sophisticated approach (geostatitical) to achieve accurate quantification of resources whereas primary deposits are more predictable due to uniform geological characteristics that geostatistical methods have been made for.

1.3 Objectives

This thesis aims to investigate the potential and deportment of critical and high-tech elements in Thalanga mine waste (tailings and waste rock) located in Charters Towers, Northern Queensland, to determine its secondary prospectivity and Acid Metalliferous Drainage potential. This will be achieved through the following specific objectives:

1. Collect representative samples at mine waste site.
2. Identify critical elements (e.g., Bi, In, Sb, As, Te, W and REEs) in concentrations of at least ten times crustal abundance as a first pass test of critical element fertility.
3. Determine the mineralogical hosts of these critical element and comment on the relationship between ore deposit geology and mineralisation style with the cycling of critical element(s) of interest in the surficial environment.
4. Perform Acid Base Accounting tests on the waste material.
5. Determine mineral processing technologies suitable for recovery of critical elements.

2.1 Critical Raw Materials

There is an urgency to research critical raw materials due to the geopolitics of sourcing and the global goal to achieve zero carbon emissions by 2050. Metallogenic minerals occur in varying abundances across different geologic terrains in the Earth's crust. While some minerals are abundant and easily sourced from various locations unless constrained by geopolitical factors, others are naturally scarce and in high demand for the green transition. "Critical raw materials are those raw materials that are economically important but have a high supply risk" (European Commission, 2020, p. 2). The European Union reviews its critical raw materials (CRMs) list every three years, with the latest update made in 2023 since its inception in 2011.

Materials of economic importance classified as critical can differ from country to country depending on several factors, including the pace of technological development, availability of the raw material as a mineable natural resource, and geopolitical tensions affecting sourcing from other countries. For example, Australia and the EU have similar lists of critical minerals, but minerals like chromium, indium, tellurium, and zirconium are considered critical in Australia's updated list, whereas Europe does not include these elements in its updated list (Australia's Critical Minerals List and Strategic Material List, 2023). The criticality of elements is evaluated based on their importance and supply risk (Whitworth, et al., 2022). The European Commission assesses raw materials individually, determining their supply risk using the parameters described below (Chernoburova & Chagnes, 2023)

$$S.R = \left[(HHI_{WGI-t})_{GS}.\frac{IR}{2} + (HHI_{WGI-t})_{EU\ sourcing}\left(1-\frac{IR}{2}\right)\right].(1-EoLRIR).SI_{SR} \qquad Equation1$$

Where HHI is the Herfindahl-Hirschman Index, WGI is the scaled World Governance Index, t is the trade adjustment of WGI, EoLRIR is the End-of-Life Recycling Input Rate, SI is the Substitution Index related to S.R, and IR is the Import Reliance. The Herfindahl-Hirschman Index term ($(HHI_{WGI-t})_{GS}$) is a measure of the market concentration of the element and is used to assess the market competitiveness considering the t-trade adjustments of the supplying countries in comparison to Global Supply (GS). In simple terms, the criticality of a metal/element in EU is characterised by two main factors; the economic importance of the element to the EU economy which hinges on the end-of use application and the added value of corresponding EU manufacturing sectors. The economic importance is corrected by the substitution index which is in close relation to the technical and cost performance of the substitutes for individual applications. Second factor is the Supply Risk, which is explained by

the Herfindahl Hirschmann index and the Import Reliance (IR), where substitution and recycling are considered risk-reducing factors.

2.2 Geometallurgy

The concept of geometallurgy in mining has existed for a long time but has been applied implicitly in resource estimation with numerous limitations. Even with the emergence of geometallurgical modeling, variables such as hardness, grindability, throughput, mill power index, recovery, and concentrate grade have been incorrectly assumed to be additive in traditional geostatistical modeling approaches (Richmond & Shaw, 2009). Before the invention and implementation of the geometallurgical approach, the exploration and mining industry used a cost-effective but less robust traditional element-based methodology to evaluate commercially important mineral deposits (Butcher, Dehaine, Menzies, & Michaux, 2023).

The geometallurgical approach was defined as an innovative method to address the limitations of traditional approaches when developing ore deposits by considering the heterogeneity of the orebody and quantifying geological variables (such as lithology, structures, and alteration) and mineralogy that affect the metallurgical performance of mineral processing (Williams & Richardson, 2004, as cited in Louwrens, 2015). Initially, Lamberg (2011) described geometallurgy not as a discipline but as an amalgamation of ore deposit geology and mineral processing to manage risk and ensure effective use of orebodies. However, he noted that the process performance parameters simulated by geometallurgical models include figures for throughput, energy consumption, concentrate grade and recovery, and tailings properties. This indicates that geometallurgical models can be extended to predict, quantify, and characterize resources in tailings.

Parian et al. (2015) and Lund & Lamberg (2014) clarified that geometallurgy is a cross-disciplinary approach that integrates information from geology, mineral processing, and subsequent downstream processes into a model to describe the spatial variability of an ore deposit necessary for planning and management. This shows that geometallurgy can be applied further along the mining value chain. "The knowledge of grade and its variation alone is not sufficient for geometallurgy, but mineralogy also defines the method of extraction and concentration" (Parian, Lamberg, Möckel, & Rosenkranz, 2015; Parbhakar-Fox, Edraki, Walters, & Bradshaw, 2011), which can ultimately provide reliable information about what goes into the tailings.

Geometallurgical modelling has gained recognition and now exists as a geometallurgical program, which seeks the continuous synergy of the mining value chain—from exploration,

production, and processing through economics to closure and rehabilitation—to ensure efficient use of resources. Since the inception and application of the geometallurgical approach in mining, there have been extensive studies and publications on the topic to enhance efficient resource utilization across the mining value chain (Lamberg, 2011; Lund & Lamberg, 2014; Parian et al., 2015; Richmond & Shaw, 2009; Lund, Lamberg, & Lindberg, 2013; Pereira, 2023; Ortiz et al., 2023; Butcher et al., 2023).

The relevance of fully extending the geometallurgical approach to mine waste characterization and management has been less discussed in the literature. However, Parbhakar-Fox & Baumgartner (2023) describe a geometallurgical approach to minimize mine waste production by properly modelling geoenvironmental domains from the exploration stage of mining. A well-organized and implemented approach to predict and classify AMD can reduce mine closure liability costs by 10% (Dowd, 2006, cited in Lottermoser, 2017). Robust geometallurgical modeling of a deposit can help classify, quantify, and design a management plan for acid-generating waste rock and tailings that could potentially be generated during mining operations, prior to actual production and processing on site.

When reconsidering tailings and waste rock as secondary sources of critical elements for the green transition and circular economy, tailings storage facilities and waste rock dumps should be seen as new orebodies that require a geometallurgical approach for evaluation and modeling. However, variations in tailings mineralization and architecture are areas where geometallurgical variables have not been extensively studied, apart from the first case study by Louwrens (2015).

2.3 Characterisation of Mine Waste

Mine waste can be heterogeneous in architecture due to post-depositional processes, which can alter the texture, geochemistry, and mineralogy through a series of chemical reactions. If the goal of characterizing mine waste is critical for recovery and geoenvironmental assessment, then knowledge of the geochemistry, mineralogy, recoverability, and acid-generating potential of the material is crucial (Guatame-Garcia, et al., 2023).

2.3.1 Geochemical and Mineralogical characterisation

Predictive environmental indicators in mining are valuable techniques that provide quantitative information against which environmental risks associated with mining and mineral resource development can be assessed (Lottermoser B., 2017). The geochemistry of mine waste, as well as that of the primary deposit, is crucial for predicting environmental risks associated with these materials and implementing immediate mitigation measures. This topic has been extensively

studied, with the fundamental understanding that mine wastes exhibit geochemical characteristics like the mined rock. The chemistry of drainage from mine wastes, which can be acid-rich, results from the oxidation of iron-sulphide minerals such as pyrite (FeS_2) and pyrrhotite ($Fe_{(1-x)}$ S) (Jamieson, 2011; Hunt et al., 2016; Parbhakar-Fox & Lottermoser, 2015; Lindsay et al., 2015).

Various geochemical methods and analyses exist to determine the elemental composition of samples, depending on whether the focus is on major, trace, or volatile elements, precious metals, or total carbon and sulphur. Often, a combination of two or more techniques is employed. The four-step acid digestion method followed by ICP-MS/AES is a commonly used technique for geochemical analysis. Mineralogy is equally important as geochemistry. Mineralogical characterization provides a comprehensive understanding of the mineral forms in which elements identified through geochemistry exist within the material. This helps identify minerals posing environmental risks. For instance, it is critical to determine whether sulphur exists as sulphide-sulphur or sulphate-sulphur, and whether acid-neutralizing minerals are primary carbonates (e.g., calcite, dolomite) readily available for neutralization, or secondary carbonates derived from silicates (e.g., chlorite, plagioclase).

Performing techniques such as mineral liberation analysis (MLA), automated mineralogy, scanning electron microscopy (SEM), and optical microscopy are essential for thorough mineralogical characterization.

2.4 Acid Mine Drainage (AMD)

Acid Mine Drainage (AMD) poses significant environmental risks associated with mining due to its long-term detrimental effects and the high costs involved in its control once it has begun. Continuous assessment of mine waste is essential throughout the life of a mine as part of effective mine waste management. Utilizing predictive environmental indicators are crucial for understanding the oxidation of sulfidic rocks and waste materials, which can lead to AMD and contamination of ground and surface waters (Noble et al., 2016).

AMD is primarily generated by the oxidation of sulphide minerals such as arsenopyrite, galena, pyrrhotite, chalcopyrite, etc. However, the oxidation of pyrite is the most well-known mechanism responsible for generating AMD. The oxidation process of pyrite proceeds as follows:

$$2FeS_2 + 7O_2 + 2H_2O = 2Fe^{2+} + 4SO_4^{2-} + 4H^+ \qquad \textit{Equation 2}$$

$$4Fe^{2+} + O_2 + 4H^+ = 4Fe^{3+} + 2H_2O$$ *Equation 3*

$$Fe^{3+} + 3H_2O = Fe(OH)_3 + 3H^+$$ *Equation 4*

$$FeS_2 + 14Fe^{3+} + 8H_2O = 15Fe^{2+} + 2SO_4^{2-} + 16H^+$$ *Equation 5*

In the presence of oxygen and water, equations 2 to 3 occur, releasing hydrogen ions into solution. Under pH conditions below 4, Fe^{3+} ions available in solution can further dissolve pyrite, as shown in equations 4 and 5. To mitigate the impacts of AMD, the mining industry conducts static and kinetic tests to classify wastes into Potentially Acid Forming (PAF), Acid Forming (AF), and Non-Acid Forming (NAF) categories (Parbhakar-Fox & Lottermoser, 2015).

The static test rapidly and cost-effectively determines the current acid generating potential of samples. Maximum acidity can also be calculated from chemical assays and the amount of different mineralogical phases present in the sample (Bouzahzah et al., 2013). In contrast, the kinetic test involves a continuous leaching process over an extended period (Chopard et al., 2017), providing information about the rate of chemical breakdown of minerals in the samples and the concentration of elements in the leachate, simulating atmospheric conditions.

A common geochemical test for AMD is the rinse and paste pH test, which offers a preliminary assessment of acid generating potential. However, these tests are not predictive because materials disturbed during mining may exhibit neutral to alkaline rinse and paste pH values but can still be high acid producers due to unoxidized sulphides (Lottermoser B. G., 2010).

The two main static tests used to determine acid forming characteristics are the Acid Base Accounting (ABA) method and the Net Acid Generation (NAG) test (Smart, et al., 2002). The ABA method separately determines Maximum Potential Acidity (MPA) and Acid Neutralizing Capacity (ANC). The difference between MPA and ANC gives the Net Acid Producing Potential (NAPP) of the material. In contrast, the NAG test involves the reaction between hydrogen peroxide and the sample to oxidize pyrite under controlled conditions, providing an overall measure of the material's acid generation potential. The NAG result represents the combined effect of sulphide oxidation and neutralization by available acid neutralizing minerals in the sample. The NAG capacity is measured in kg H_2SO_4 / tonne and serves as a screening tool against the rinse and paste pH tests, cross-checking with the NAPP from ABA, which is also measured in the same unit.

The single addition NAG test is suitable for samples containing less than 0.3 g of sulphide-sulphur, while the multi-addition test is appropriate for samples containing more than 0.3 g of

sulphide-sulphur (Parbhakar-Fox et al., 2011). However, there are no universally documented controlling variables for the NAG test, and procedural errors are expected as outlined in the AMIRA P387A Handbook (Chopard et al., 2017; Parbhakar-Fox et al., 2018). Research efforts have focused on refining the NAG test, particularly the multi-addition method, to minimize discrepancies in results and interpretation. Despite these advancements, challenges persist, particularly due to the absence of a global standard for NAG pH testing, contrasting with established standards for ABA (Parbhakar-Fox, Fox, Ferguson, Hill, & Maynard, 2018).

2.5 Process and Recovery Technologies of CRM

According to the metal wheel proposed by Verhoef, Gerard, & Reuter (2004) and Bellenfant et al. (2013) as shown in Figure 1, metallurgical processes in metal processing follow a structured order. Primary metals or carrier metals are in the inner wedge, metals extracted as by-products occupy the white circle, and those that end up in waste are found in the outermost layer (Tinti et al., 2023). While most Critical Raw Materials (CRMs) originate from by-products of primary polymetallic ores, they often accumulate in residues (Bellenfant et al., 2013).

The highly heterogeneous properties of mine waste, resulting from various extraction processes of primary ores, necessitate a reassessment of the economic and technological feasibility of re-processing residues to recover specific CRMs found in tailings and waste rock. Researchers have proposed several reprocessing techniques, including phytomining, traditional methods like comminution, flotation, hydrometallurgy, and pyrometallurgy. Each technology has unique strengths and weaknesses, highlighting the importance of adopting a geometallurgical approach to characterize and select the optimal technology for CRM extraction from the initial stages of mining (Parbhakar-Fox & Baumgartner, 2023). In terms of Thalanga mine waste, which has a particle size distribution (PSD) with P_{90} = 75 μm, reprocessing by grinding will be cost-ineffective. Even though re-grinding has the potential to produce fresh mineral surfaces amenable to flotation, these materials may have undergone some degree of oxidation. This oxidation makes enrichment by flotation less suitable due to the surface interactions involved. Density and magnetic separation methods (Shaking table, Spiral, LIMS, HIMS, WHIMS or HGMS) could be the best simple approaches to recommend give the high pyrite content in the tailings.

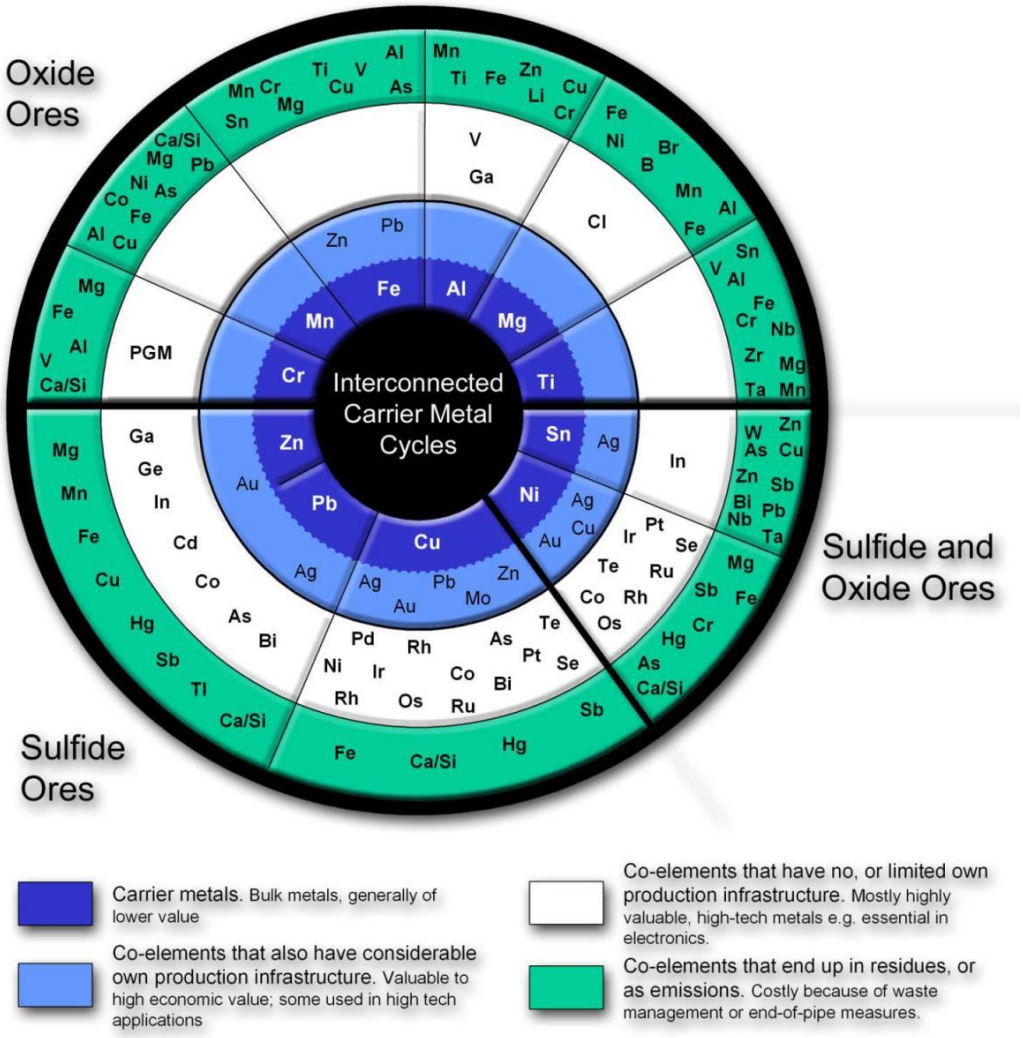

Figure 1: The Metal Wheel (Bellenfant, D'Hugues, Bodenan, & Cassard, 2013)

2.6 Study Area and Access to Site

The Charters Towers Regional Council Area is situated in North-eastern Queensland, approximately 690 miles north of Brisbane. Thalanga Mine is located 65 km west-southwest of Charters Towers, positioned at approximately latitude S 20° 20' 11.69" and longitude **E** 145° 46' 23.38". Access to Thalanga is primarily provided via the Flinders Highway, west of Charters Towers, with further access within the site facilitated by existing station tracks.

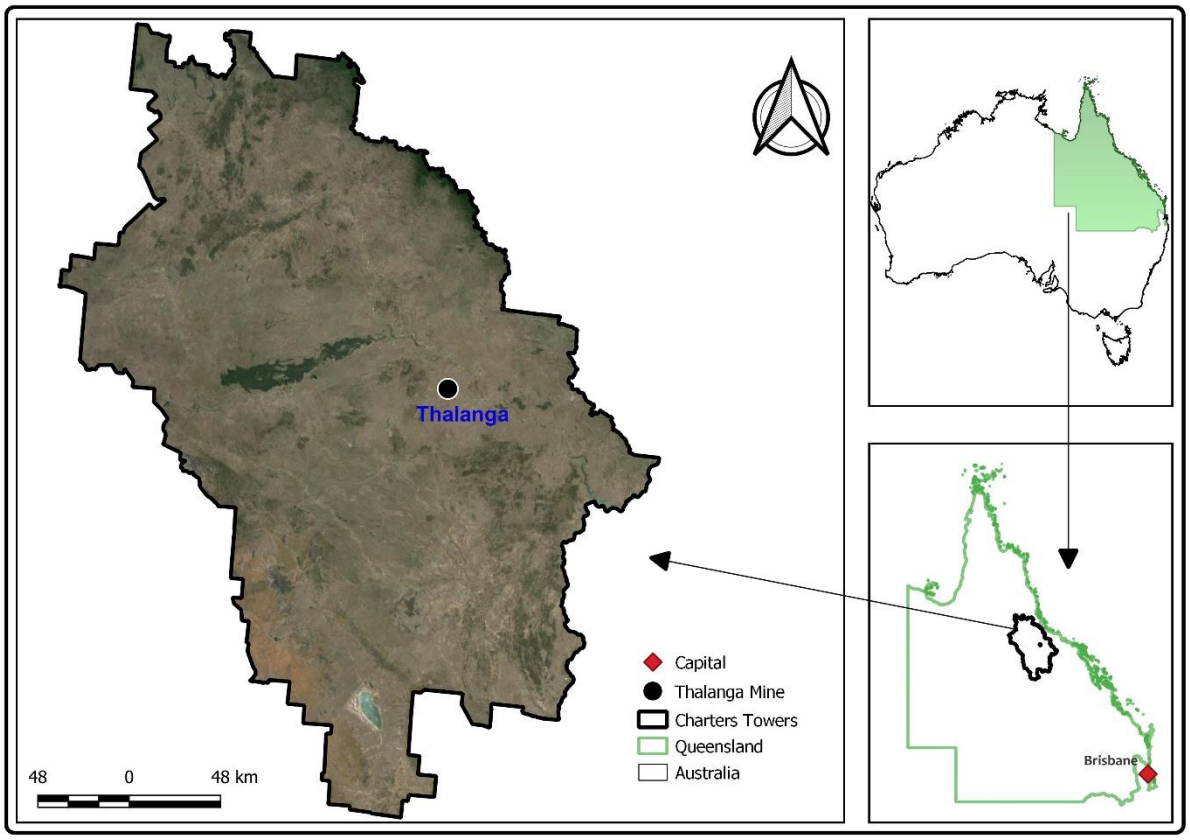

Figure 2: Study Area

2.7 Deposit Geology and Mining History

2.7.1 Regional Geology

The Tasman fold belt system encompasses the eastern third of the Australian continent, characterized by a complex orogeny comprising five sub-orogenic provinces (Walshe, Heithersay, & Morrison, 1995). The Thomson orogen, situated in the northern part of the Tasman system, features tectonic structures trending approximately east-west, orthogonal to the predominantly north-south trending Tasmanides. This geological framework reflects a profoundly heterogeneous crustal architecture, which remains incompletely understood due to the complex history of deformation and limited exposure of the Thomson Orogeny in central Queensland (Abdullah & Rosenbaum, 2017; Glen et al., 2010; Klootwijk, 2023; Burton & Trigg, 2014; Berry et al., 1999; Betts et al., 2015).

Charters Towers is located within the Mount Windsor sub-province. Deposits in this area trend east-west and are often buried beneath thick volcano-sedimentary successions of the Seventy Mile Range Group, although some deposits are exposed in certain provinces, as shown in Figure 3 (Henderson R. A., 1986).

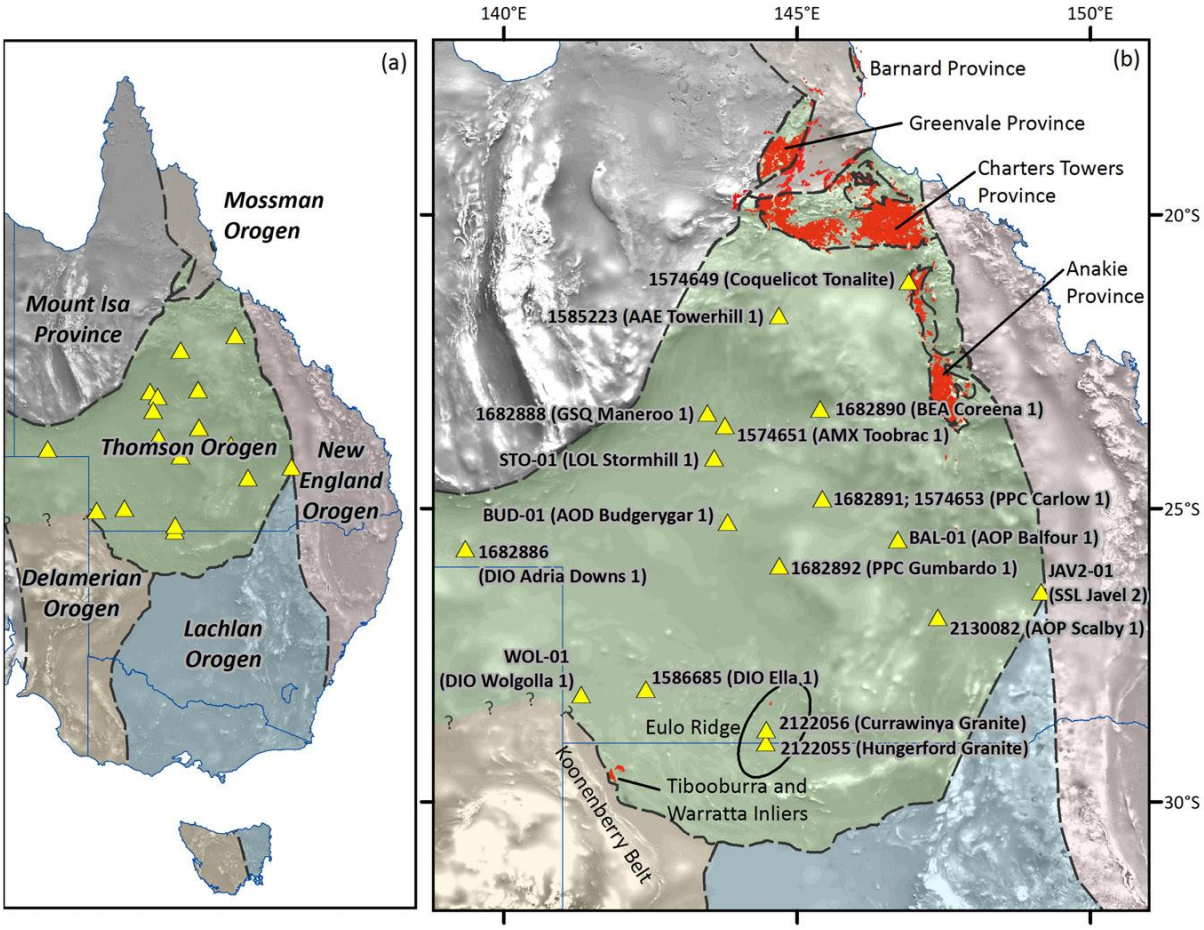

Figure 3: The Tasmanides showing key provinces and drill holes in the Thomson's orogeny. Red zone shows areas where deposit outcrops. After (Cross, et al., 2018)

The Charters Towers province in Northern Queensland consists of late Neoproterozoic and early Paleozoic metamorphic rocks, Ordovician sedimentary and volcaniclastic rocks, and multiple intrusions ranging from Ordovician to Permian in age (Fergusson, Henderson, Lewthwaite, Philips, & Withnall, 2005). According to Berry et al. (1999) and Ferguson et al. (2005), the Mount Windsor Province's geological history began with continental rifting from the Gondwanan margin during the Delamerian orogeny around 485 million years ago (Ma). This rifting caused slab rollback and the formation of rift basins. The extensional tectonic environment led to the development of the Mount Windsor volcanics. Between 450-440 Ma, crustal shortening along the NE-SW axis resulted in the accretion of the Charters Towers Province ribbon onto the Gondwana margin, causing deformation of the pre-450 Ma rocks in the province. Intrusive rocks of the Silurian-Devonian Pama province were emplaced during the subsequent rifting associated with slab rollback. The Carboniferous-Permian Kennedy igneous deposits were formed from back-arc magmatism induced by westward dipping subduction and slab rollback of the proto-Pacific oceanic crust east of the Charters Towers Province (Betts et al., 2012; Fergusson et al., 2005).

The Mount Windsor sub-province is predominantly igneous / metaigneous. It includes rhyolite, dacite and minor andesite, basalt, pyroclastic products and interbedded sedimentary rocks (Henderson, 1986). This succession is divided into four formations that constitute the Seventy Mile Range Group. Deposited in a back-arc basin during the rifting associated with slab rollback around 500-465 Ma (Betts, Stewart, & Armit, 2012), the east-west trending Seventy Mile Range Group hosts stratiform polymetallic volcanic-hosted massive sulphide (VHMS) mineralization. The post-depositional emplacement of the proximal Ravenswood granodiorite complex influenced the original formation of the Mount Windsor mineralisation and dominated its metamorphic history (Henderson R. , 1986). The Thalanga deposit is synchronous with the Mount Windsor Volcanics formation. Mineralisation may have formed during or shortly after magmatic crystallisation (Cross, et al., 2018). Zircon U-Pb dating, and Hf-O isotopes indicates that, the Mount Windsor volcanics have formed during 479 ±5 Ma (Perkins, Walshe, & Morrison, 1995)

The Puddler Creek Formation forms the basement of the Cambro-Ordovician volcano-sedimentary succession of the Seventy Mile Range Group. Mafic dykes and sills are prominent in the Puddler Creek sedimentary formation but do not extend into the overlying Mount Windsor metavolcanics and metasedimentary formations (Berry et al., 1999). The Mount Windsor volcanics was emplaced in a subaqueous environment, resulting in the formation of rhyolitic, dacitic, and andesitic rocks with metamorphism that increases from low-grade prehnite-pumpellyite facies in the east to greenschist facies in the Highway-Reward area to the west (Doyle, 2001).

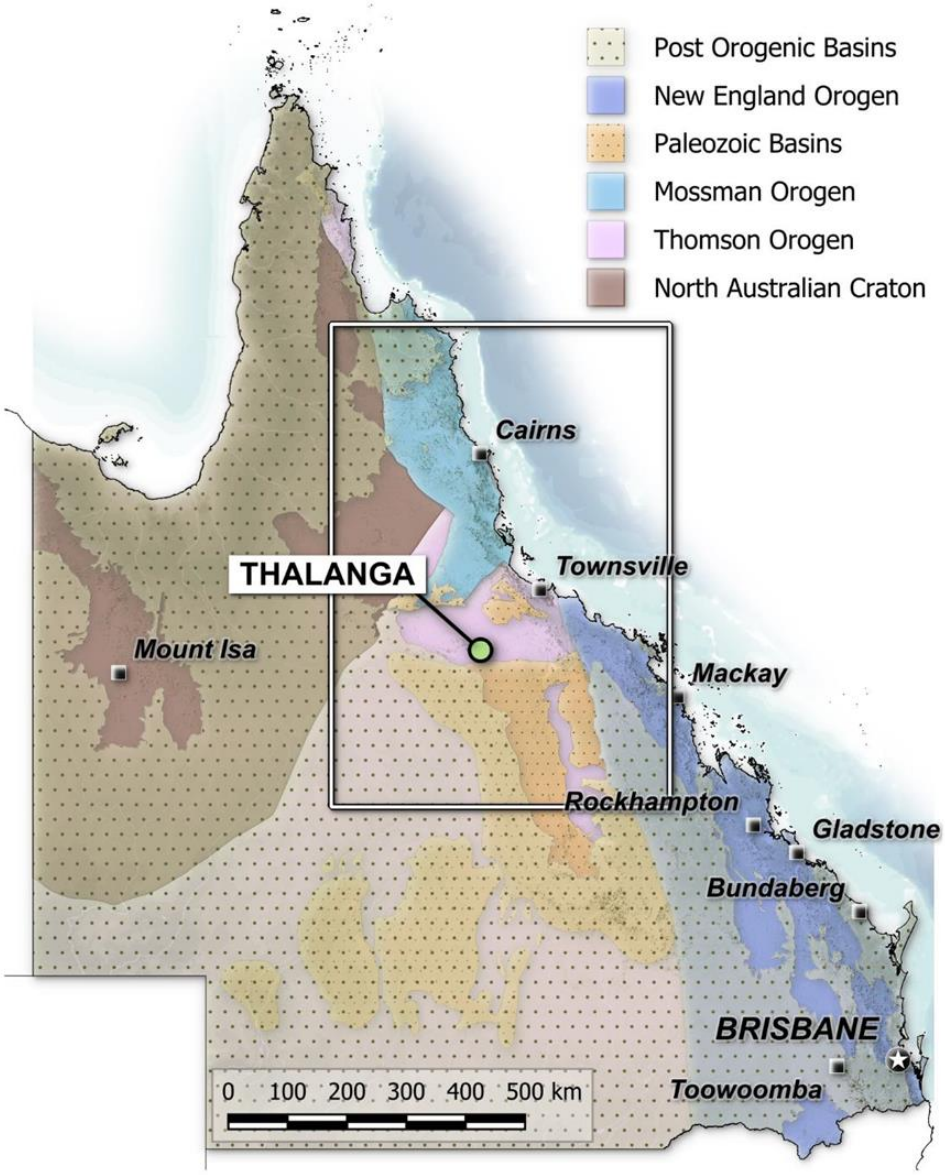

Figure 4: Location of Thalanga deposit showing outline for regional map of Queensland (source, GSQ)

The conformably overlying Thalanga deposit exhibits metamorphic grades increasing from actinolite to amphibolite facies at Waddys Mill. The Cambro-Ordovician sequence has been intruded by the Ordovician to Devonian granodiorite complex of the Ravenswood batholiths (Henderson, 1986). The Seventy Mile Range Group, trending 165 km east-west, has been divided into four successions hosting VMS deposits of base and precious metals (Pb-Zn-Cu-Au-Ag). The stratiform massive sulphide deposits mainly occur in the Mount Windsor and Trooper Creek Formations, with Thalanga and Highway-Reward deposits rich in Pb-Zn-Cu-Ag and Cu-Au, respectively (Doyle & Huston, 1999).

2.7.2 Deposit Local Geology

The Thalanga deposit is a Cu-Pb-Zn-Ag-Au VHMS deposit occurring within Mount Windsor volcanics, at the contact with dacites of the overlying trooper Trooper Creek Formation (Paulick, et al., 2001). The Thalanga deposit occurs as thin tabular pockets of mineralized lenses, while the Highway-Reward occurs as vertical veins and veinlets of mineralized pipes, likely formed by permeable conduits in the underlying formation allowing hydrothermal fluids to rise at Highway-Reward. The main ore lenses at Thalanga include Thalanga East, Thalanga Central, West, Far West Thalanga, Vomacka, and the recent Orient (Paulick & McPhie, 1999).

The succession of the Seventy Mile Range Group is summarized in Figure 5 (Paulick & McPhie, 1999) following the work of Large (1992) on Australian VHMS deposits. The host rock succession at the Thalanga deposit consists of altered rhyolite in the footwall and a volcano-sedimentary sequence dominated by dacite to rhyodacite in the hanging wall (Paulick, Herrmann, & Gemmell, 2001). The Highway-Reward deposit comprises coherent rhyolite, rhyodacite, and dacite, with associated non-stratified breccia facies that have been resedimented by syn-eruptive volcanic processes, preserving clast shapes (Doyle & McPhie, 2000).

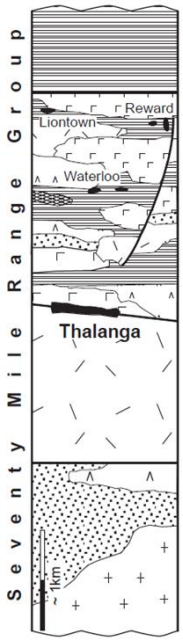

Formation	Age	Lithology
Rollston Range Formation	**Early Ordovician** (Bendigonian-Chewtonian; fossils [1])	sandstone, siltstone and mudstone
Trooper Creek Formation	**Early Ordovician** (Lancefieldian 2-Lancefieldian 3; fossils [1])	andesitic, dacitic and rhyolitic lavas, intrusions and associated breccia; mudstone, siltstone, sandstone; pumice-lithic breccia; silica ironstone; massive sulphide
Mount Windsor Formation	**Early Ordovician** (481 ± 5 Ma and 485 ± 5 Ma; SHRIMP dating [2])	rhyolitic lavas and intrusions; monomictic rhyolitic breccia (minor sandstone)
Puddler Creek Formation	**? Late Cambrian**	sandstone and greywacke; alkalibasalt and trachyandesite lavas and sills
Lolworth-Ravenswood Batholith		basal contact intruded by the Lolworth-Ravenswood Batholith

Figure 5: Generalised stratigraphic column for the Seventy Mile Range Group in Mt Windsor Province by (Paulick & McPhie, 1999) after (Large, Australian Volcanic-Hosted Massive Sulphide Deposits: Features, Styles, and Genetic Models, 1992).

2.7.3 Geochemistry and Mineralogy of the Deposit

Ridley (2013) defines VHMS deposits as stratabound bodies of hydrothermal sulphides that typically form at or near the seafloor, adjacent to active magmatic centres, in relatively deep marine environments. He identifies three main settings for VHMS deposits, including the "Kuroko" type, which is analogous to those found in the Mount Windsor Sub-province in Queensland, as discussed in other literature (Large, 1992; Paulick et al., 2001; Doyle & McPhie, 2000; Henderson, 1986; Withnall, 1982). Figure 6 provides a brief overview of VHMS structure. While the mineralogy and geochemistry of VHMS deposits may be similar, there can be slight differences in their alteration halos.

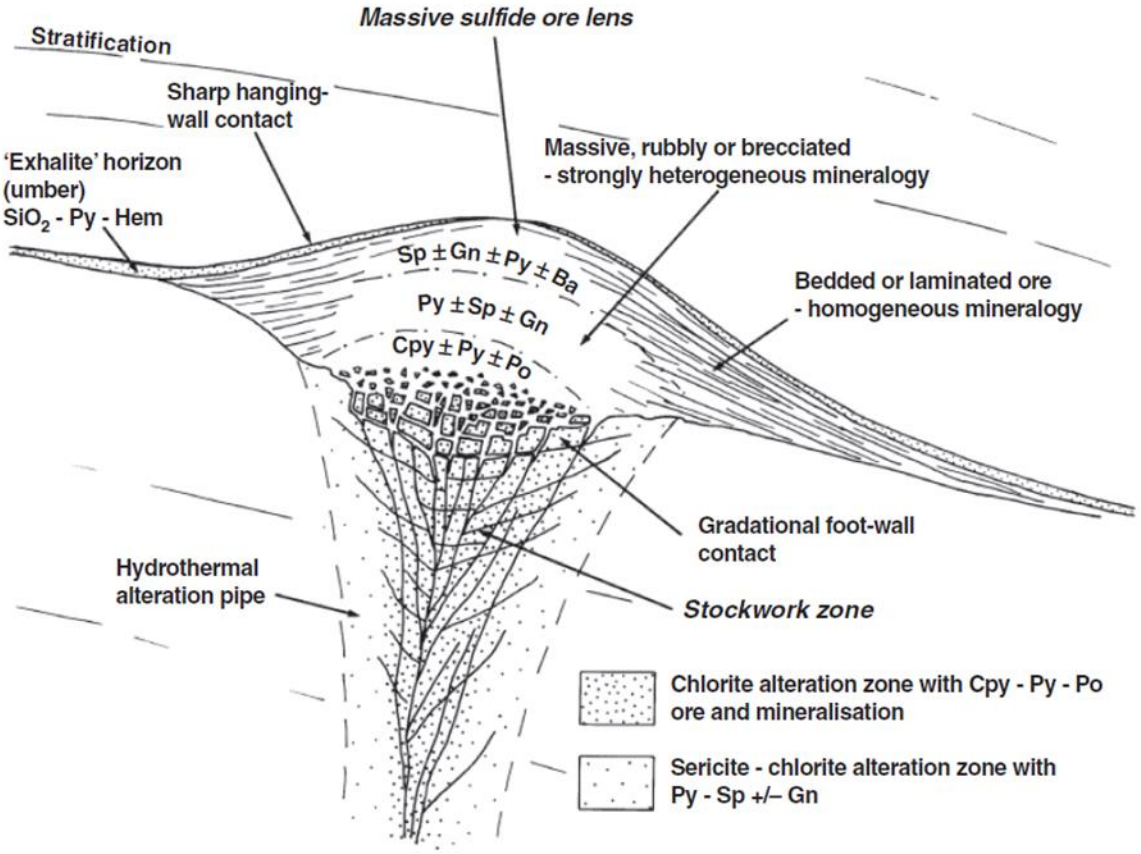

Figure 6: Idealized internal Structure and distribution of ore types within a lenticular VHMS deposit; By (Ridley, 2013) after (Lydon, 1988) Mineral abbreviations: Ba – barite; Cpy – chalcopyrite; Gn – galena; Hem – haematite; Po – pyrrhotite; Py – pyrite; Sp – sphalerite

Thalanga Mineralogy: The main lenses of the Thalanga deposit are characterized by a surface expression of flooded goethite-limonite gossan with localized barite. Mineralization occurs in zones dominated by silicification, sericitization, and pyritization within the underlying rhyolitic pyroclasts. The local mineralogy includes chlorite, actinolite, carbonate, biotite, barite, chalcopyrite, sphalerite, and galena (Withnall, 1982). Gangue minerals at

Thalanga include chlorite, tremolite, calcite, dolomite, barite, magnetite, and quartz (Paulick et al., 2001).

Intense quartz-pyrite alteration is associated with the rhyolite of the footwall, while weak albite and anorthite are associated with the dacitic hanging wall. Alteration in the footwall is destructive, primarily affecting primary feldspar (Large et al., 2001). The alteration box plot and lithogeochemistry associated with VHMS deposits extensively elaborates on the intensity of sericite and chlorite alteration in the footwall volcanics, which closely resembles Kuroko-type deposits. There is a breakdown and replacement of sodic plagioclase by sericite and chlorite in the outer part of the alteration system. Chlorite-rich assemblages replace sericite near the massive sulphide mineralization in the footwall pipe, resulting in a loss of Na_2O and CaO and a gain of K_2O. As zonation progresses closer to the footwall pipe, there is a loss of K_2O and a gain in FeO and MgO (rich in siderite and dolomite), indicating more intense alteration characterized by pyritization and chloritization.

The greenschist regional and contact metamorphism post-dating deposit formation has further modified the hydrothermal mineral assemblage, forming chlorite, muscovite, biotite, tremolite, and spessartine-almandine (Paulick, et al. 2001). The alteration facies and geochemistry of the hanging and foot walls of the Thalanga deposit are summarized in Figure 7 and Figure 8 (Paulick et al., 2001). Tetrahedrite is associated with arsenopyrite and chalcopyrite at Thalanga, but no tellurides have been identified (Simpson, 2001; Hill, 1996).

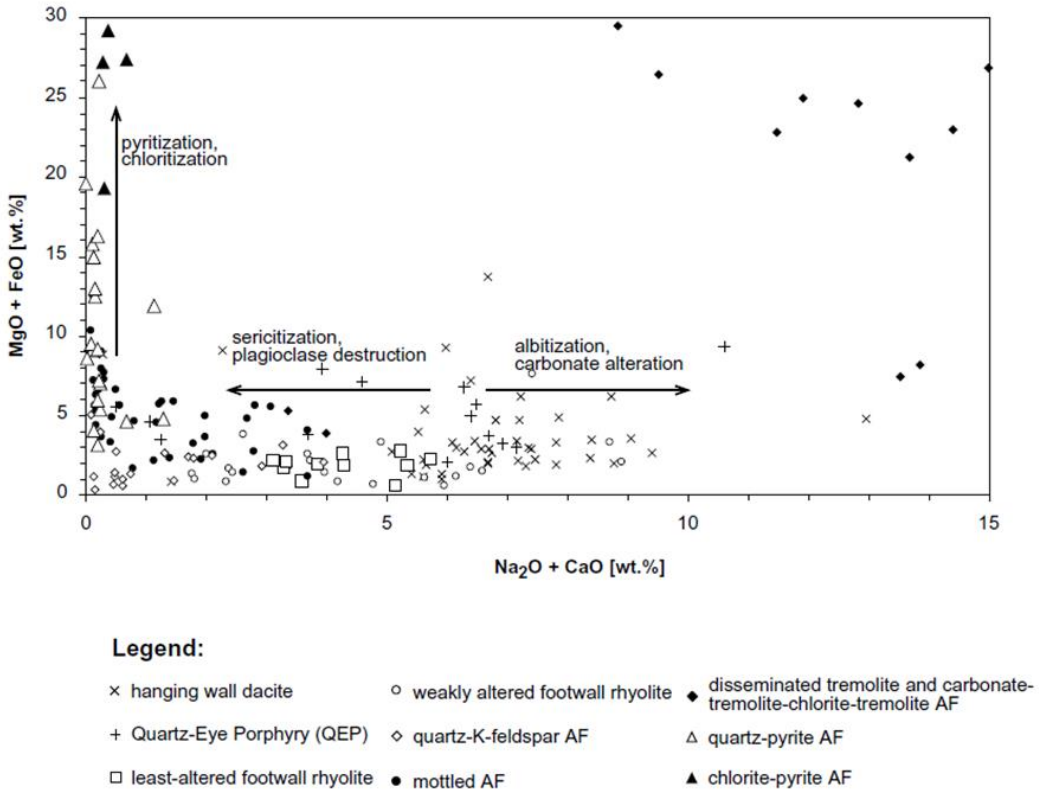

Figure 7: Alteration facies of Thalanga deposit (Paulick, et al., 2001)

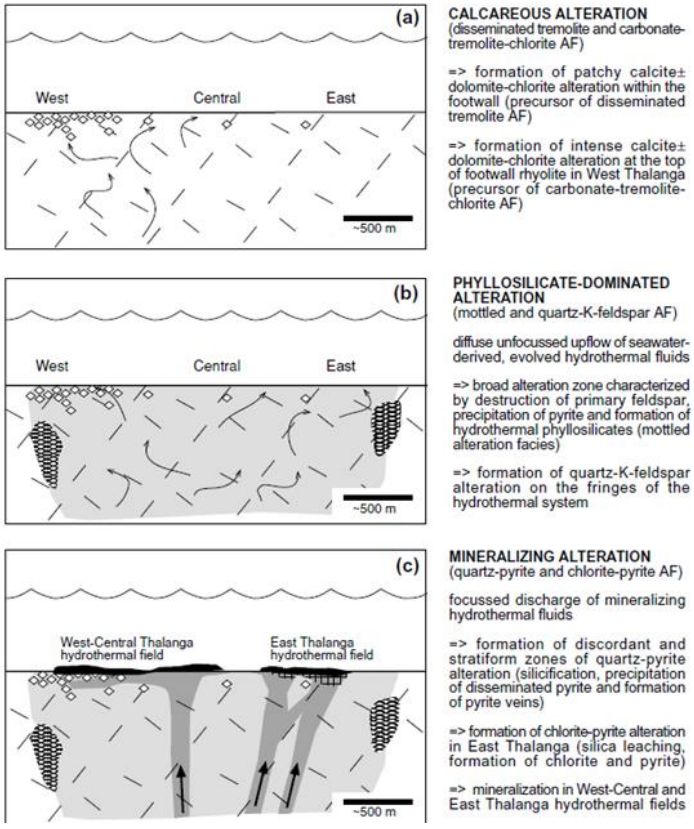

Figure 8: Geochemical characteristics and Mineral alteration zones of Thalanga VHMS (Paulick, et al., 2001)

Highway-Reward mineralogy: The Highway-Reward VHMS deposit is characterized as a Cu-Au deposit comprising two primary discordant pyrite-chalcopyrite pipes: Highway and Reward (Beams et al., 1998; Withnall, 1982). Situated in the upper part of the Trooper Creek formation, the deposit is primarily composed of clastic breccia featuring plagioclase-porphyritic andesite, jasper, rhyolite, and dacite with a chlorite-carbonate-rich matrix (Berry et al., 1992).

Mineralization within the Highway-Reward deposit can be classified into five main types:

1. Primary pyrite-chalcopyrite pipes. i.e. massive sulphide mineralisation within the central core of the Highway-Reward pipes
2. Supergene Cu (Chalcocite and Covellite) and Au above the Reward pipe.
3. Gossanous Cu-Au rich mineralization above the sulphide zone.
4. Disseminated, vein-style and stratabound pyrite-sphalerite-galena-barite mineralization at the margins of the pipes in the hanging wall.
5. Footwall and Hanging wall pyrite-quartz veins.

The gold oxide zone consists of fine-grained siliceous breccia and orange coloured gossanous barite. The alteration mineralization of the Highway-Reward deposit is zoned by assemblages of chlorite-sericite±quartz, chlorite±anhydrite±gypsum, quartz-sericite±pyrite, sericite-chlorite-feldspar-quartz, and hematite±chlorite-sericite-albite-quartz (Doyle & Huston, 1999; Herrmann, et al., 2001). Presence of electrum and tennantite associated with pyrite and chalcopyrite.

Balcooma mineralogy: The Balcooma deposit in the Greenvale area is a metamorphosed VHMS deposit rich in Pb-Zn-Cu-Au, characterized by massive pyrite associated with metamorphosed siliceous exhalites (Harvey, 1989; Huston et al., 1992). Mineralization at Balcooma is represented by two main types: dominant copper mineralization and less dominant Zn-Pb-Cu mineralization.

The mineralized zones are hosted within a sequence of quartz-muscovite-biotite-staurolite schist and quartz-muscovite-biotite schist. Chalcopyrite is commonly associated with pyrite, while massive chalcopyrite occurs alongside pyrrhotite. The Balcooma mylonites are primarily composed of rhyolitic to dacitic, featuring vitric and lapilli tuff, agglomerate, and interlayered pelite, arenite, and conglomerates (Henderson R. A., 1986). These mylonites contain phenocrysts of plagioclase feldspar, with quartz, muscovite, feldspar, and minor biotite also present due to metamorphic processes (Withnall, 1982).

Electrum at Balcooma is often associated with chalcopyrite and bismuth minerals, and less commonly with galena, occurring as remobilized minerals within cracks in pyrite grains (Huston, et al., 1992).

2.7.4 Mining History and Current Operations

The Thalanga polymetallic deposit, hosted within the Mt Windsor subprovince, was initially discovered in 1975 (Gregory & Hartley, 1982; Miller et al., 2001; Kilgariff, 2003). Exploration efforts preceding its discovery in the 1970s identified potential VHMS mineralization in the Mt Windsor subprovince, with early reports mentioning occurrences of barite (Herrmann, 1995). Since the discovery of Thalanga, numerous exploration campaigns have been conducted in the Mt Windsor formation to further delineate and expand knowledge of the polymetallic deposit in the area. Key exploration companies involved in these efforts include Pennaroya (1975), Pancontinental/RGC (1977-1990), Aberfoyle/Aztec (1983-1985), CRAE (1984), Freeport/Mt Burgess Gold (1984-1988), Conatus (1987-1990), Metallic Minerals/Queensland Gold (1995-1998), Newcrest (2005-2007), and Red River Resources Limited (2015) (Tamaduk, 2018; Kilgariff, 2003).

These exploration campaigns employed a variety of methods including stream and sediment sampling, ground magnetic surveys, induced polarization, airborne electromagnetic surveys, radiometric surveys, rock chip sampling, geological mapping, and diamond drilling. Over time, the Thalanga deposits were systematically drilled, with significant intersections at Thalanga West and West45 in 1980, although the orientation of the ore bodies was not fully understood until the mid-1990s.

Mining operations at Thalanga commenced in 1989 with open-pit mining of supergene polymetallic Cu-Pb-Zn ores by Pancontinental, followed by underground mining of primary polymetallic Cu-Pb-Zn ores in 1991. Renison Goldfields Consolidated acquired the operation in 1995. When Thalanga ore was depleted in 1998, ore from the Highway Reward deposit was mined and processed at Thalanga. Sterlite purchased the operation in 1999 and continued mining from Highway Reward until October 2002, when deep underground mining ceased, and the mine closed in 2005 (Kilgariff, 2003).

In 2006, Kagara Mining acquired Thalanga and mined ore from the Vomacka open pit and the Balcooma deposit. Kagara developed the West 45 decline in 2011 and mined until the company went into administration in 2012. The project remained under care and maintenance until 2014, when Red River Resources acquired it and initiated development of the West 45 underground mine in 2017. Production from West 45 ceased in 2020, and the mine has been under care and

maintenance by the Queensland Government (Queensland Government, 2024) since 2022 following Red River Resources' entry into administration. Thalanga ceased operations in 2022. It is currently under care an

The processing plant originally used at Teutonic Bore in Western Australia was relocated to Thalanga for ore processing (Kilgariff, 2003). The plant initially processed supergene Cu-Pb-Zn ores from Thalanga and later treated ores from the Highway Reward and Balcooma deposits. Adjustments were made to the plant operations to accommodate the different ore sources. Despite efforts to store tailings into cells corresponding to specific ore sources, some cells were inadequately labelled, making it challenging to correlate them geochemically and mineralogically with specific deposits. Additionally, it is unclear from the literature whether ore blending occurred during processing. If blending did occur, it would contribute to variability in the geochemical and mineralogical composition of tailings within the Tailings Storage Facility (TSF), emphasizing the heterogeneity of waste characterization vertically and laterally.

According to the National Resources Authority (NRA, 2018) and (SLR Consulting Pty Ltd, 2020), tailings cells at Thalanga were designed as follows: Cells 2 to 5 contain tailings from Thalanga, Cell 6 contains tailings from the Reward open cut, and Cells 1 and 7 contain tailings from the Highway and Reward deep. Cell 8 contains tailings of materials from Balcooma and cell 9, reprocessed tailings of Reward deep tailings, and tailings from Vomacka (SLR Consulting Pty Ltd, 2020). Figure 9, likely represents the recent tailings dam, and can be traced back to ores from the current operating sites including Vomacka, Far West mine.

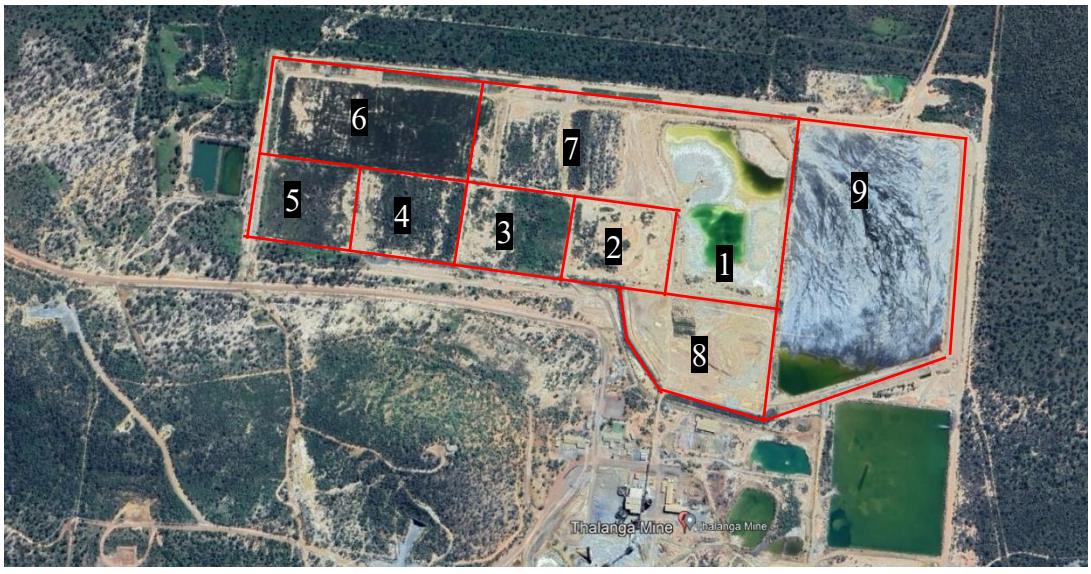

Figure 9: Tailings cell annotation of Thalanga mine

This research utilizes analytical techniques to conduct preliminary assessments and explore the potential for Acid AMD and critical elements content in Thalanga mine waste (tailings and waste rock). Sampling and analytical procedures enable the general characterization of both the deposit and waste materials. The study design, outlined in Figure 10, encompasses sample collection, preparation, geochemical and mineralogical analysis, Acid Base Accounting, and assessment of critical element distribution.

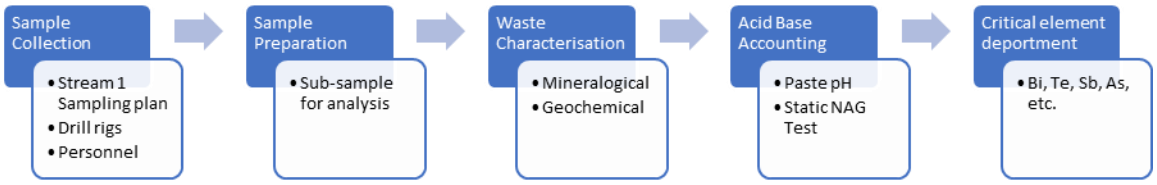

Figure 10: Summary of study design

3.1 Sample Collection

Samples were collected from Thalanga mine between October 30th and November 5th, 2023, as part of preliminary sampling for waste characterization. The layout of the Thalanga mine site is depicted in Figure 11A. The waste dump has been categorized into Potential Acid Forming (PAF) and Non-Acid Forming (NAF) materials, with NAF rocks serving as a perimeter barrier for the PAF cell. Grab samples (Waste rock samples) were obtained from accessible areas, each weighing approximately 2-2.5 kg.

Sonic drilling was used to extract samples from old tailings, reaching depths of up to 12 meters in sections of the tailings dam that were stable. A total of 80-160 samples, each weighing 2-2.5 kg, were collected by Sonic drilling. Auger drilling was used to recover samples from wet and unstable parts of the tailings, reaching depths of up to 8 meters. A total of 40-80 samples, each weighing 2-2.5 kg, were collected by auger drill method. The provisional sampling plan was adjusted on-site based on prevailing conditions, as illustrated in Figure 11B and Figure 12.

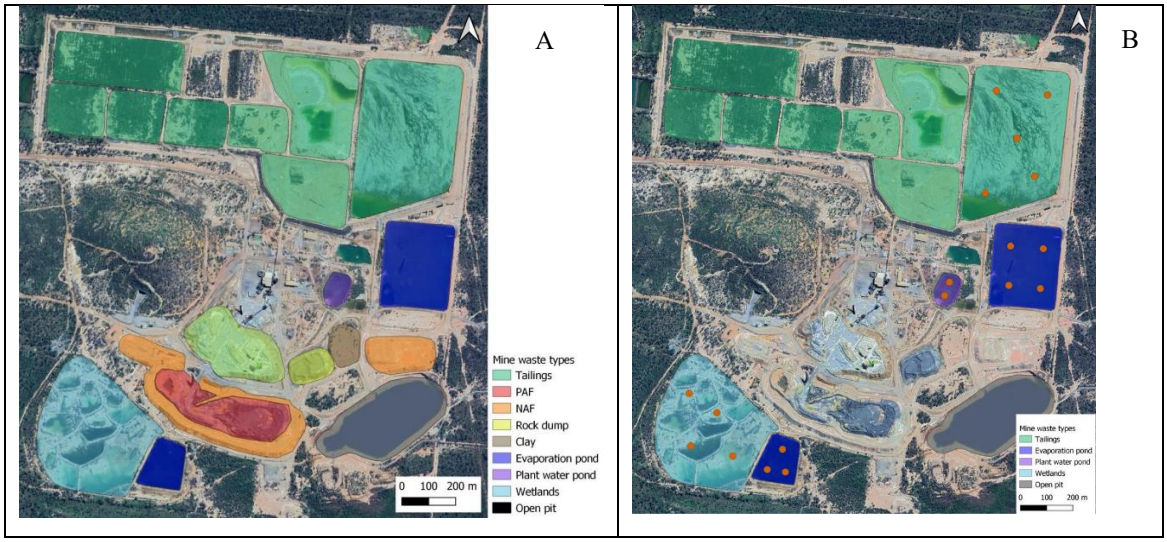

Figure 11: Aerial View of Proposed GSQ sampling points (Source: MIWATCH Sampling Plan Report)

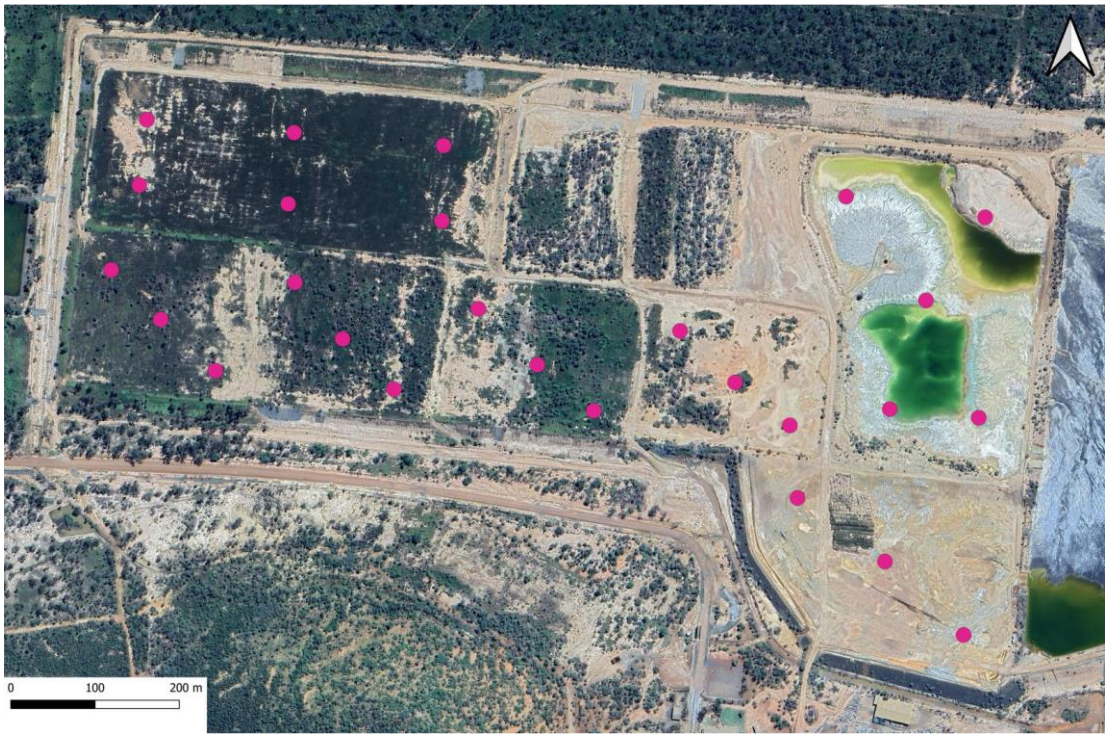

Figure 12: Aerial view of Proposed GA S2 sampling point (Tailings). (Source: MIWATCH Sampling Plan Report)

3.2 Sub-sampling and Sample Preparation.

Three sample classes were distinguished and sampled: A total of 37 waste rock samples were collected from both the PAF and NAF cells, each weighing 2-2.5 kg, and their respective geographic locations are shown in Figure 11. Varying degrees of oxidation were observed on the rock surfaces.

Tailings samples were obtained from 30 drill holes distributed across the old, capped tailings, as shown in Figure 12. Each hole was drilled to a depth of approximately 12 meters using sonic drilling, a vibratory method that fluidizes particles to the drill string, minimizing friction and ensuring representative, undisturbed samples (Guatame-Garcia, et al., 2023). A total of 179 samples were collected from all drill holes at intervals of 0-1 meter, where changes in facies (such as grain size or visible pyrite) were identified. Sample logs from top to bottom are presented in Figure 58 (Appendix B).

In areas where the drilling rig could not operate due to lack of competent ground conditions, an auger drill was used to access samples up to 8 meters deep at similar intervals. A total of 38 samples were collected from GSQ tailings.

Overall, approximately 254 samples were collected from both Thalanga tailings and waste rock. These samples were transported to the Zillmere Exploration Data Centre for preparation before being sent to ALS Brisbane. All samples were re-labelled, and certified standards (including blanks) and duplicates were inserted to ensure data quality. Standards such as OREAS 630b were used, with one standard inserted in every pack of 20 samples, occasionally in packs of 10 or 15 samples.

At ALS Geochemistry, Brisbane, sample preparation depended on the material type (rock, rock chips, and pulps). Pulps were dried for several hours in an oven at 60°C. Rock samples were crushed to 70% passing 2 mm, and 250 g of the material was subsampled by splitting and pulverized to 85% passing 75 µm. Clean and barren quartz was used to clean the crusher and pulverizer after each sample to prevent contamination.

3.3 Geochemical Analysis

The prepared pulps underwent geochemical analysis at ALS. Given that no single analytical method can determine the concentration of all elements, a combination of methods was employed based on the mineralogical hosts of elements and considerations regarding potential element loss. Specifically, ME-MS61, ME-MS81, and pXRF34 methods were utilized.

ME-MS61 Method: This method comprehensively analyses trace, minor, and major elements in pulverized samples. It involves a four-acid digestion using hydrochloric acid (HCl), nitric acid (HNO_3), hydrofluoric acid (HF), and perchloric acid ($HClO_4$), followed by analysis with Inductively Coupled Plasma Atomic Emission Spectrometry (ICP-AES) for major elements and Inductively Coupled Plasma Mass Spectrometry (ICP-MS) for trace elements. A sample mass of 0.25 g is used.

ME-MS81 Method: This method is designed for the analysis of rare earth elements (REE) and a wide range of trace elements in samples with low concentrations. The sample is homogenized, and 0.25 g is fused into a glass bead with lithium borate flux at temperatures between 900-1100°C. Lithium borate facilitates matrix breakdown, ensuring uniform incorporation of all elements into the bead. The resulting bead is dissolved using strong nitric acid, hydrochloric acid, or hydrofluoric acid, and the solution is analysed by ICP-MS for elemental concentrations.

p-XRF34 Method: This non-destructive, in-situ analysis method employs portable X-Ray Fluorescence Spectrometry to rapidly determine the elemental composition of samples before detailed laboratory analysis.

ME-IR08 Method: This method determines total sulphur and carbon content, particularly in cases where these elements exceed detection limits in previous tests. It involves a combustion process that oxidizes carbon and sulphur into CO_2 and SO_2 gases, detected using infrared detectors.

3.3.1 Acid Base Accounting

Acid Base Accounting was conducted on the samples using static methods, specifically the modified Net Acid Generating (NAG) and paste pH tests. To assess the potential variation in Acid Mine Drainage (AMD) across the tailings storage facility (TSF), 58 samples were selected from master pulps returned from ALS, comprising 19 waste rock samples and 38 tailings samples from 8 drill holes. Samples with high contents of S% and Fe% accordung to the geochemical assay were selected for the worst case scenario test.

The paste pH test evaluated the presence of readily formed acidity and alkalinity (Parbhakar-Fox et al., 2018; Smart et al., 2002; Noble et al., 2016). In this test, 20 ml of deionized water was added to 10 g of sample in a test tube at a solid-water ratio of 1:2 (w/w), stirred, and left to react overnight. pH measurements were taken the following day using a TPS-ORP pH device (SN: 2102-309691) calibrated to pH 2, 4, and 7 before measurement.

Due to time and budget constraints, 28 samples from 6 drill holes and 11 waste rock samples were selected from the initial 58 samples for the NAG test (n=38). The NAG test followed guidelines from the AMIRA P387A Handbook (Smart et al., 2002) with modifications (Parbhakar-Fox et al., 2018). In this test, 250 ml of destabilized H_2O_2 at a pH range between 4.5 and 6 was added to 2.5 g of sample in an Erlenmeyer flask to oxidize sulphides and assess the acid-forming potential of the sample.

MODIFIED NAG TEST (MULTI-ADDITION METHOD)

The multi-addition NAG method was used with 15% w/v of H_2O_2 in the following steps.

1. 100ml of H_2O_2 was added to the sample and allowed to react for 2hrs or until effervescence ceases. The 100ml is not added at a go as some samples can react rapidly and boil over the Erlenmeyer flask. It is added bit by bit depending on the reactivity of the sample
2. The sample is heated for 2hrs at 150 ˚C
3. The sample is cooled to room temperature and another 100ml of H_2O_2 was added as in step 1 and step 2 also repeated.
4. The remaining 50ml is added to the sample and allowed to react overnight before step 2 is carried out.

The NAG pH was measured using a calibrated pH meter after the sample had cooled to room temperature. The leachate was subsequently filtered using a 595/1/2 filter. All solid residues from the filtered leachates were rinsed and dried for mineralogical analysis.

A 2 ml aliquot of the filtrate was taken and diluted tenfold, then preserved with 0.4 ml of HNO_3 for further geochemical analysis of dissolved environmentally liable elements.

STANDARDIZATION OF NaOH SOLUTION DETERMINATION OF NAG CAPACITY

To determine the NAG capacity of the samples, the leachate was titrated against standard NaOH solution. First, 4 g and 20 g of NaOH pellets were separately dissolved in 200 mL of deionised water in beakers to prepare 0.1 M and 0.5 M NaOH solutions, respectively. These solutions were then transferred into 1000 mL volumetric flasks and topped up with deionized water to the mark, resulting in solutions with precise concentrations of 0.1 M and 0.5 M. It's important to note that these concentrations are approximate and may introduce errors when estimating NAG capacity. For accurate determination of concentrations, titration of these NaOH solutions was conducted against standard oxalic acid ($C_2H_2O_4 \cdot 2H_2O$), employing phenolphthalein as an indicator.

Figure 13: Acid-Base titration

Procedure:

Dissolve exactly 1.5759 g of hydrated oxalic acid ($C_2H_2O_4$) in a 100 ml deionised water and transfer the solution into a 250 ml volumetric flask. Top it up to the mark.

$$\text{M } (C_2H_2O_4{\cdot}2H_2O) = \frac{Mass(C_2H_2O_4{\cdot}2H_2O)}{Molar\ mass} \times 4 = \frac{1.5759}{126.07} \times 4 = 0.0500\ moldm^{-3}$$

For the 0.1 M NaOH standardization, pipette 10 ml of oxalic acid into three 250 ml Erlenmeyer flasks separately and add two drops of phenolphthalein to each. Titrate it against NaOH solution. Read and record the volume level in the burette when the solution turns pink or rose. Repeat for all the three test and find the average titre volume, V_{NaOH}.

To calculate the exact concentration of NaOH, I use the assumption that, to reach neutrality, the same number of moles of NaOH and oxalic acid are needed.

$$M_{NaOH} \times V_{NaOH} = 2 \times (M_{C_2H_2O_4} \times V_{C_2H_2O_4}),$$

$$M_{NaOH} = \frac{2\times(M_{C_2H_2O_4}\times V_{C_2H_2O_4}}{V_{NaOH}} \qquad \textit{Equation 6}$$

For the 0.5 M NaOH standardization, the same procedure was followed with 50 ml of Oxalic acid. The exact concentration of NaOH calculated was 0.0948 M and 0.489 M.

DETERMINATION OF NAG CAPACITY

Leachates with Nag pH < 2.0 were titrated against 0.489 M NaOH whiles those with pH > 2.0 were titrated against 0.1 M NaOH.

During the titration, the volume of NaOH consumed by the leachate at pH of 4.5 and 7.0 were read and recorded. The NAG capacity is calculated for each sample at both pH values using eq7 below.

$$NAG(kgH_2SO_4/tonne) = \frac{49 \times V \times M}{W} \qquad \textit{Equation 7}$$

where V= titre volume of NaOH, M= molarity of the NaOH, and W is the weight of the sample reacted.

Some of the precipitates formed during titration were filtered and dried for SEM analysis.

SEQUENTIAL NAG TEST

After the multi-addition method, three samples from the cells 2, 4 and 8 of the tailings respectively were analysed to compare the pyrite oxidation ability of Multi-addition and Sequential or Multi-stage Nag test.

Procedure:

2.5 g of sample is measured into 250 ml Erlenmeyer flask

250 ml of H_2O_2 is added to the sample and allowed to react until two hours or effervescence stops.

The sample is heated between 150˚C-250˚C for another two hours and allowed to cool to room temperature. The pH is measured and noted

The sample was filtered, and the leachate titrated against standard NaOH solution like the procedure in the multi-addition method. The NAG capacity is calculated and recorded with the titre value at pH of 7.

The residue is rinsed thoroughly with deionised water to ensure there is no peroxide in it. The procedure is repeated with the residue until the pH of the NAG liquor is above 4.5.

The total NAG capacity is calculated by adding the individual NAG capacities obtained at each test.

3.3.2 Mineralogical Analysis

To assess the bulk mineralogy and physical characteristics, particularly of pyrite (including shape, particle size, and mineral associations), representative sub-samples were extracted from

the master pulps for examination using a Mineral Liberation Analyser (MLA). Data from twelve samples were analysed for mineralogy, texture, and liberation using Dataview software.

Samples of interest were selected based on mineralogy and NAG test results. It was studied further for mineralogical analysis via Polished Block Analysis using Scanning Electron Microscopy (SEM) and Optical Microscopy at the GeMMe Mineralogy Laboratory in ULiège.

Some samples with high sulphur content were put to complete pyrite oxidation analysis using both the original sample and rinsed residues post-NAG test. Samples exhibiting high sulphur content, but low acid-generating potential were analysed for pyrite liberation.

POLISHED BLOCK PREPARATION

Polished block-grain mount specimens were prepared for select samples and their corresponding residues obtained after the NAG test. This step aimed to enhance understanding of the extent of pyrite oxidation, and liberation within the samples.

To mitigate operational biases such as preferential plucking during polishing, segregation of denser and/or larger particles, and inadequate dispersion of granules (Pirard & Sardini, 2011), procedures outlined in Bouzahzah et al., (2015) were followed. It is important to highlight that this method represents an advancement over traditional approaches and is typical of ULiège within the GeMMe group. Its uniqueness lies in its ability to eliminate errors related to particle-particle agglomeration and differential settlement.

MATERIALS

Struers Epoxy Resin	Nano Carbon (Black Carbon)	Struers degassing Chamber
Hardener	Mechanical Stirrer	Vevor Vacuum chamber
Mould		

For each polished block mould, a specific recipe is prepared in the following sequence: epoxy resin combined with nano-carbon, mechanically stirred for three hours. The mixture undergoes degassing in the Struers degassing chamber to remove bubbles before adding the hardener. After manual stirring, the mixture is poured into the mould containing the sample and stirred again to ensure uniform homogeneous distribution of particles within the resin. The sample is then allowed to cure for a minimum of 8 hours.

Figure 14: Degassing chambers. (Struers)

BLOCK POLISHING

The polishing process entails multiple stages of grinding, progressing from coarse to fine surfaces using Struers' MD grinding discs. These abrasive discs are enhanced with water or diamond suspension during polishing. At ULiège, we use the Tegramin-30 Struers machine, shown in Figure 15. Coarse abrasive particles ranging from 125 µm to 7 µm are used with water as a lubricant, while particles from 9 µm to 1 µm utilize diamond suspension. The MD discs used in this project fall into categories of Plane (coarse) grinding and Fine grinding (Struers, 2018). The final three steps are particularly time-consuming, requiring the polished blocks to undergo ultrasonic bath immersion between each step to remove debris lodged in cavities. The first water-based polishing step is relatively swift.

Table 1: Abrasive types used for the block polishing

Plane Grinding Disc	**Abrasive particle size**
MD Piano 120	125 µm
MD Piano 220	68 µm
MD Piano 500	30 µm
MD Piano 1200	15 µm

MD Piano 2000	7 µm
Fine Grinding Disc	**Abrasive particle size**
MD-Largo	9 µm
Polishing cloth	**Abrasive particle size**
MD- Dur	3 µm
MD- Dur	1 µm

Figure 15: Tegramin-30 Struers

3.3.3 Critical Element Deportment

Polished blocks were prepared for analysis and deportment of critical elements. Prior to SEM imaging and analysis of the samples, the polished blocks with mounted samples are imaged with an optical microscope (Zeiss AxioImager M2m) with an XYZ motorized stage to obtain tiled images which enhances identification of areas of interest when mounted under the Scanning Electron Microscope with precision. In ULiège the Mineralogic Mining System-ZEISS is used. It automatically quantifies minerals by measuring the chemical composition of minerals through detection of elements in X-ray spectrum for each pixel analysed. The system is Zeiss Sigma 300 field Emission Gun equipped with two Bruker (xFlash 6| 30-Xray) Energy Dispersive Spectrometers as shown in Figure 16. SEM-EDS analysis of the samples was performed under vacuum using a probe current of 2.3 nA with an accelerating voltage of 20 kV at a working distance of 8.5 mm. Spot mode analysis was used with an EDS dwell time of 1 s. These are user defined parameters. The identification of mineral phases is determined using classification data developed from the optical microscopy SEM-BSE study.

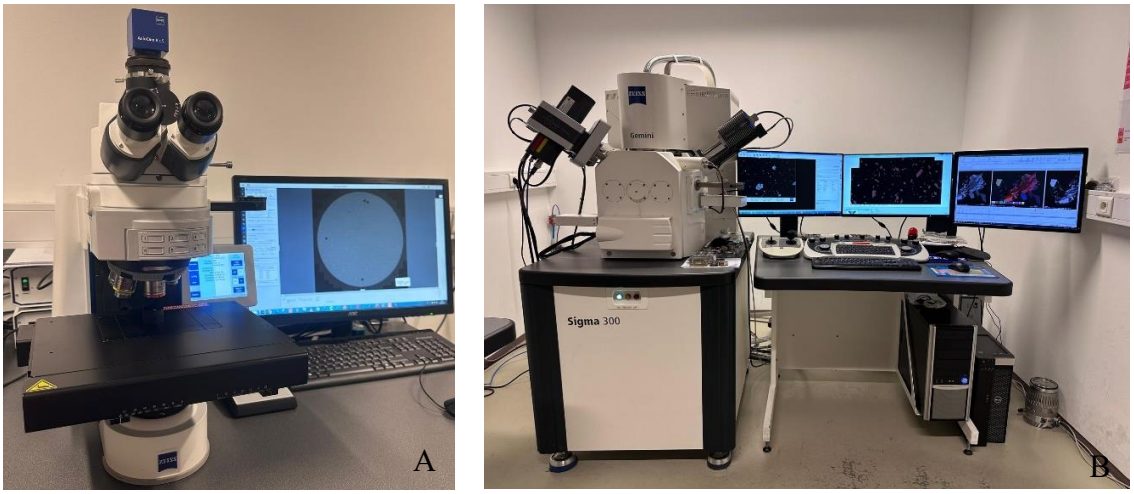

Figure 16: A) Optical Microscope AxioImagerM2m and B) Zeiss Mineralogic SEM

SEM was used for the bright phase mineral search, leveraging Backscattered Electron (BSE) intensity to identify and characterize minerals. This approach relies on the fact that minerals with higher average atomic numbers appear brighter than the surrounding matrix. The critical elements of interest in this study have atomic numbers higher than Fe and S, making them easily distinguishable within sulphide minerals.

Samples were metalized, a process where a thin layer carbon is applied to the polished block to enhance electron conductivity in non-conductive samples and prevent charging under the electron beam. Parameters such as contrast, resolution, threshold, and segmentation (Region of Interest - ROI) were optimized to capture high-quality images and maximize data acquisition.

Bright phases identified in the BSE images were further analysed using Energy Dispersive X-ray Spectroscopy (EDS) in spot mode. Spectra obtained from EDS were quantified using Quantax software to determine the weight percentages of elements present in the bright phases. Elemental compositions obtained from EDS were compared to known mineral compositions to identify the minerals present in the bright phases.

Integration of geochemical assay results and SEM mineralogical data allowed for correlation of concentrations of each critical element with specific mineral phases. Modal mineralogy was calculated, and the content of each critical element within each mineral phase will be determined by multiplying the element content in each mineral phase by its proportion in the sample.

A mass balance check is supposed to be performed to ensure consistency, verifying that the sum of critical element contents across all mineral phases matched their respective geochemical assay results.

Chapter Four Results

4.1 Tailings Physical Characteristics

The tailings were deposited in cells classified according to the site of origin of the processed ore. The three sites from which materials were processed at the Thalanga plant had similar physical characteristics but different mineralogical and geochemical characteristics. The old tailings, comprising Cells 2, 3, 4, 5, 6, 7, 8 and 9 as shown in Figure 9, were covered with about 0.2 meters of clayey material. These tailings were saturated beneath the cover, making it difficult to physically identify facies from the retrieved cores. The common physical characteristic of the tailings across all cells was a dark colour and visible pyrite in the core samples. A sonic drill was used for coring samples up to 10 meters deep, as the old tailings were quite stable. The fresh tailings had no cover system. There were pockets of salt precipitates across the surface of the fresh tailing, especially in the dry areas of the cell. However, the competency of this part allowed for only auger drilling.

Cells 2, 3, 4, and 5 contained tailings of ore materials mined from the Thalanga open cut and underground mine (Thalanga central, West 45, and Far West). These materials showed related mineralogical, geochemical, and textural similarities. Beneath the clay covering of the cells, percolated meteoric water caused minute oxidation of the very topmost tailings to about 0.2 meters deep. The tailings were saturated with water, making retrieval of cores difficult. Cell 6 contained tailings from ore processed from Reward Open cut, characteristic of supergene copper tails. Cells 1/7, and 8 were the most acid-generating cells, containing processed ore materials from Thalanga, Highway and Reward Deep, (the divide between cell 1 and 7 failed around 2000 causing the two tailings to mix up). Cell 8 contains tailings of ore from Balcooma. Cell 9 contains tailings of processed ore from Vomacka however it initially received tailings from the reprocessed tailings of Highway-Reward.

The waste rock samples were pre-classified during dumping into Potentially Acid Forming (PAF) and Non-Acid Forming (NAF). The PAF rocks were deposited at the centre, while the NAF rocks were used as a peripheral shield for the PAF, as shown in Figure 11. Salt precipitates were taken from the depression zones between the waste dump and the ROM pad where meteoric water draining from rocks had routed. The initial waste rock was moved from the original position to fill the Thalanga central open cut after 9 years of fighting AMD as a way of containing the acidic water. With time, waste from other sites were used to fill it completely and the peripheral barricade with NAF rocks were put in place.

4.1.2 Tailings textural characteristics

MLA and SEM were used to study the morphology of the grains and particle size. Three samples were used to study particle size distribution (PSD) and mineral grain size distribution of the waste materials: THA-T061 from tailings Cell 4 representing material from Thalanga deposit, THLG-18 from tailings Cell 9 representing the most neutral pH cell, and THA-33 from the waste rock. The PSD of THA-T061 (Figure 17) has a P_{90} of 75 µm and does not vary significantly across its depth. The mineral grain size distribution by chalcopyrite, pyrite, and pyrrhotite are P_{90}(chp, py, pyrrh) = 53 µm, 45 µm, and 16 µm respectively, as shown in Figure 18. Since the P_{90} of the PSD is 125 µm and larger than the individual grain sizes, particles may form from the agglomeration of several mineral grains, as evident in the mineral map in Figure 23.

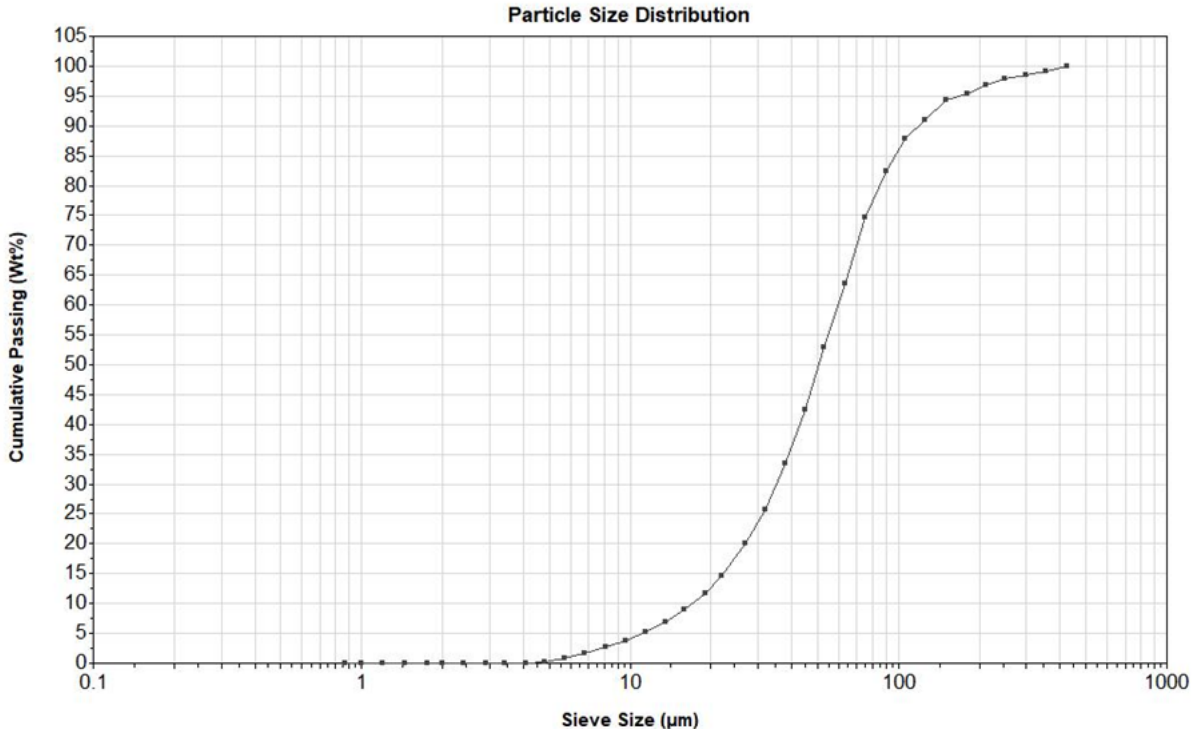

Figure 17: PSD of THA-T061 (Thalanga ore tailings), cell 4

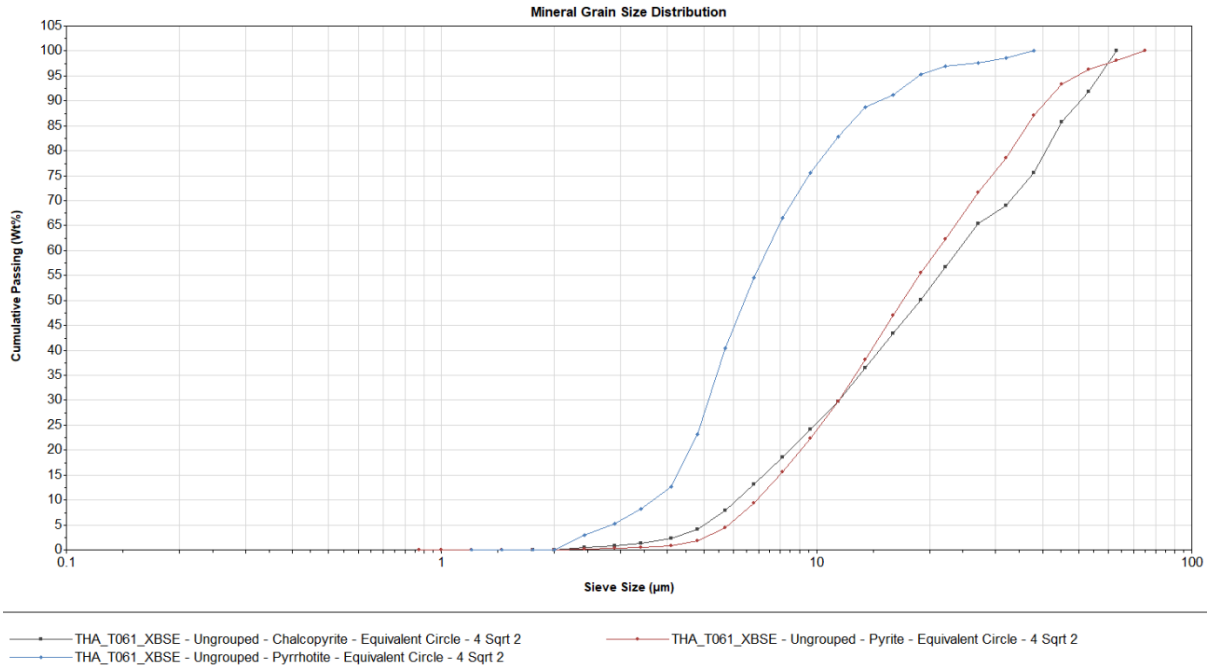

Figure 18: Liberated mineral grain size distribution of THA-T061 (Thalanga Tailings cell 4)

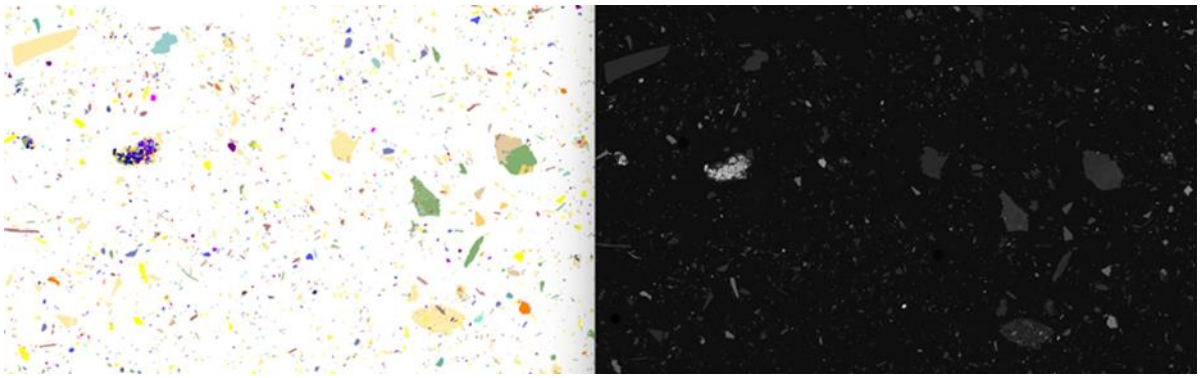

Figure 19: Grain Morphology and texture of THA-T061 (Thalanga tailings) cell 4

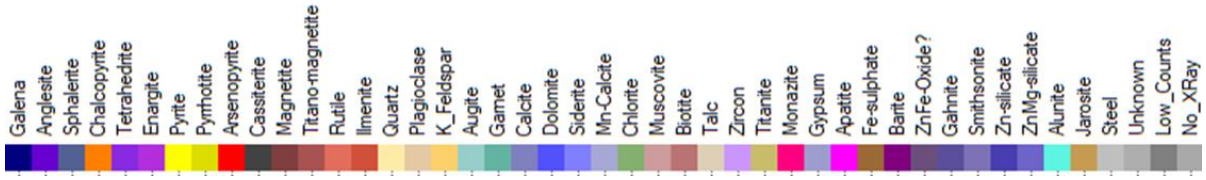

Figure 20: Mineral map legend of THA-T061

The PSD (P_{90}) of THLG-18 is 90µm. However, the mineral grain size distribution is recorded as $P_{90(chp, py, pyrrh)}$ = 45µm, 45µm, and 22µm respectively as shown in Figure 21 and Figure 22. The PSD can also be inferred to be similar across the depth of the cell without significant variation.

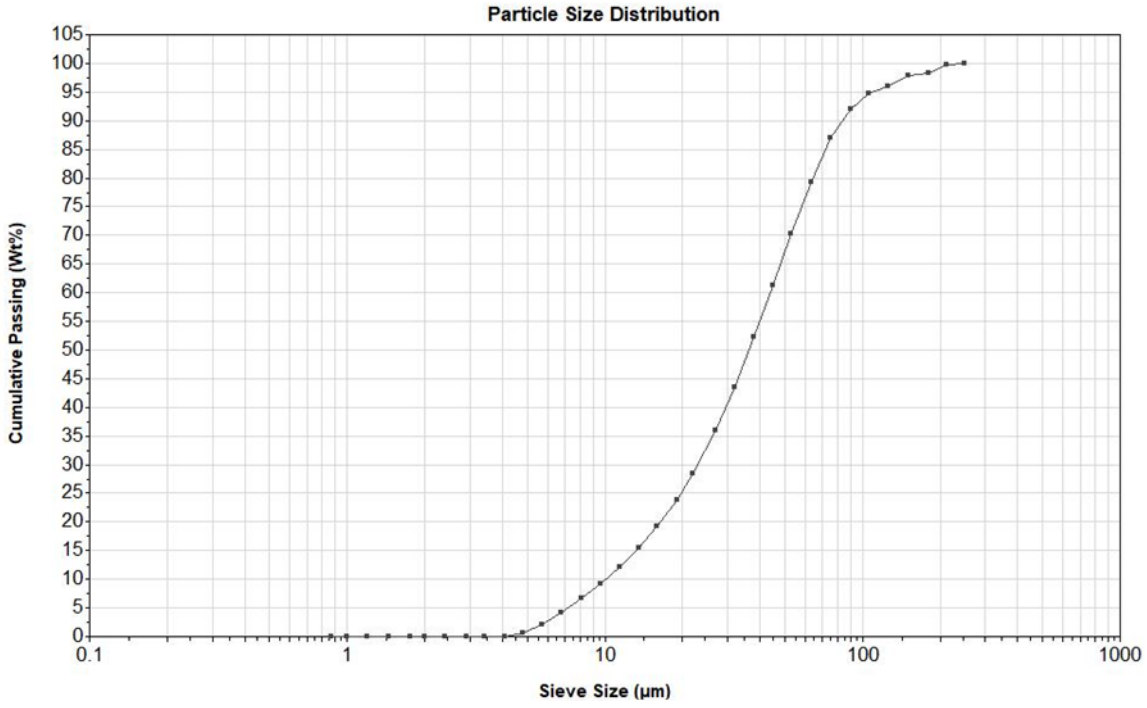

Figure 21: PSD of THLG-18 (Neutral tailings), cell 9

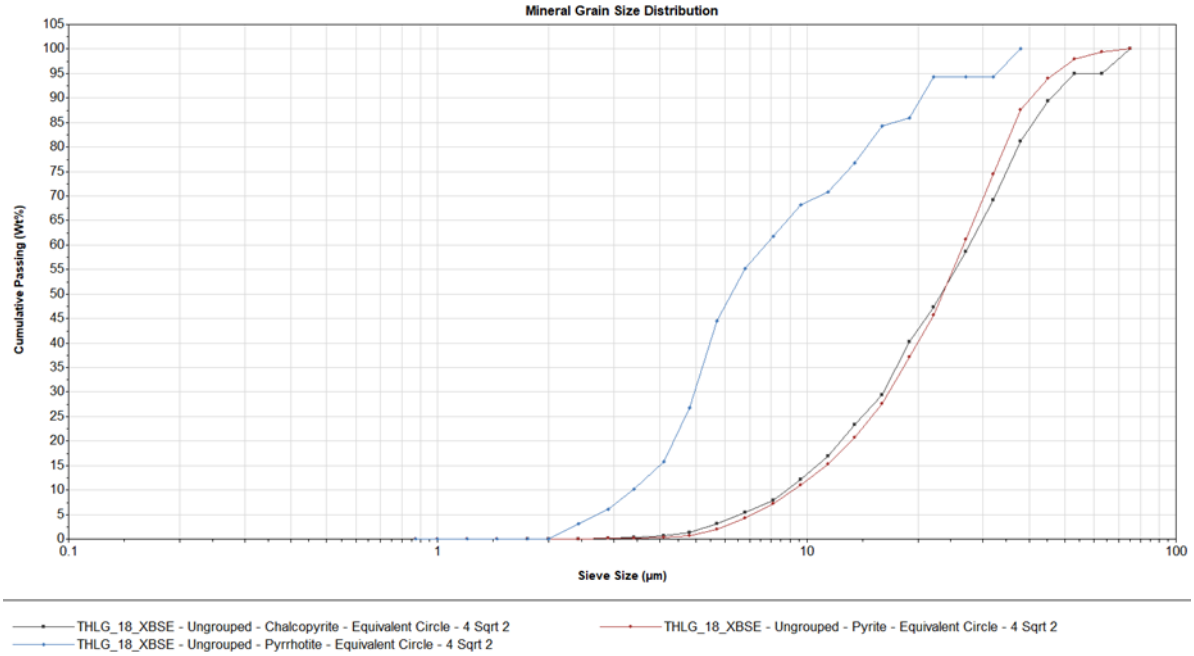

Figure 22: Liberated mineral grain size distribution of THLG-18, cell 9

Figure 23: Grain Morphology and Texture of THLG-18, cell 9

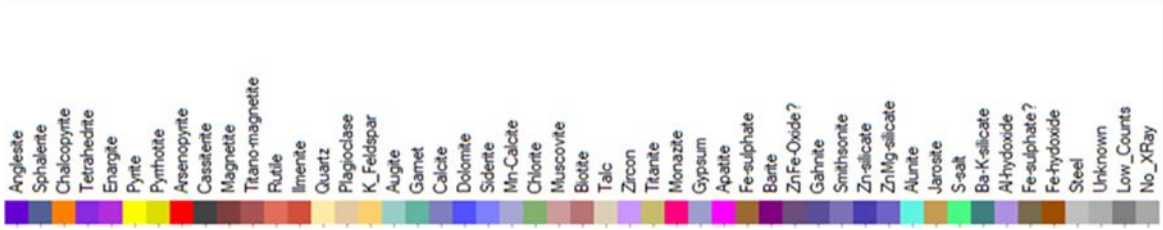

Figure 24: Mineral Map Legend for THLG-18

The pulverized waste rock has particle size distribution (PSD) with a P_{90}=1200 µm, as shown in Figure 25. Chalcopyrite (cpy), pyrite (py), and pyrrhotite (pyrrh) have P_{90} values of 850 µm, 1400 µm, and 150 µm, respectively. Notably, the pyrite grains are particularly large and prominent in the waste rock, as illustrated in Figure 27 Figure 27.

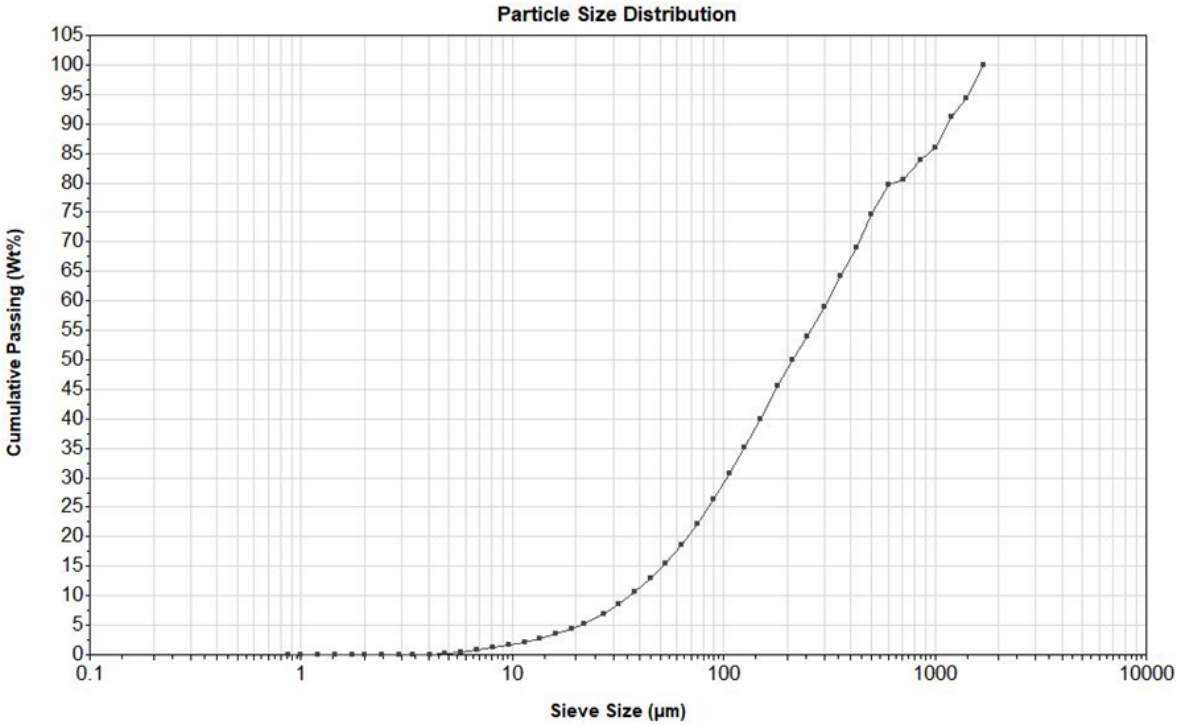

Figure 25: PSD of THA-33, waste rock

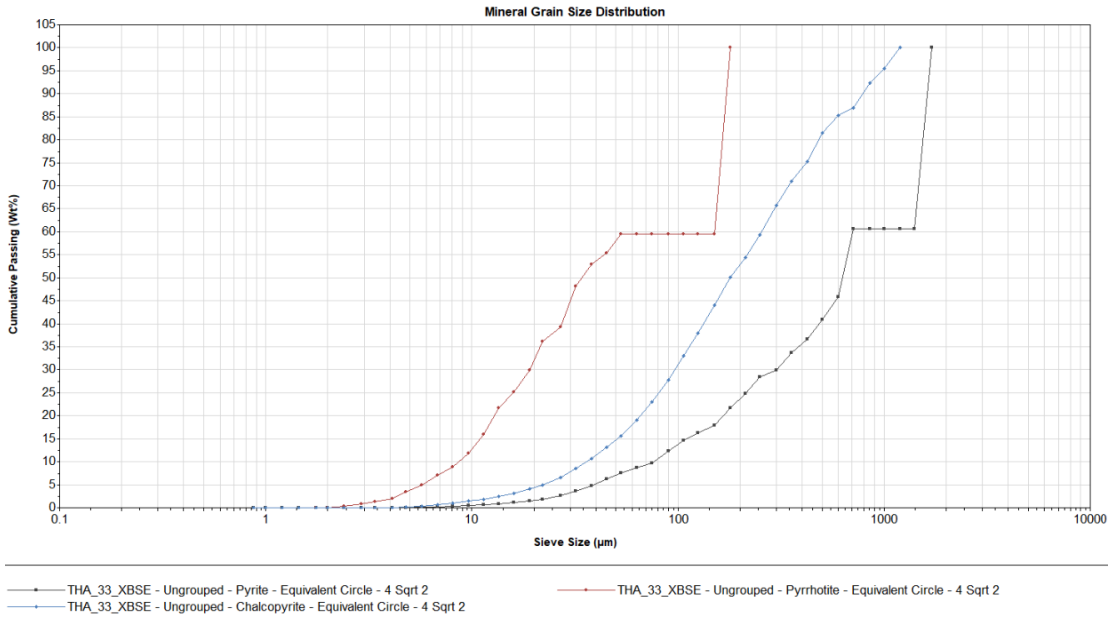

Figure 26: Liberated mineral grain size distribution of THA-33 waste rock

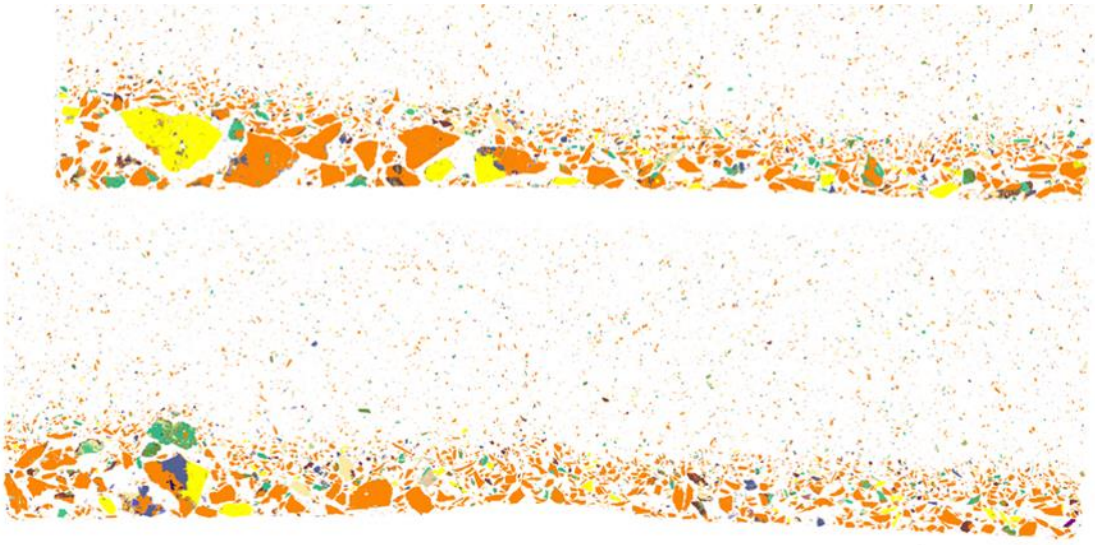

Figure 27: Grain Morphology and Texture for THA-33

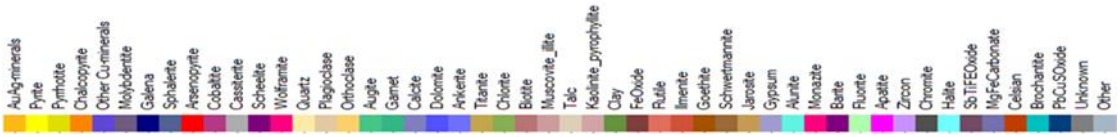

Figure 28: Mineral Map legend for THA-33

In general, the PSD of the tailings ranges between 10 µm and 250 µm, as indicated by the two PSD curves for tailings. Conversely, the PSD of the waste rock can be as large as 500 µm. Most mineral grains are liberated at the P_{90}, except those encapsulated in agglomerates associated with the tailings. The minerals predominantly exhibit anhedral, subrounded, and elongated shapes, as seen from the MLA mineral maps. The textural features of cell 4 at depth suggest that the slurry/material was transported a short distance from the spigot point before sedimentation, allowing minimal time for particle segregation and vertical size classification.

4.2 Geochemical Characteristics

Element concentrations measured by p-XRF and ICP-MS/AES showed high levels of Fe and S in the tailings and waste rock, reaching up to 48.2% Fe and 41.3% S, with averages of 16.93% and 16.30%, respectively. While Au was not analysed in this project, potentially economic metals such as Cu and Zn were found at average concentrations of 0.3% and 0.4%, respectively, as shown in Figure 29. Potentially harmful elements such as As, Ag, Cd, Sb, Pb, and Zn was also in abundant concentrations in the waste materials.

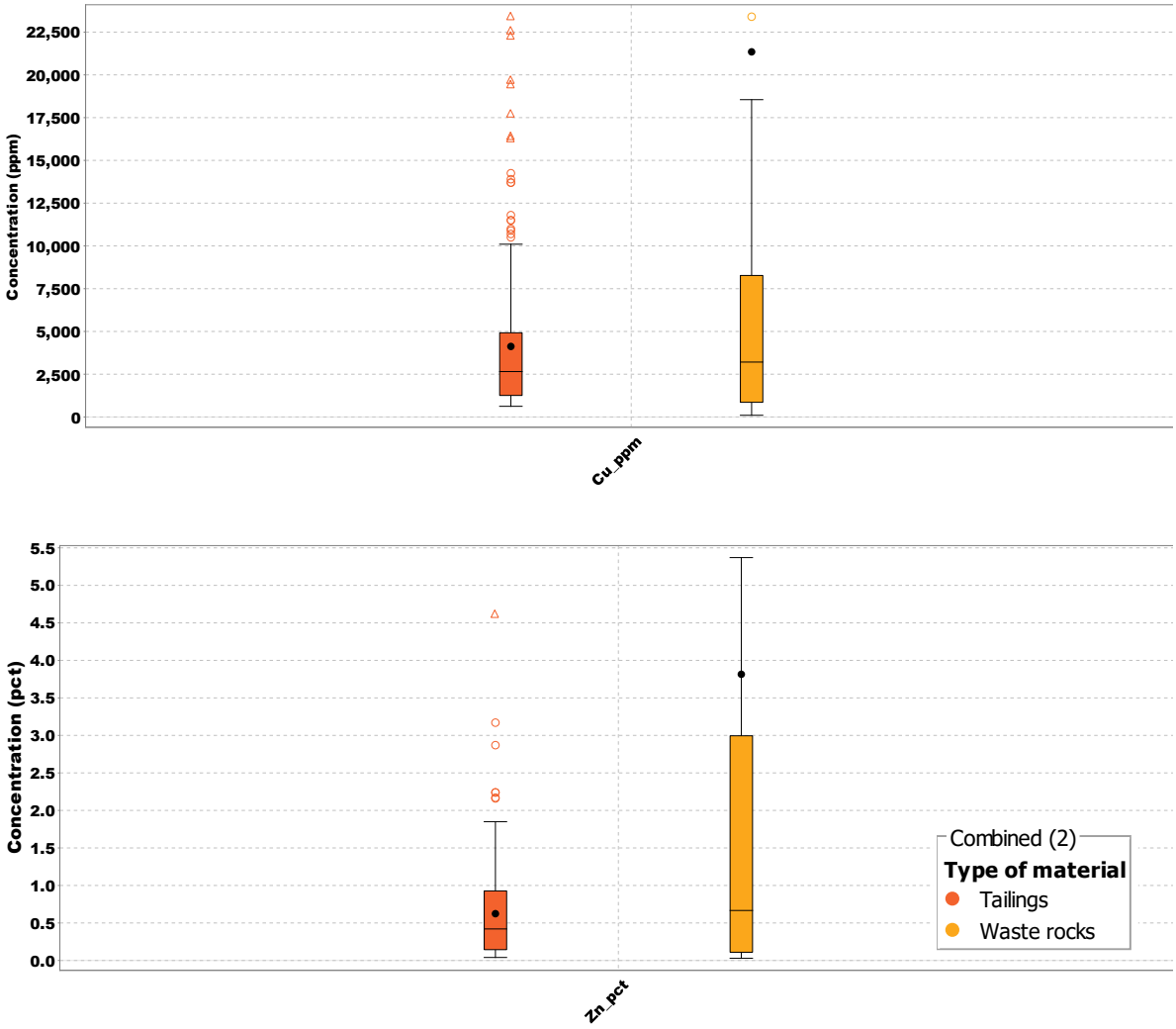

Figure 29: Concentration of Copper and Zinc in Thalanga waste

4.2.2 Geochemistry of CRMs

Elements considered critical by the Australian Government Department of Industry, Science, and Resources were studied, including some elements that are not considered critical by the EU. Elements at least ten times more abundant than the average crustal abundance were selected for detailed examination. Figure 30 shows a ratio between the site-specific concentration of these critical elements at Thalanga and their average crustal abundance. The graph only shows the number of times a particular critical element is abundant in Thalanga waste as compared to average crustal abundance.

Elements such as As, Bi, In, Sb, Se, and Te, which are associated with Thalanga mine waste, are on Australia's CRM list. However, only As, Bi, and Sb are captured among the European CRM list updated in 2023. The concentrations of these elements in Thalanga mine waste are more than 100 times the average crustal abundance. The high concentration of these elements in salt precipitates indicates their potential to be remobilized and transported in solution.

The critical elements are more concentrated in the tailings than in the waste rock probably because most of them are considered penalty element and are rejected into the tailings during the processing stage.

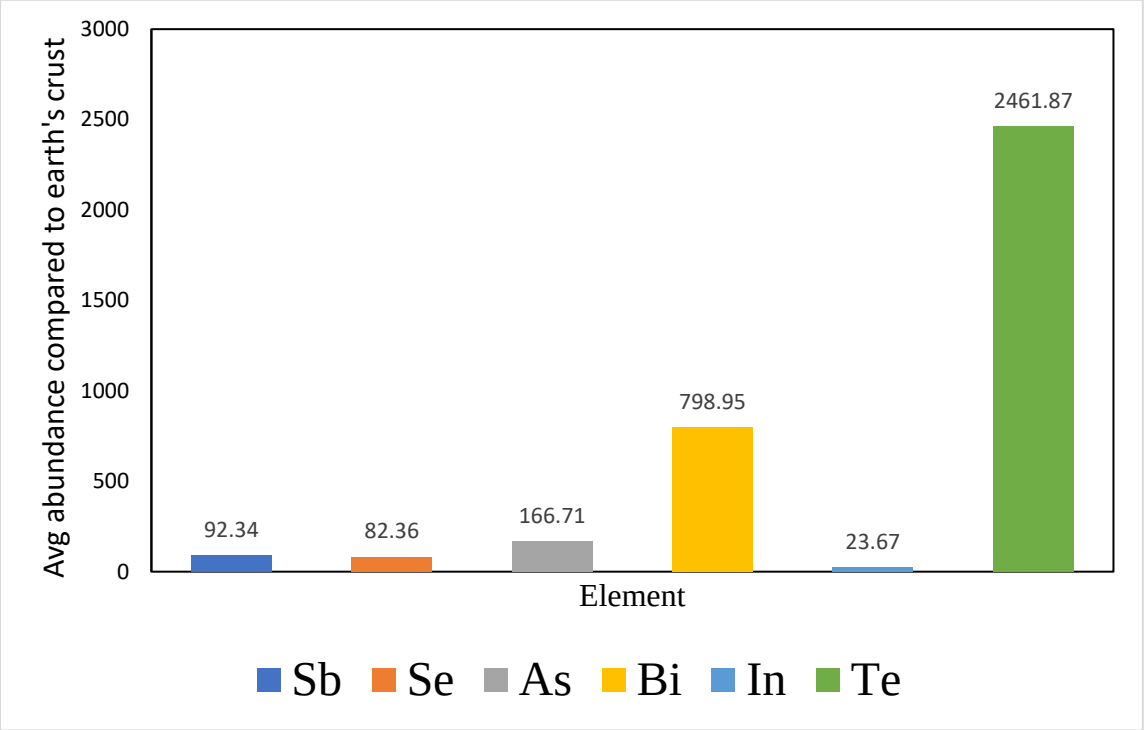

Figure 30: Average critical element abundance in Thalanga as compared to average crustal abundance (Levinson, 1974)

Figure 30 shows the concentrations in ppm, with As, Bi, and Sb having appreciable levels. Although the concentration of Te in Thalanga waste is low, its abundance relative to average crustal abundance makes it worthy to look at. Indium, on the other hand, has an average concentration of 1 ppm, which is not significantly greater than its average crustal abundance of 0.16 ppm.

A careful analysis of the data indicates that, the outliers in the tailings, as shown in Figure 31, are not true outliers but reflect concentrations in specific cells and may have relationship with the type of ore processed from a particular mining site. Upper outliers of Bi and Sb are associated with the Thalanga deposit in cells 2, 3, 4, and 5. Upper outliers of In are found in all tailings cells but are particularly high in cells 7 and 8, which have high Fe and S contents.

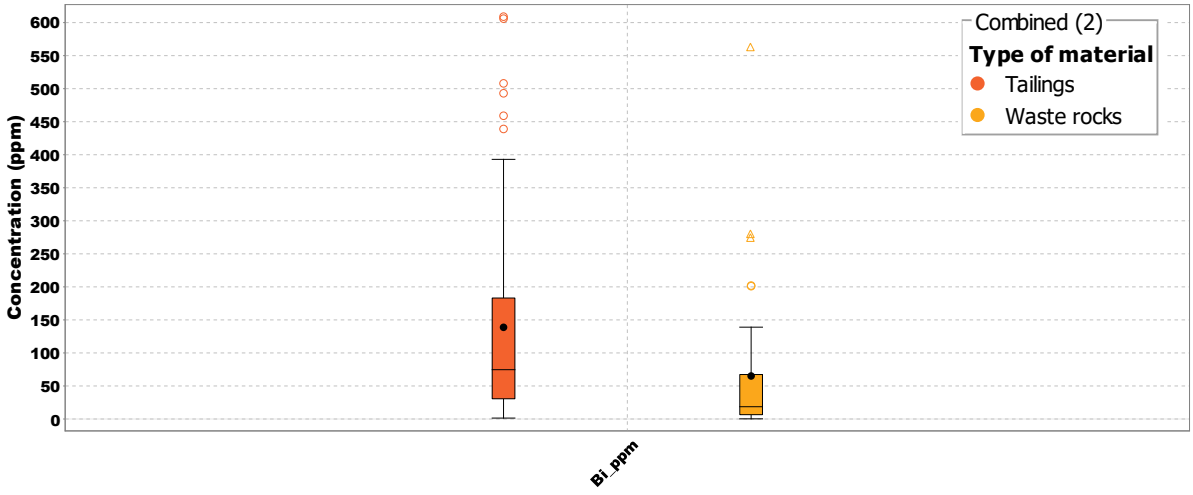

Figure 31: Concentration of Bi in waste (tailings and waste rocks)

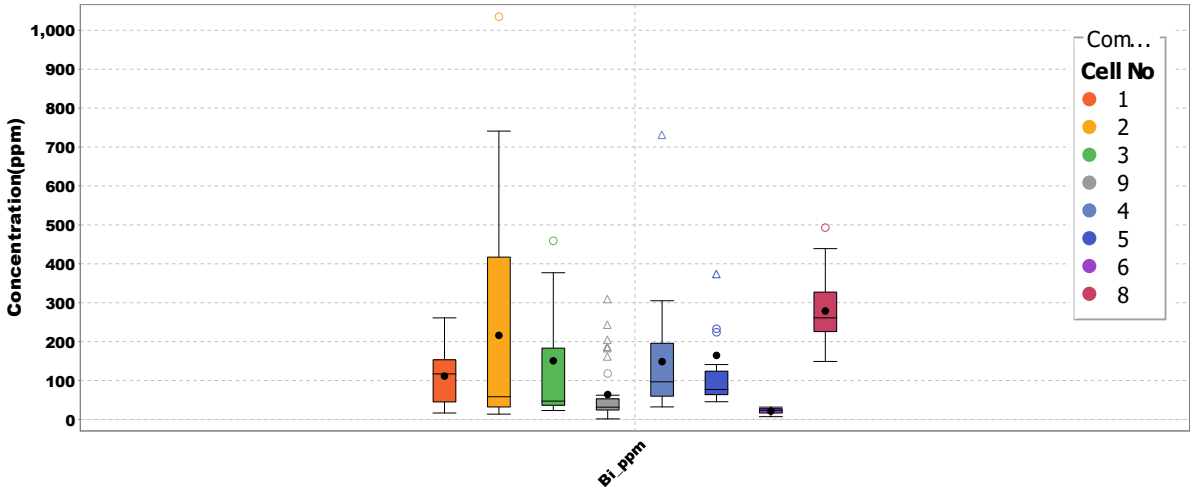

Figure 32: Concentration of Bi according to tailings cell

4.2.3 Acid Base Accounting

The experimental results for the Net Acid Generation (NAG) Capacity, NAG pH, and paste pH, indicates that the most acid generating materials are from the cell 8 with the lowest NAG pH of 1.69. The less acid generating materials are from cell 9 with a NAG pH of 7.9. Materials from these cells yielded a NAG capacity of 279 kg H_2SO_4/tonne and 0 kg H_2SO_4/tonne.

The scatter plot of sulphur (S%) versus paste pH and sulphur (S%) versus NAG pH shows how sulphur relates to the pH and how reliable both tests can be. Ideally, sulphide sulphur correlates well with pH and shows that that pH values decreases as sulphide sulphur increases. In this

study, the sulphur comprises of both sulphide sulphur and sulphate sulphur. From Figure 33, about 20 samples have paste pH values above 6 and as high as pH of 8. However, the same sulphur plot against NAG pH in Figure 34 shows a shift of 15 of these samples towards pH less than 6. Generally, it can be deduced that the oxidation of pyrite using peroxide (NAG pH test) is many times more effective than oxidation with deionised water (paste pH). In this instance of the paste pH test, one cannot confidently conclude whether it is pyrite that is not readily acid generating, or it is carbonates that are readily released giving the sample such high paste pH. This is because paste pH primarily assesses immediate acid-generating sulphate salts and high surface area pyrite and carbonates (Weber, et al., 2006). Nevertheless, in the absence of materials to carry out NAG pH test especially on site, paste pH can give valuable information otherwise it is not as reliable as NAG pH.

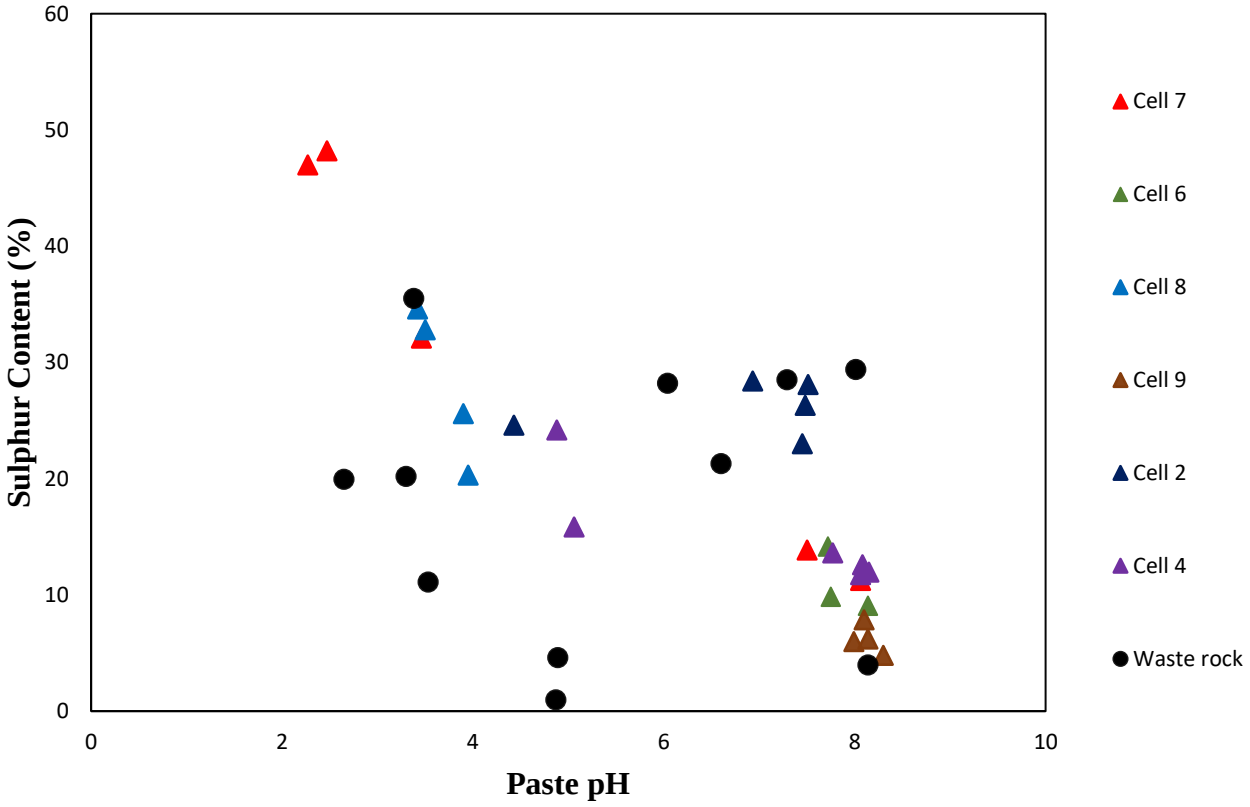

Figure 33: Sulphur content (%) vs Paste pH

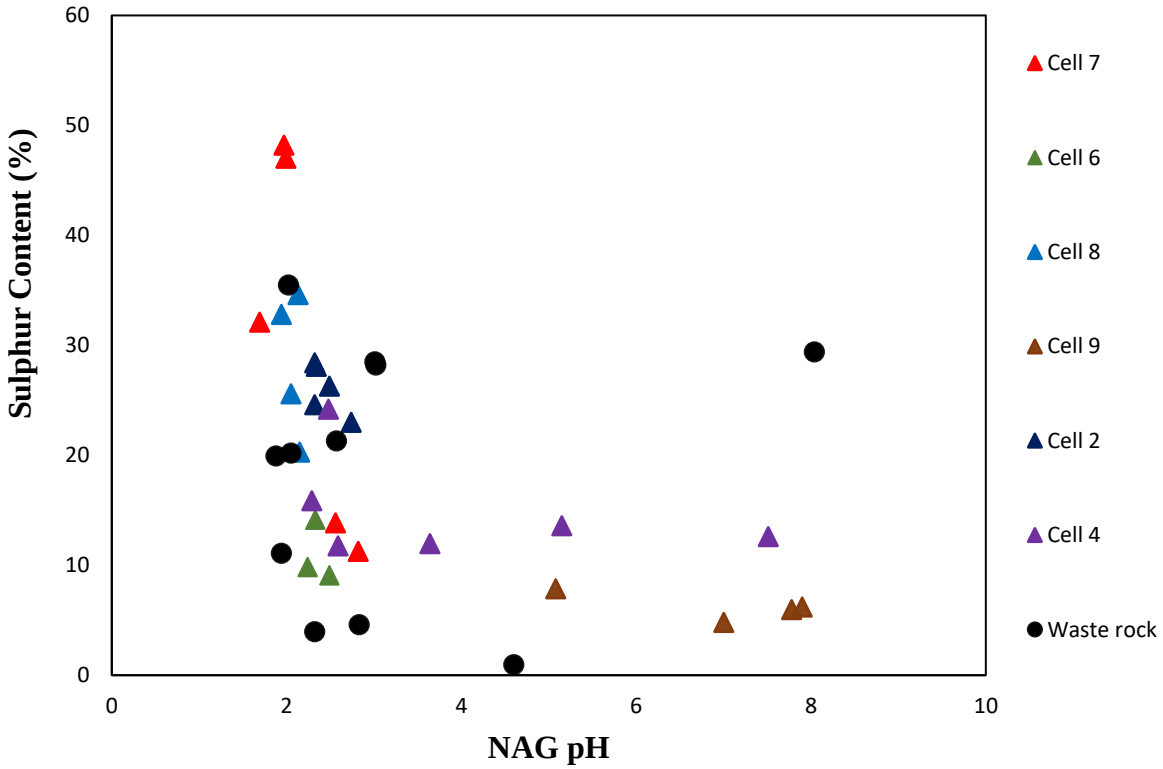

Figure 34: Sulphur content (%) vs NAG pH

Having obtained information on the general paste and NAG pH value range of the Thalanga waste, a downhole plot of S%, Fe%, paste pH, NAG pH, and NAG capacity was made to examine the variation of NAG capacity and pH across depths within cell and between cells. The values along drill holes were used to deduce variations at depth and across the span of the tailings dam. In almost all cells, the S% and Fe% are approximately in a 1:1 ratio within each hole but differ from cell to cell. The distribution of S% and Fe% down the hole does not follow any regular pattern that could be attributed to the remobilisation of minerals or leachates in situ. For instance, a statement cannot be made that acidity or pyrite content increases downhole or otherwise. The tailings near the surface have not experienced significant oxidation possibly due to the cover.

The percentages of S and Fe within each cell are mostly related to their respective NAG pH and NAG capacity. Cells 2 and 6 have appreciably high S and Fe content but not a very high NAG capacity compared to cells 7 and 8. Firstly, this could be due to the presence of some readily neutralising carbonate or silicate minerals and secondly, the presence of numerous agglomerates that hinder pyrite reaction with the hydrogen peroxide. There is a variation in NAG pH and net acidity across the depth of each cell (Figure 35). This indicates that the deposition episodes of tailings in each cell may have come from similar ore deposits but with

variable grades or concentrations of sulphide minerals like pyrite and pyrrhotite at different depths.

By reconstructing each deposit's architecture in terms of grade with reference to the sulphide concentration in the tailings, it can be inferred that all cells were filled with tailings of ore that increased in grade at depth in situ. Consequently, the concentration of S% and Fe% at the surface of the tailing storage is high because oxides of the ore were processed first and stored at the bottom of the cell. However, the data from cell 6, as presented in Figure 35, shows an exception. The tailings at the surface of cell 6 have lower S and Fe content compared to the bottom of the cell.

Cell	S%	Fe%	Paste pH	NAG pH	NAG Capacity
2	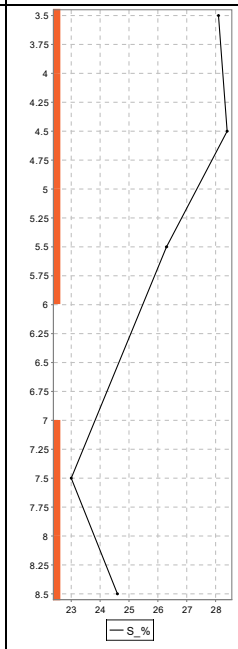 S_%	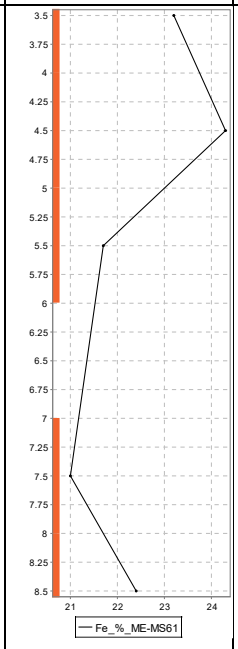 Fe_%_ME-MS61	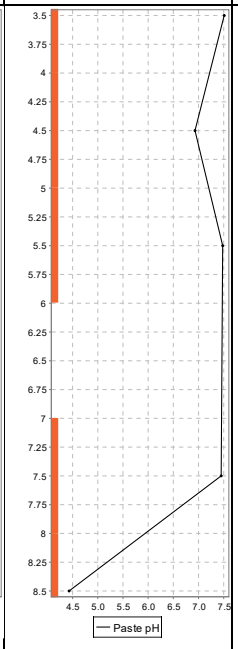 Paste pH	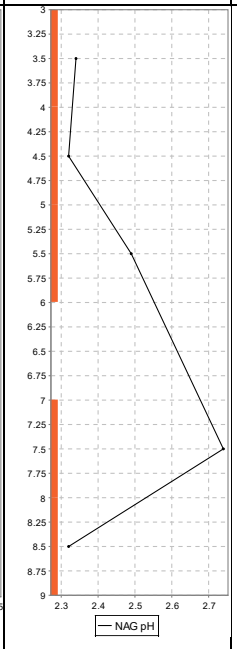 NAG pH	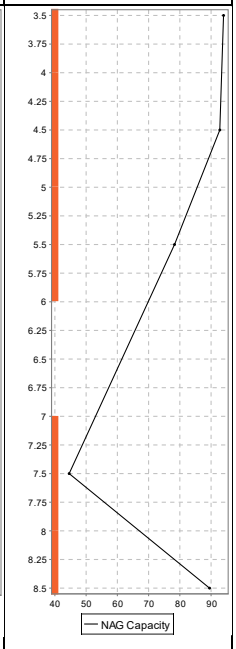 NAG Capacity
6	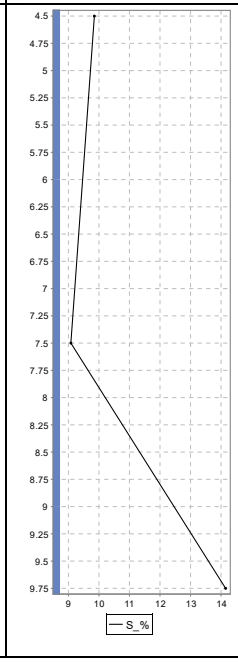 S_%	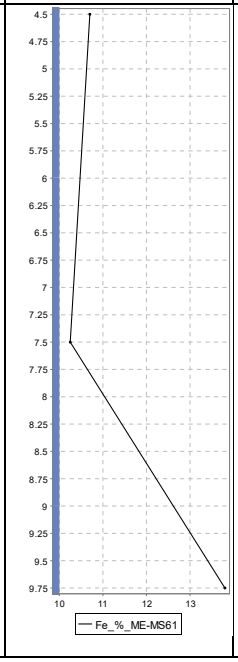 Fe_%_ME-MS61	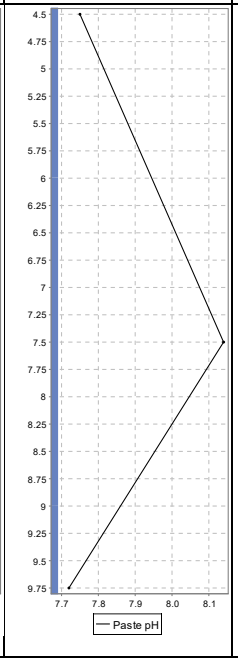 Paste pH	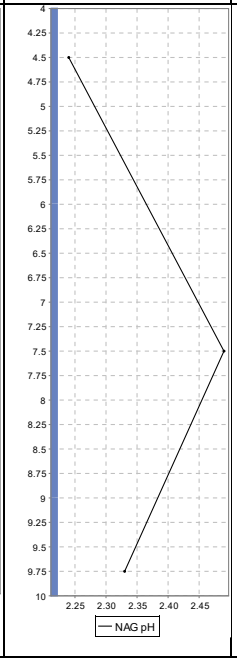 NAG pH	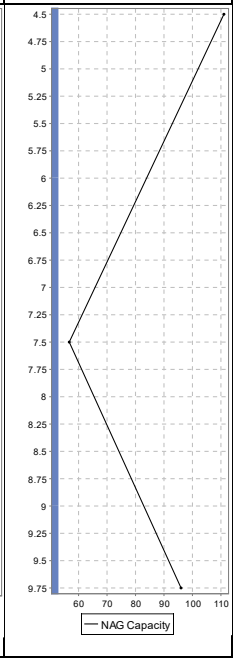 NAG Capacity

7	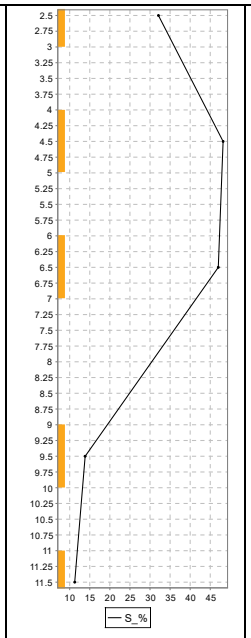 S_%	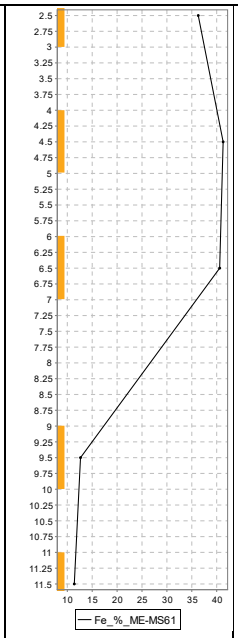 Fe_%_ME-MS61	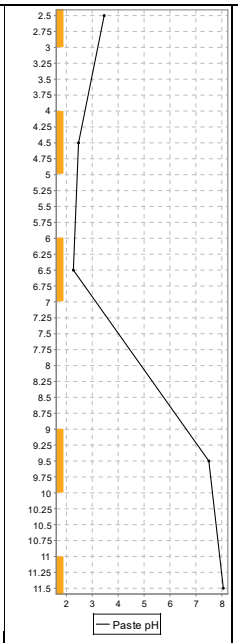 Paste pH	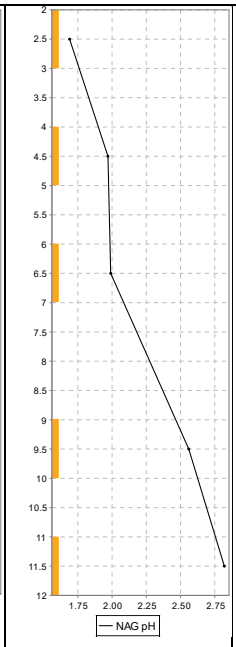 NAG pH	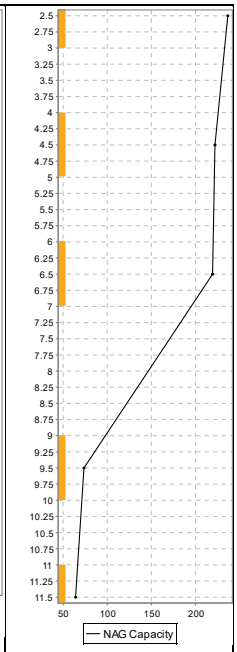 NAG Capacity
8	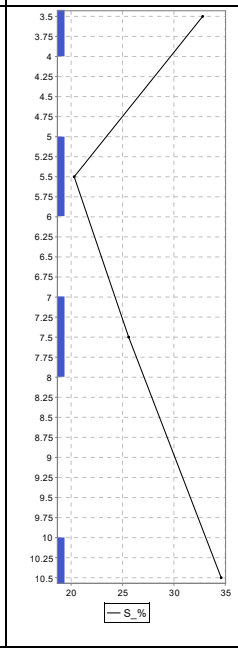 S_%	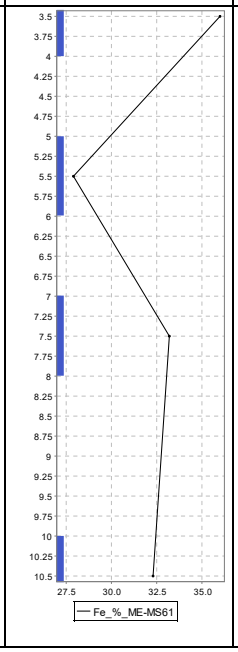 Fe_%_ME-MS61	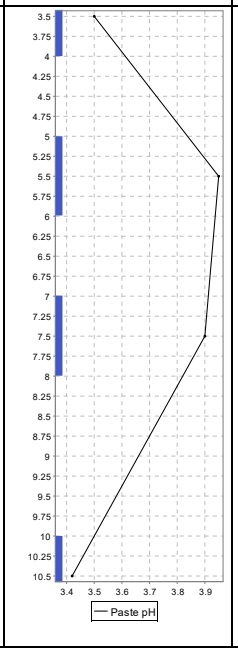 Paste pH	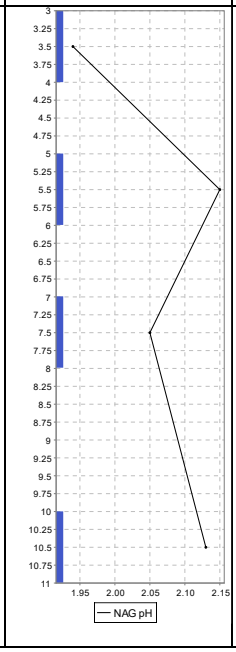 NAG pH	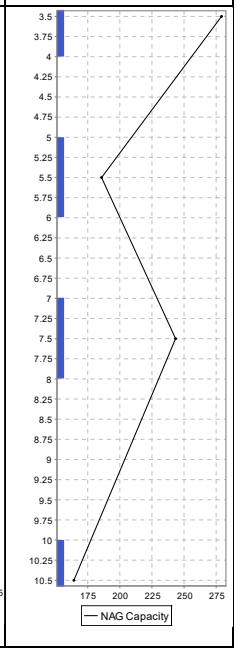 NAG Capacity

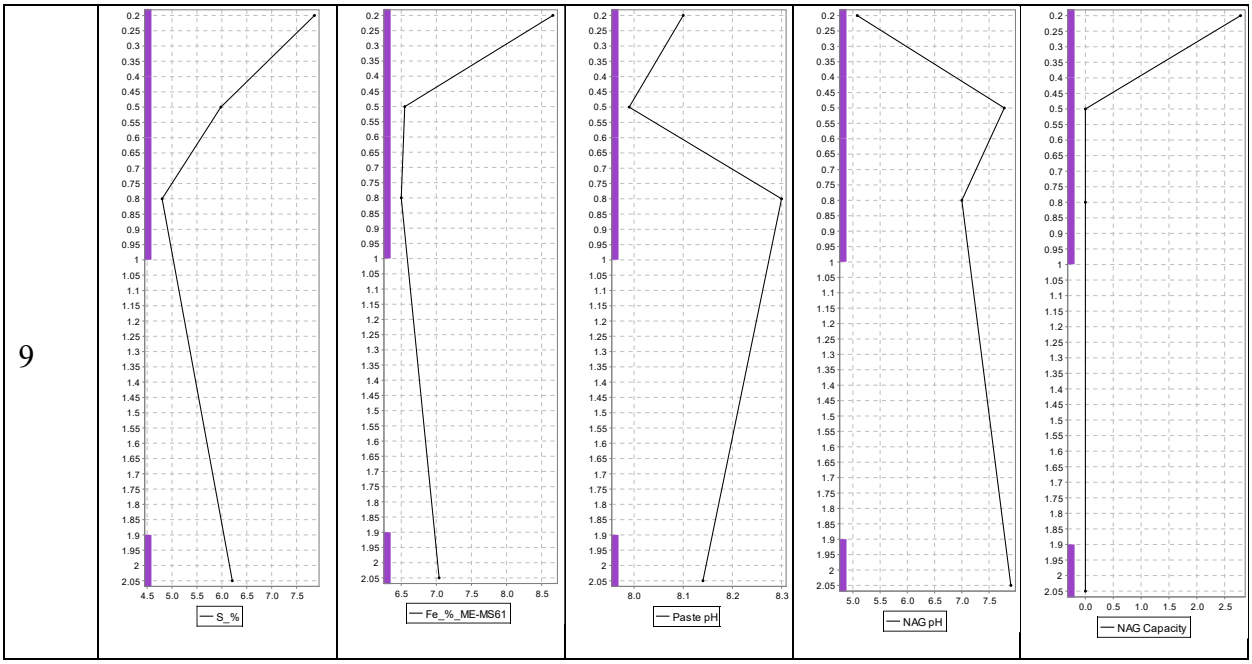

Figure 35: Downhole plot of NAG results of the tailings using one drill hole data from each cell

4.2.4 Classification of Acid Generation Potential

Two standard geoenvironmental classification schemes were used to identify non-acid forming (NAF) and acid forming (AF) samples: Weber, et al., (2006) and the AMIRA Project P387A. The results of paste pH were plotted against NAG pH following Weber et al. (2006) to classify the samples of each cell into NAF, AF, and PAF, as shown in Figure 36.

The results indicate that samples with paste pH > 6 and NAG pH < 4 are potentially acid forming with a lag time or delay in acid generation upon contact with oxygen. Most of the samples in this category are from cells containing Thalanga tailings. Samples within the NAF category is non-acid generating upon contact with oxygen and water; this occurs when both paste and NAG pH values are above 6 and 4.5, respectively. Since NAG results do not explicitly determine the acid-neutralizing capacity of samples, NAF in most cases should not be considered completely neutral. These are mostly samples from cell 9 and waste rock dumps.

Samples classified as extremely acid forming (EAF) have low paste pH and low NAG pH and are immediately acid generating upon contact with water and oxygen, allowing no time for proper management and mitigation measures once they have started. Some waste rock and tailings from cells 7 and 8 (processed ore from Highway Reward deep) fall into this category. Samples with very low paste pH but high NAG pH, or low NAG pH and low NAG capacity are classified as uncertain and require thorough screening to understand their acid-generating characteristics. Ideally, a low NAG pH sample should correspond to a very high NAG capacity,

and vice-versa. There was only one sample (a waste rock sample) in this category, which is completely different from all other samples in both physical appearance and mineralogy. It has no neutralizing potential with very low sulphur content, a sign of an already oxidized material.

In general, the observations made during the NAG experimental test (see Figure 57 in Appendix A) agree with the classification. Samples that immediately and violently reacted with H_2O_2 but were quiet during the heating stage ended up having very low NAG pH and were classified as EAF. Samples that mildly reacted with H_2O_2 and gradually increased in effervescence and boiling during the reaction and heating stages had pH values categorized into AF and PAF. Samples that showed no reaction with H_2O_2, no effervescence, bubbling, or boiling during the reaction stage but became violent during the heating stage, generating large bubbles and boiling, had pH values around 6-8.

The heating stage of the test can then be said to catalyse the release of neutralizing minerals if any are present, while the reaction stage primarily oxidizes and releases acid from pyrites. This was confirmed by Parbhakar-Fox,et al., (2018).

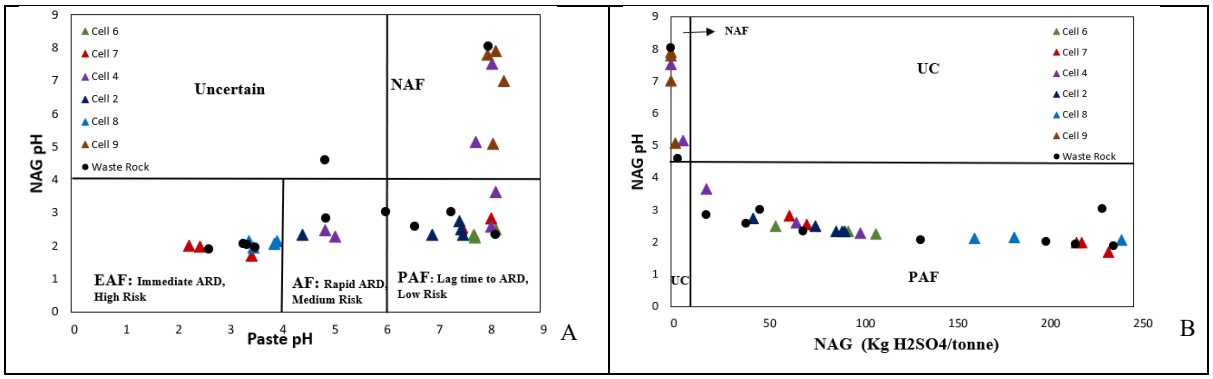

Figure 36: ABA static test classification scheme for potentially acid Generation. (A) NAG pH against paste pH after (Weber, et al., 2006); (B) NAG pH against NAG capacity after (Smart, et al., 2002); UC-uncertain, PAF- Potentially Acid Forming, AF- Acid Forming, EAF- Extremely Acid Forming, NAF- Non-Acid Forming

The second classification scheme (Figure 36B), based on Smart et al. (2002), is a modified version that plots NAG pH against NAG capacity in kg H_2SO_4/t. This plot serves as a confirmation of the classification by Weber et al. (2006), as both schemes are similar. Originally, Smart et al. (2002) plotted NAG pH against net acid producing potential (NAPP), for classification. Since this project focused on experimentally determined Net Acid Generation (NAG) capacity rather than calculated Net Acid Producing Potential (NAPP), it was appropriate to modify the plot accordingly.

According to the AMIRA Project P387A, the threshold for acid-generating samples by the static NAG test is 5 kg H_2SO_4/t. Below this NAG capacity, a sample is considered non-acid generating. However, before reaching a conclusion, the test must be calibrated to the specific site, and proper mineralogical characterization must support the assertion of non-acid generation below 5 kg H_2SO_4/t. Here, the classification is divided into PAF, NAF, and UC.

From Figure 36B, approximately 70% of Thalanga waste samples analysed are potentially acid generating. Samples that recorded high NAG capacity (>150 kg H_2SO_4/t) and low pH (1-2.5) are the same samples classified as high-risk AMD materials in the Weber et al. (2006) scheme. The NAF and UC samples in both classification schemes are consistent. Samples with NAG capacity above 20 kg H_2SO_4/t are considered highly acid generating and require proper and immediate management and mitigation plans. Samples with up to 9 kg H_2SO_4/t NAG capacity are considered to contain low acidic salt, whereas samples with up to 30 kg H_2SO_4/t are considered to have high acidic salt (Weber et al., 2006).

Unlike NAPP, which can have negative values indicating a net neutralizing capacity of the sample, NAG measures up to zero, denoting non-acid generating.

4.2.5 Sequential NAG Test

To investigate the degree of oxidation of pyrite by the modified NAG method, the sequential NAG test was performed on two samples from the tailings cell 8 and 4: THA-T175 from cell 8 (high NAG capacity with high S and Fe content), THA-T061 from cell 4 (low NAG capacity with high S and Fe content. The objective was to compare the degree of oxidation of pyrite using these two methods by comparing their NAG capacity to the Sobek NAPP value as well as comparing the mineralogy between their original samples, residue of the multi-addition NAG method, and residue of the sequential NAG method (see Table 6 and Table 7 in Appendix A for data). This comparison was prompted by observing that the estimated MPA and the NAG capacity of the samples had a difference that cannot be realistically balanced by the limited neutralizing minerals in the mine waste. The residue from the final stage of the sequential test, residue of the modified NAG test, and the original sample were studied under the microscope and SEM to understand the mineralogical changes before and after the tests.

Table 2: Comparison of Multi-Addition NAG and Sequential NAG results

Sample	NAG of multi-addition test (kg H_2SO_4/t)	Max. Producing Acidity (MPA) (kg H_2SO_4/t)	Unrealistic Neutralising Capacity (kg H_2SO_4/t)	NAG of Sequential test (kg H_2SO_4/t)	Actual Experimentally determined Neutralising Capacity
THA-T175	279.18	1025	745.82	782.47	242.53
THA-T061	6.68	425	418.32	0	425

Table 2 above indicates that only 50.8% and 100% of pyrite in samples THA-T175 and THA-T061, respectively, was oxidized by the multi-addition method, assuming the sequential method oxidizes all pyrites. From the table, the sequential test indicates that the actual neutralising capacity of the sample THA-T175 is 242.53 kg CO_3 /t and was 50% less than the MPA. The neutralising capacity for THA-T061 was 425 kg CO_3 /t and was equal to the MPA even though all neutralising minerals did not react during the multi-addition stage. This is why the NAG capacity was 6 kg H_2SO_4/t instead of zero. The MPA was calculated using the S% from ICP-MS assuming all sulphur is coming from pyrite as used in (Chopard, Benzaazoua, Bouzahzah, & Plante, 2017). The ideal method should have been to use the MLA data (i.e. minerals; pyrite and pyrrhotite), but in this case ICP-MS results was more reliable. It is assumed that the comparison does not include sulphate-sulphur in the estimation of MPA. SEM and optical microscopy were used to study the residues of each test to confirm the dissolution of pyrite in each method.

4.3 Mineralogical Characteristics

4.3.1 Mineral Abundance

MLA analysis on bulk samples (n=12, 6-tailings, and 6-waste rock) indicated the presence of quartz, muscovite, pyrite, pyrrhotite, chalcopyrite, chlorite, Fe-oxyhydroxides, barite, sphalerite, galena, calcite, dolomite, gypsum and jarosite in both the tailings and waste rock. These minerals were categorized into iron-sulphides (pyrite and pyrrhotite), other sulphides (chalcopyrite, sphalerite, galena, etc.), carbonates, neutralizing silicates, other silicates, sulphates, and Fe-Ti-oxides (see Table 8 in Appendix A).

Figure 39 presents the MLA analysis of the six tailing samples, detailing the mineral weight percentages. The mineralogical characteristics of each sample are compared and related to their

respective geochemical and NAG results in other graphs shown in Figure 38 and Figure 38. The NAG capacity at pH 4.5 and 7.0 represents the acidity calculated when the NAG liquor was titrated to these pH levels. Titration to pH 4.5 accounts for the acidity due to Fe, Al and most of H^+. The additional acidity between pH 4.5 and pH 7 typically arises from soluble metals such as Cu and Zn from chalcopyrite and sphalerite, with corresponding release H^+ (Smart, et al., 2002).

All six samples exhibit significant S% and Fe% concentrations, with the highest values observed in samples from cells 1/7 and 8. Samples from cells 4 and 2, both containing Thalanga ore tailings, also show appreciable S% and Fe%. Sample THA-T061 from cell 4, despite its high S% and Fe%, resulting in a high Fe-sulphide mineral content, has a very low NAG capacity. This discrepancy can be explained by the mineralogy of the sample, which indicates significant neutralizing capacity from silicates and carbonates. In addition to the presence of significant neutralising silicates, most of the pyrite and pyrrhotite are trapped in agglomerates becoming inaccessible to hydrogen peroxide for oxidation within the time frame of the test. These samples were rich in only pyrite as the source of acidity with very low wt% pyrrhotite. The NAG capacity/acidity of the remaining samples correlates with their Fe-sulphide content and limited neutralizing silicates and carbonates, especially in cells 2, 7, and 8.

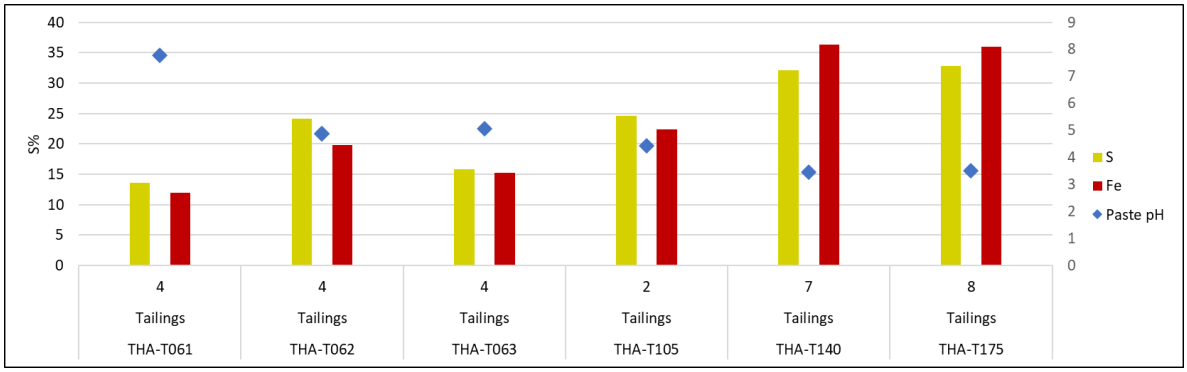

Figure 37: Geochemistry of selected tailings sample

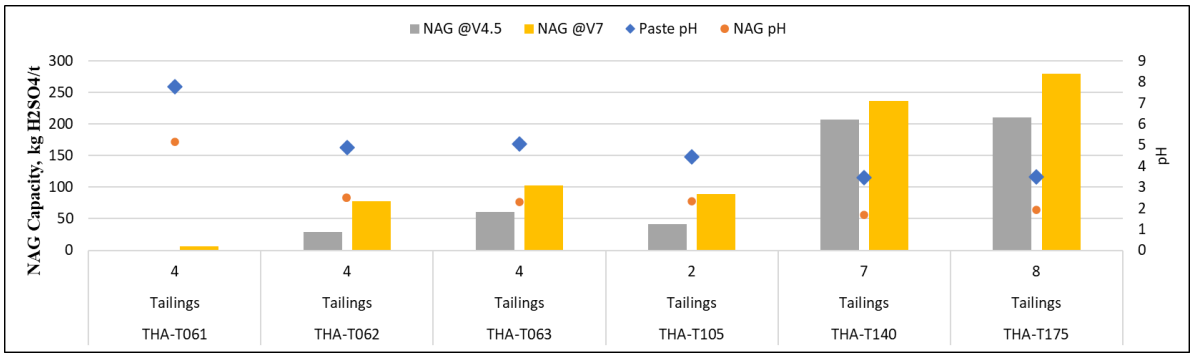

Figure 38: NAG results of the selected tailings sample

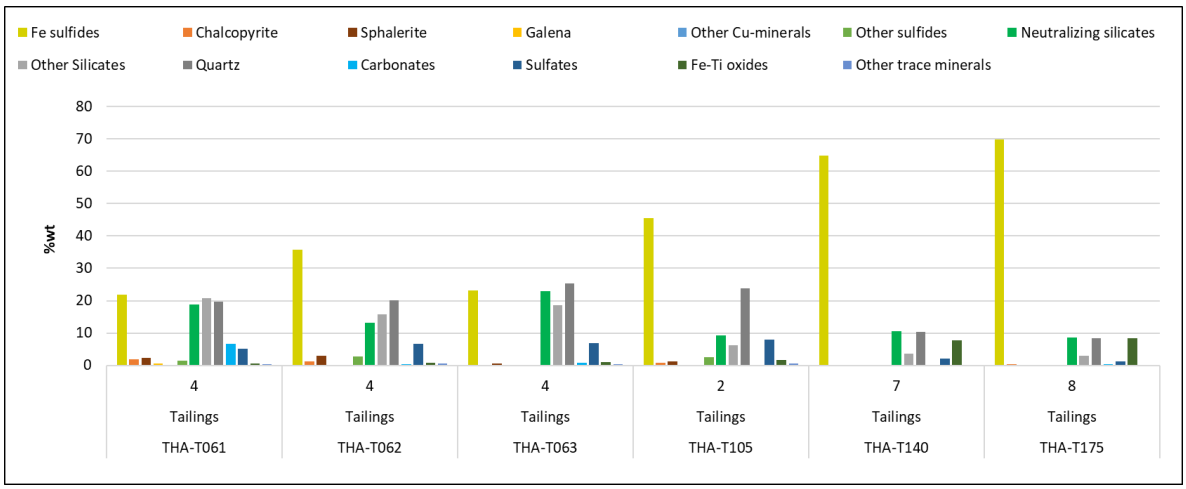

Figure 39: Mineralogy of selected tailings sample

Degree of Oxidation of Pyrite under 15% H_2O_2

Sequential NAG tests were performed on both samples. It took six NAG test stages to oxidize all the pyrite in THA-T175 for its pH to reach 7. in each stage, the residue from the previous stage was rinsed and used for the next stage. One stage sequential NAG test was enough to bring THA-T061 to a neutral pH. The mineral maps generated from analysis of the original sample and residues after the test are shown in Figure 41 and Figure 41.

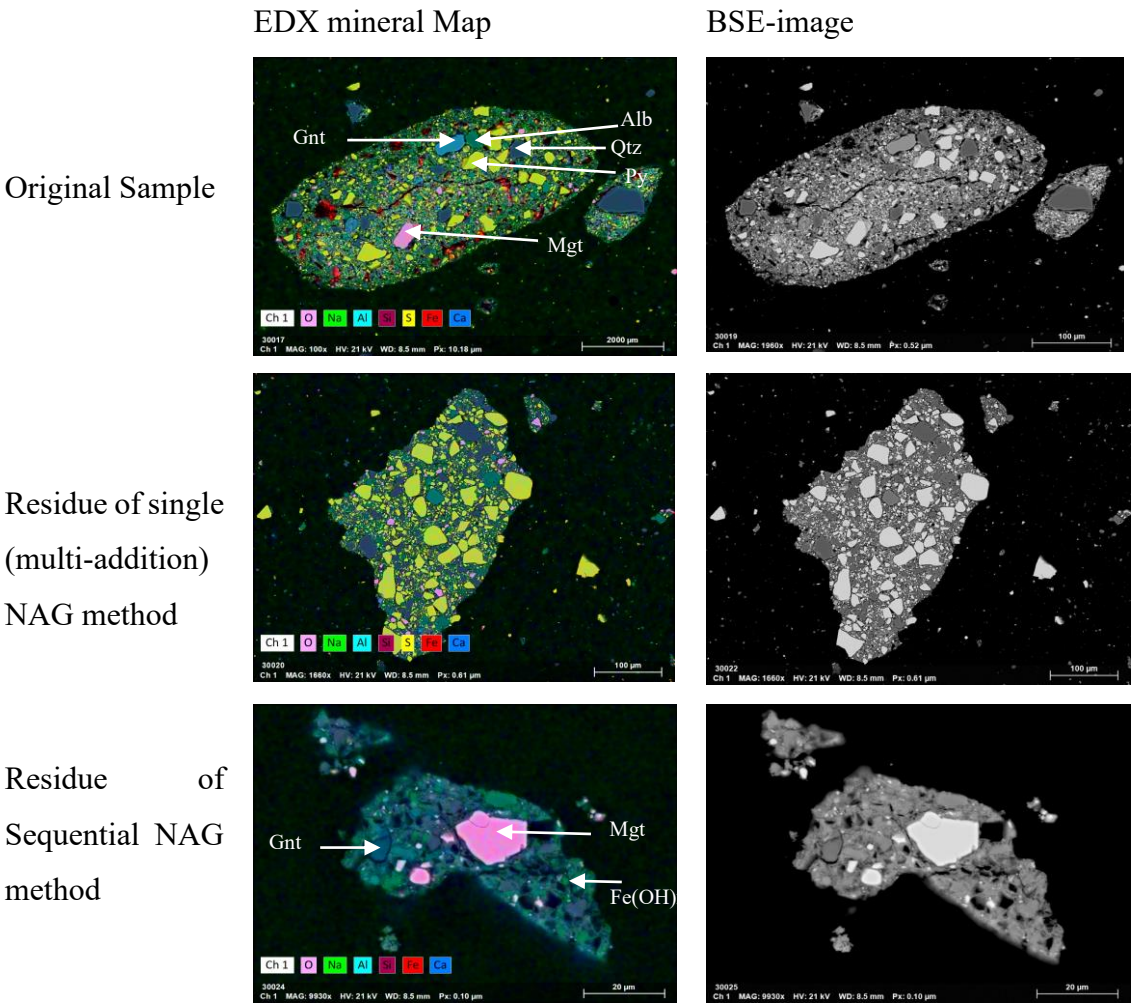

Figure 40: SEM analysis of THA-T175 to check degree of oxidation and leaching of pyrites. Py- pyrite, Gnt- garnet, Mgt- magnetite, Alb- albite, Qtz- quartz, Fe(OH)x – secondary iron-hydroxide.

In the case of THA-T 61 shown in Figure 41, even though there were appreciable neutralising silicates to justify the overall low single addition NAG capacity and zero sequential NAG capacity, unoxidized pyrite can be seen in the original sample, and residues of both single addition and sequential addition NAG test. This implies that, neutralising minerals were easily dissolved and leached faster than the pyrites. From the optical microscopy of the original sample, a lot of agglomerates can be seen which serves as potential hinderance to oxidation of pyrite. Hence the NAG capacity obtained in both single and sequential addition methods are not representative of the pyrite contained in the sample as indicated by MLA and optical microscopy.

Original Sample	Residue of Single Addition Nag Test	Residue of Sequential Addition Nag test
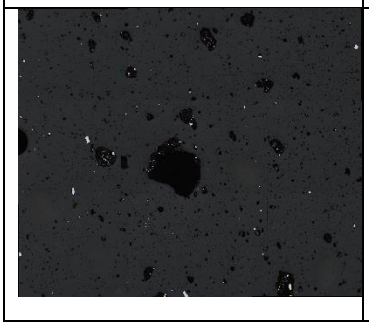		

Figure 41: Optical microscopy analysis of THA-T061 to check degree of oxidation and leaching of pyrites by the methods

The MLA analysis of the six waste rock samples revealed some samples with uncertain characteristics, such as THA-11 and THA-29. THA-11 fell within the uncertain zone of the NAG classification scheme. This (THA-11) sample appeared red in colour physically and has very low S% and Fe% geochemically but exhibited a circum-neutral paste pH. Mineralogically, it is predominantly composed of quartz and Fe-oxyhydroxides. The few grains of pyrite present had the tendency of giving it that circum-neutral pH because there are no neutralising minerals. Perhaps, this is an already oxidized material.

THA-29, on the other hand, has high S% and Fe% content, yet shows neutral paste and NAG pH values (pH=8), and zero NAG capacity. Sample THA-02 required a significant amount of NaOH after reaching pH 4.5 during titration. Unlike other samples that produced a reddish-brown precipitate at this pH, THA-02 produced a white precipitate. The white precipitate formation can be attributed to zinc, which precipitates as white when it comes out of solution. Coincidentally, MLA analysis indicated that THA-02 contained approximately 45% sphalerite.

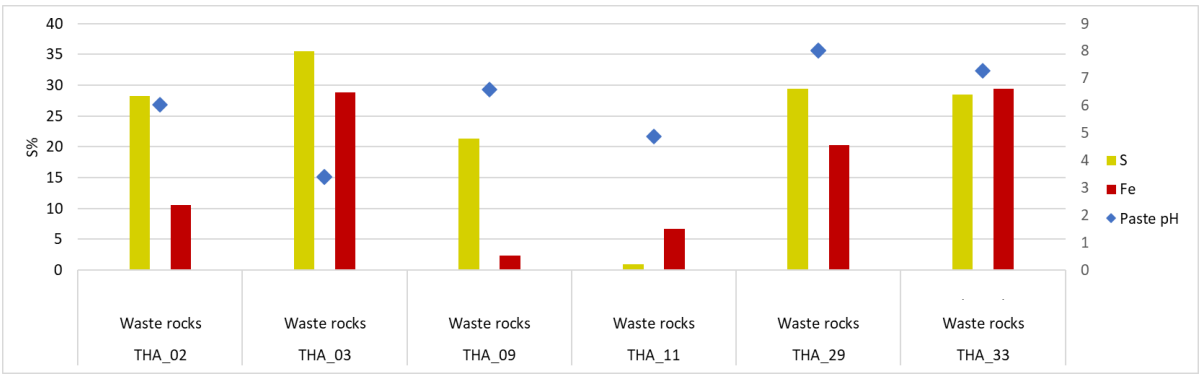

Figure 42: Geochemistry of Selected waste rock samples

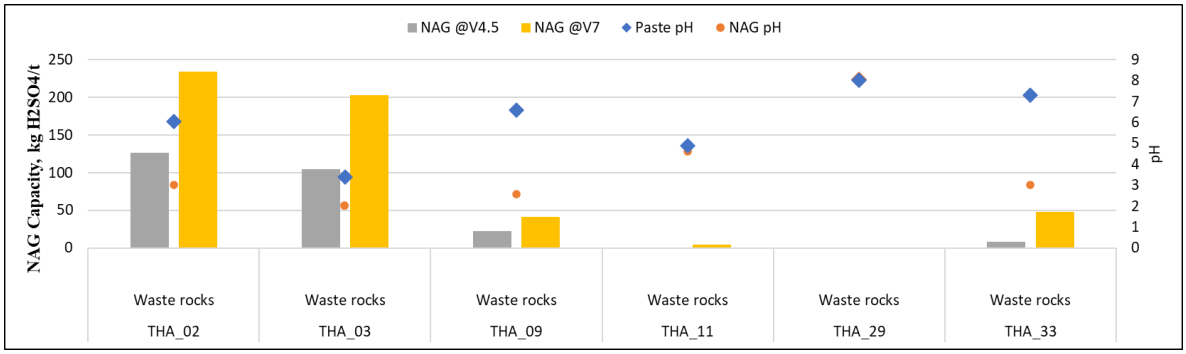

Figure 43: NAG results of selected waste rock samples

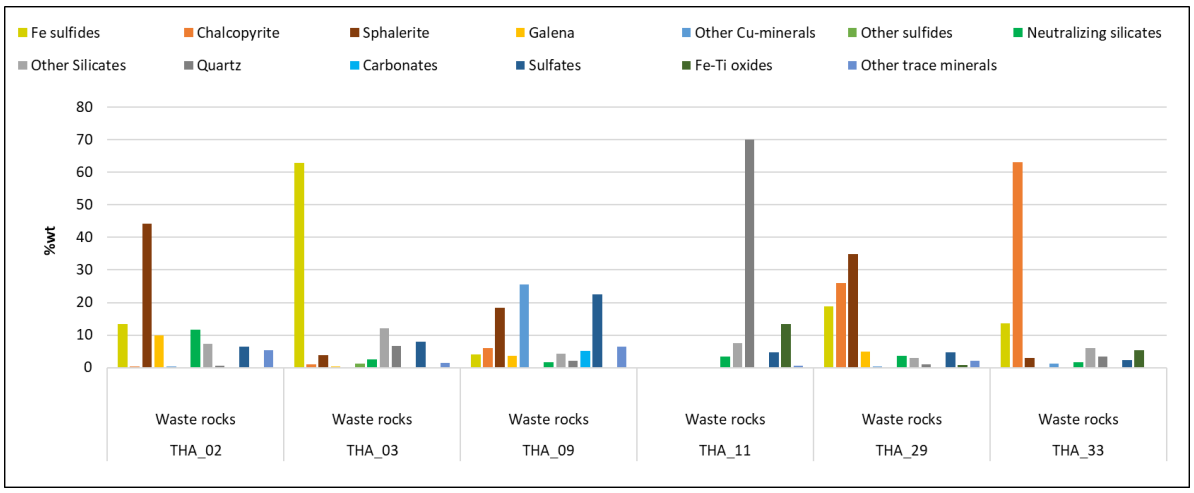

Figure 44: Mineralogy of selected waste rock samples

In general, samples THA-02, THA-03, and THA-33 shows elevated percentages of sphalerite, pyrite, and chalcopyrite, respectively. This is unusual for waste rock unless there was a misclassification during the mining operation, or a high cut-off grade was applied to the ore or a complex interlocking mineral texture that made processing such material uneconomic at the time of operation. (SLR Consulting Pty Ltd, 2020) records the average grade of Thalanga from 1989 to 1998 as 8.52% zinc, 2.65% lead, and 1.62% copper whiles (Gregory, Hartley, & Wills, 1990) reports 8% zinc equivalent cut-off grade at 2.2% copper, 3.9% lead, 12.3% zinc, 99g/t silver and 0.6g/t gold calculated from diamond drilled core during primary mineral resource (indicated and measured). Further mineralogical analysis on samples THA-11, THA-02, and THA-29 (Figure 45) indicates the following:

Sample THA-11 has circum-neutral pH despite low S% and Fe% and was classified as uncertain by classification schemes. This is because the sample contains mainly quartz within a matrix of iron-oxyhydroxides and barium silicates. With no neutralising minerals the few accessible pyrite grains can give the sample a circum-neutral pH even at very low Fe% and S%. The sample is full of Fe-hydroxides, hence its red colour.

In sample THA-02, pyrite grains are trapped in agglomerates (Figure 45) and may have prevented effective interaction between pyrite and hydrogen-peroxide. However, sphalerite is abundantly present in both liberated and agglomerated forms. Beyond pH 6, Zn^{2+} released into solution forms a white precipitate, releasing H^{+}, which combines with SO_4 to form H_2SO_4 and consumes more NaOH to reach neutral pH. This accounted for the high NAG capacity of the sample.

The mineralogy of sample THA-29 shows appreciable amounts of pyrite, chalcopyrite, and sphalerite. According to Chopard, et al., (2017), chalcopyrite, galena, and sphalerite contribute to acid generation. The zero NAG of this sample can be attributed to numerous agglomerations trapping the sulphides within a matrix of silicates. Once the sulphides at the periphery of agglomerates are oxidized, Fe-oxyhydroxides precipitate around the entire agglomerate, preventing further oxidation of inner sulphides. This can equally relate to free sulphides in the presence of limited oxidation. Precipitates of iron hydroxides from the neutralisation reaction can coat and prevent these minerals from further oxidation. The SEM images are shown in Figure 45.

Sample	EDX Mineral map	BSE- image
THA-11	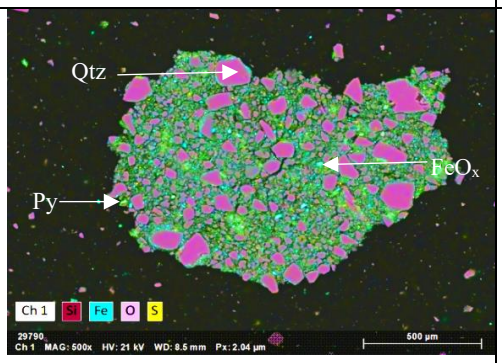	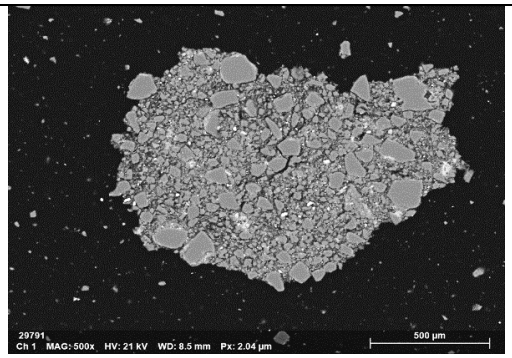
THA-29	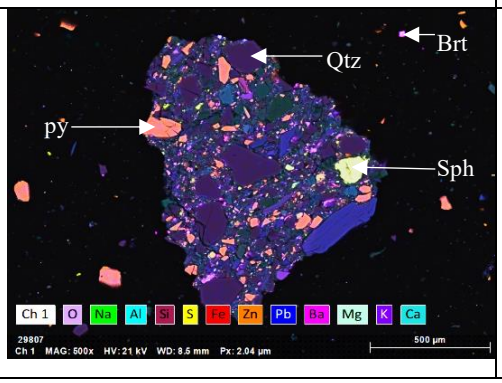	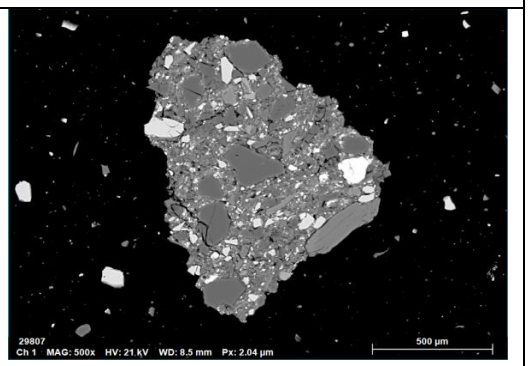

Figure 45: SEM mineral analysis of sample- (THA-11), sample classified as uncertain, (THA-02), sample with high consumption of NaOH and formation of white precipitate during titration, (THA-29); High S% and Fe% but zero NAG. Py-pyrite, sph-sphalerite, cpy-chalcopyrite, Gn- galena, Qtz- Quartz, Brt- Barite.

4.4 Critical Element Mineralogy

The mineralogy of the critical elements was studied using SEM-EDS to understand their respective phases and associations. The critical elements, however, are mostly present at concentrations below the detection limit of EDS. In some cases, As, Bi and Sb could be detected in micro-inclusions in the sulphides. Tellurium and selenium were difficult to identify.

4.4.1 Bismuth

The analysis of sample THA-T175 for Se indicated the presence of Bi in various forms. Only one Se-rich phase is in association with lead was identified. Multiple Bi-rich phases were found, including native Bismuth, Bismuth in pyrite, Bismuth in galena, and Bismuth associated with lead, as shown in Figure 46. About 26 bright phase grains were analysed for bismuth but 11 grains contained bismuth. One grain of native bismuth was found. Barite and Barium silicate were common in the samples. See (Table 9 Appendix B) for spectrum of bismuth grains and other mineral grains.

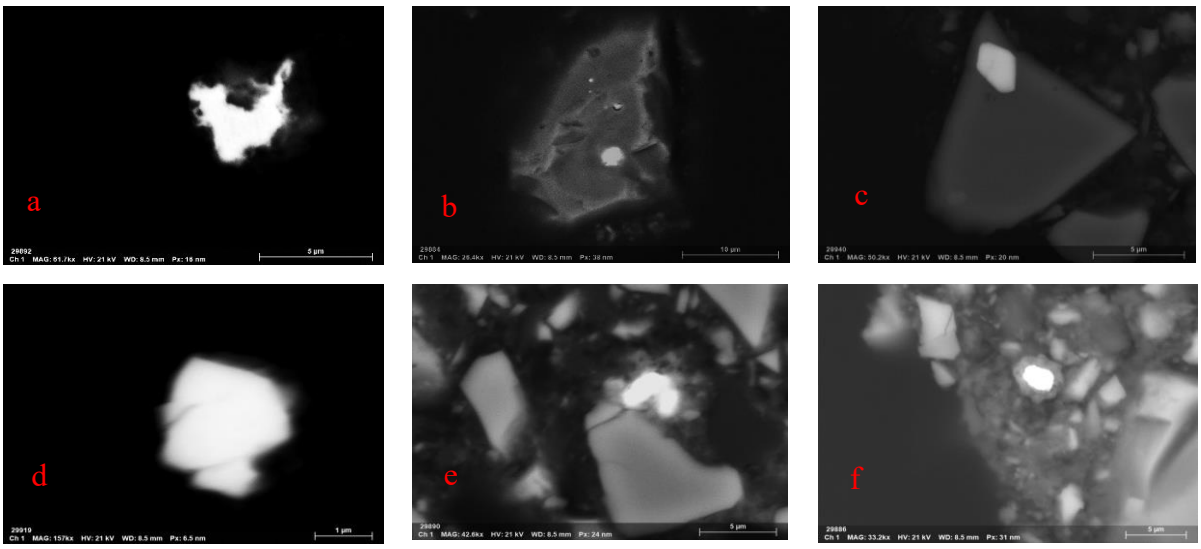

Figure 46: Bright Phase search for Bi. a) Native Bismuth b) Bismuth associated with lead and copper as inclusion in pyrite c) Bismuth associated with copper and sulphur, d) Bismuth phosphate e) Bi in association with lead and iron f) Bi in solution with Pb, Sb, Ag, Fe

4.4.2 Arsenic and Antimony

Antimony was identified in tetrahedrite and sometimes in a complex association with copper, zinc, and arsenic. According to the stoichiometries (see Table 10 Appendix B), Figure 48 (A) shows tetrahedrite grain with its spectrum giving information on the elemental combination of the proposed mineral. Figure 48(B) is a typical example of tetrahedrite-tennantite series with its spectrum having arsenic and antimony undergoing crystal lattice substitution or co-precipitation during hydrothermal fluid transport (Klein & Dutrow, (2008) and Habashi,

(2001)). Arsenic on the other hand was found in arsenopyrite Figure 47 and in the tetrahedrite-tennantite series with antimony, copper, and iron (see Table 10 Appendix B). Over 2,100 bright phase minerals were searched including pyrite and minerals brighter than pyrite. Six grains were analysed for antimony and arsenic in the form of tetrahedrite and arsenopyrite respectively. Over 40 grains of tetrahedrite-tennantite series were identified. Five grains of scheelite and cassiterite were identified and shown in (Figure 62)

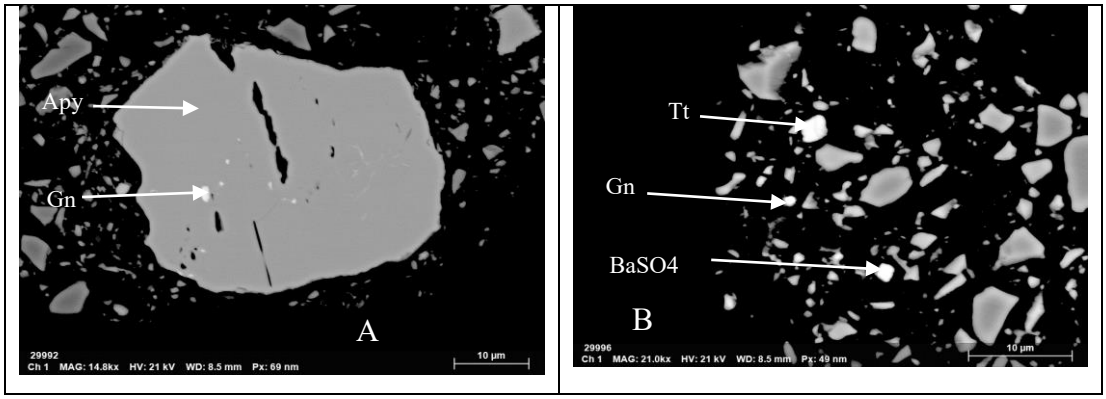

Figure 47: Arsenopyrite with galena inclusion B) Tetrahedrite-tennantite series. Apy- arsenopyrite, Gn- galena, Tt- tetrahedrite-tennantite grain, BaSO4- Barium sulphate.

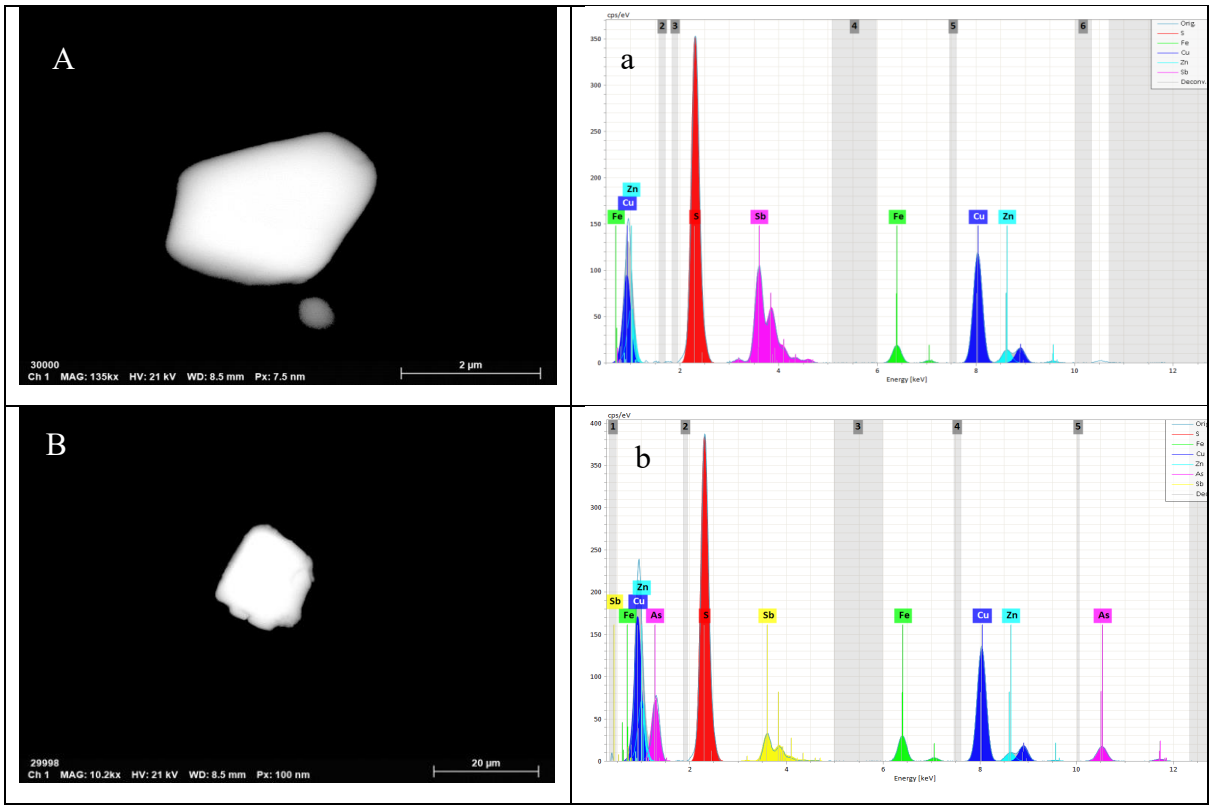

Figure 48: A) and a) -Tetrahedrite grain and spectrum; B) and b) Complex phase of Sb and As (Sample THA-03 (waste rock))

4.4. Selenium and Tellurium

One grain of Selenium was identified Figure 49. However, it occurs in association with lead. The only exclusive Lead-Selenium mineral is Clausthalite but the stoichiometry (90.39% Pb, 2.65% Se, 6.97% S) in this case did not relate to Clausthalite (PbSe- 72.41% Pb and 27.59% Se). Nonetheless, it can also be sulphate of selenium (e.g. selenide). Tellurium could not be identified in all the specimens analysed because they may exist as trace elements in other abundant minerals or as trace elements in another abundant bright phase which can overshadow it even though ICP-MS detected tellurium.

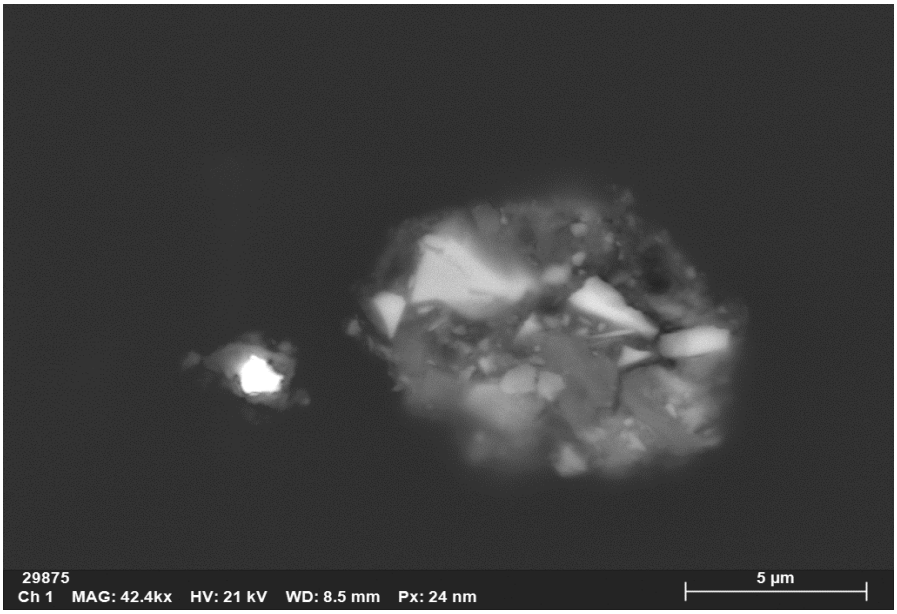

Figure 49: Selenium associated with galena

4.4.3 Element Deportment

For a robust element deportment to be carried out, the number of grains upon which the analysis is performed should be of appreciably high to minimize errors in average stoichiometry of each phase. For this project the number of selenium, antimony, and arsenic grains identified were very few to allow elemental deportment. The difference between the stoichiometry of two grains if the same mineral was too wide in most cases to be able to average and match it to any known mineral in the mineral database (4700+ minerals from minerals.com). It becomes difficult to conclusively assign a mineral name to a phase. However, few minerals which were close to the stoichiometry of bismuth and with more than 50% of like what was identified include Ximengite, Bismite, Sillenite, Arsenobismite, Beyerite, Neyite, Muckeite, etc. (See Table 12, Table 13, and Appendix B). The deportment of bismuth was attempted. About 19 Bi-rich phases in total were analysed. Eight different combinations of elements to form bismuth

mineral was identified but could not be classified as distinct mineral phase. To do element to mineral conversion, the weight percentage of each supposed mineral phase is calculated manually using equ.8 was used

$$wt\%_{mineral\ phase} = \frac{wt\%_{element\ in\ sample}}{wt\%_{element\ in\ mineral\ phase}} \times 100 \qquad \textit{Equation 8}$$

Table 3: ICP-MS for sample THA-T175 Bi deportment

Element	Bi	Pb	Cu	Fe	S	Ag	Sb	O	P
ICP-MS (%)	0.0274%	0.0288%	0.1785%	36%	32.80%	0.000404%	0.00118%	-	0.009%

Table 4: Stoichiometry of elements in Bi mineral Phase 1

	Element	S%	Fe%	Cu%	Pb%	Bi%	Sum %
Phase 1	Grain 1	30.13	26.97	1.32	19.18	22.4	100
	Grain 2	25.36	16.02	1.4	28.4	28.83	100.01

Table 5: Stoichiometry of elements in Bi mineral Phase 2

	Element	S%	Fe%	Pb%	Bi%	sum
Phase 2	Grain 1	9.12	16.45	10.42	64.01	100
	Grain 2	25.75	18.1	42.22	13.92	99.99
	Grain 3	40.04	52.74	4.22	3	100
	Grain 4	8.06	15.02	36.53	40.39	100

To be able to do proper element to mineral conversion and proceed to element deportment, at least there must be one element that is not shared between phases (i.e. a full rank composition table that is possible to invert). Almost all key elements relevant for element to mineral conversion in this project are shared between two or more phases which makes it impossible to proceed to element deportment.

5.1 Environmental Liability of Thalanga Mine Waste

Pyrite and pyrrhotite are the main sulphide minerals driving acid generation in Thalanga tailings and waste rock. Significant contribution comes from the pyrite as pyrrhotite is in very low abundance compared to pyrite (See Table 8 Appendix A). Pyrite in the tailings is mostly liberated (Figure 19) with abundant free surface areas available for oxidation across the cells. The worst-case scenario method used to assess the AMD was applied across the span of the tailings by plotting a compositional variation map using Fe and S concentrations to determine which part to focus on (Figure 50). Figure 51 shows the selected holes on tailings dam and sample points for waste rock used for the study.

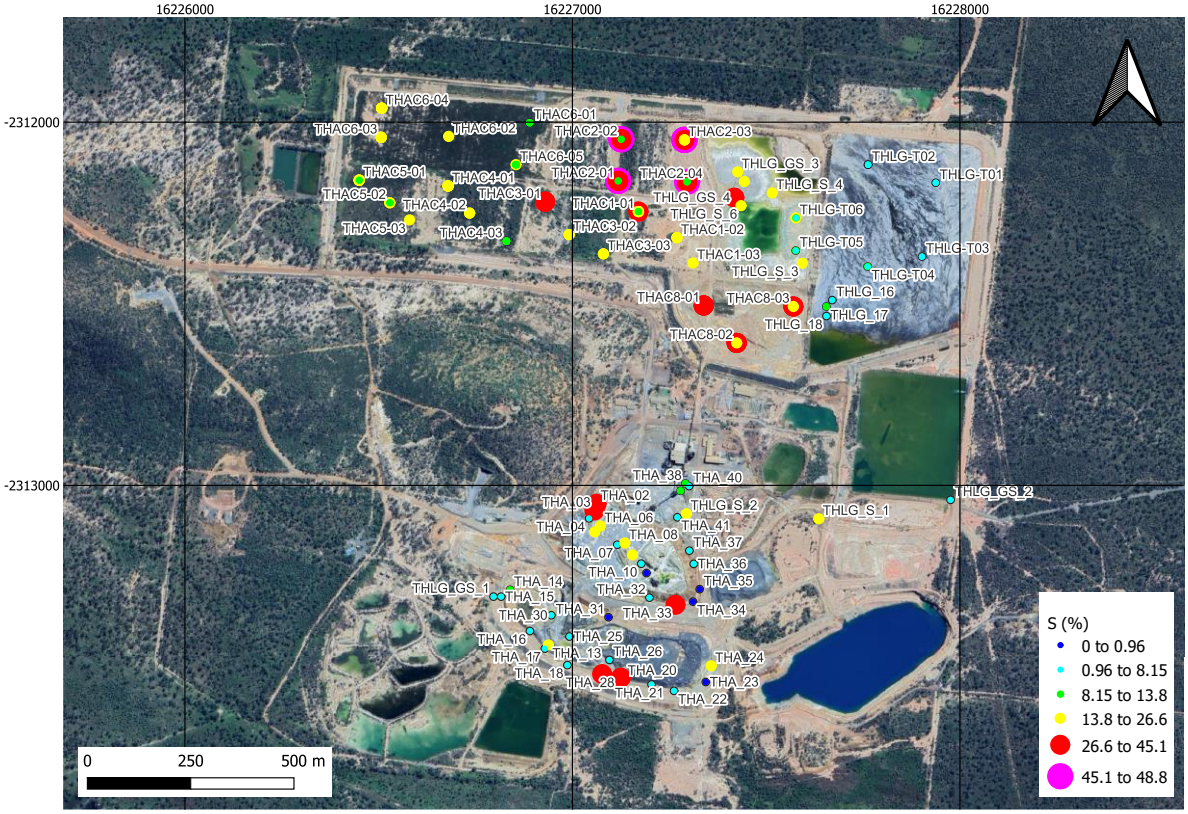

Figure 50: Compositional map for entire drill holes and sample points

The cover system of the old tailings is good as it has impeded oxidation of pyrite even to the upper part of the tailings. The unoxidized tailings pose a threat to AMD unless the cover system is continually maintained to deprive the high pyrite concentration of oxygen. Samples from both upper and lower layers of the tailings gave acidic pH. Grain morphology and textures analysed from the MLA data shows elevated pyrite concentration e.g. THAC-02 (cell 7) =62.24 wt.% THAC08 (cell 8)= 67.74 wt.% (see Table 8 Appendix A). The concentration and

liberation of pyrite grains in the tailings increases amenability to oxidation and hence the acid generating potential. Acid neutralising minerals exist as silicates and carbonates. Although there are more neutralising silicates than carbonates, they are still not enough to neutralize the generated acid from pyrite oxidation. This is evident in the samples from cell four and two which represent materials from Thalanga site (Figure 39). In these samples, neutralising silicates are in the form of chlorite, plagioclase, K-feldspar in total concentrations of 18.91wt%, 13.11wt%, 22.88wt% (see Table 8 Appendix A)

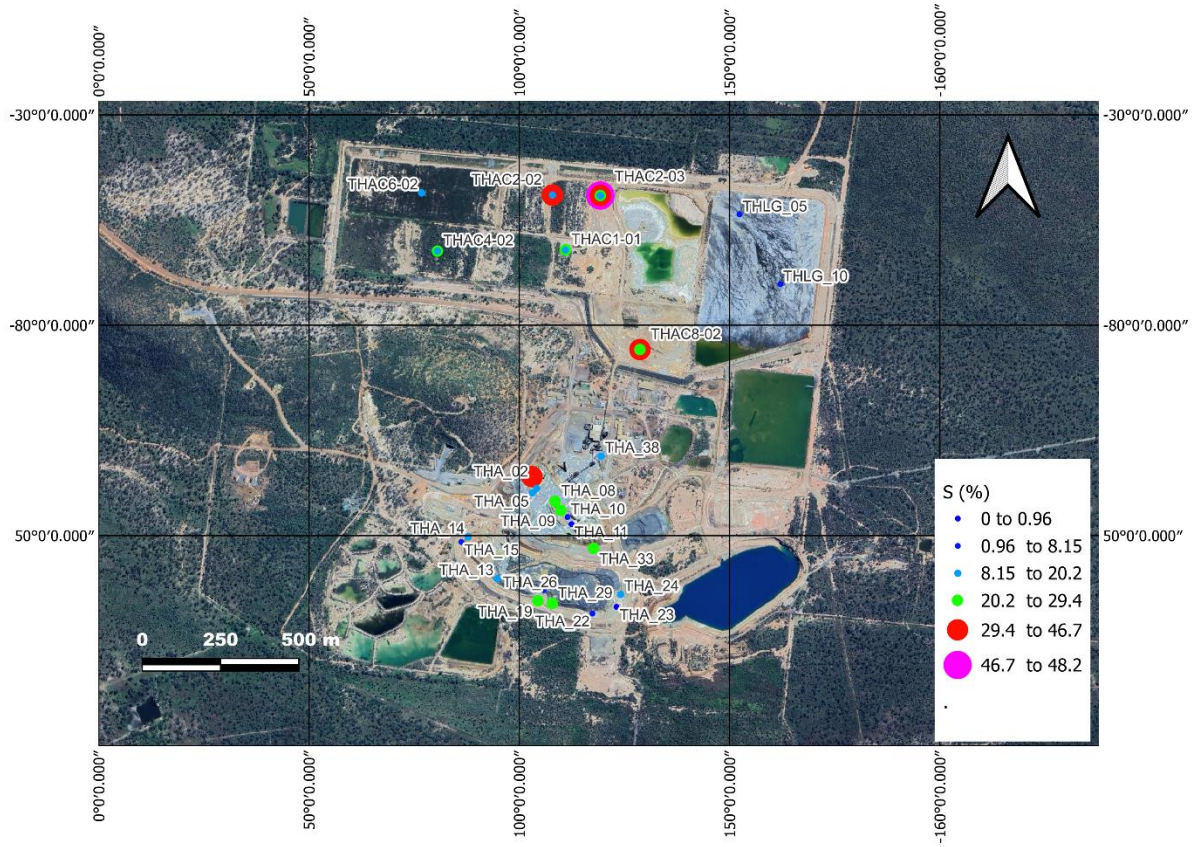

Figure 51: Drill holes and sample points for analysed samples

5.1.1 Pyrite Characteristics and NAG Tests

Pyrite in the samples exist in the form of free pyrite and agglomerated pyrite associating with silicates and secondary iron-oxides. The multi-addition NAG (single addition) method was not robust enough to oxidize completely both free and agglomerated pyrite in the sample as the sequential NAG method did. This was demonstrated in Figure 40: SEM analysis of THA-T175 to check degree of oxidation and leaching of pyrites. Py- pyrite, Gnt- garnet, Mgt- magnetite, Alb- albite, Qtz- quartz, Fe(OH)x – secondary iron-hydroxide.

In the case of THA-T 61 shown in Figure 41, even though there were appreciable neutralising silicates to justify the overall low single addition NAG capacity and zero sequential NAG

capacity, unoxidized pyrite can be seen in the original sample, and residues of both single addition and sequential addition NAG test. This implies that, neutralising minerals were easily dissolved and leached faster than the pyrites. From the optical microscopy of the original sample, a lot of agglomerates can be seen which serves as potential hinderance to oxidation of pyrite. Hence the NAG capacity obtained in both single and sequential addition methods are not representative of the pyrite contained in the sample as indicated by MLA and optical microscopy, where the residues from the two methods were compared. This indicates that the multi-addition method (single addition) only gives partial quantification of the acid generating potential of a sample and therefore cannot be relied on for a complete quantitative measure of AMD.

However, a combination of sequential method and Sobek calculation method is a sure way to accurately estimate the maximum producing acidity (MPA), and indirectly determine the acid neutralising potential (ANC) using the net acid generating potential (NAG or NAPP). One reason that could be tied to the partial pyrite oxidating ability of multi-addition method is the early formation of iron-oxyhydroxides ($Fe(OH)_3$) around pyrites and agglomerates. This occurs after H_2O_2 during the first addition has been consumed, for partial pyrite oxidation. This triggers the release of OH^- from neutralising minerals which reacts with the partially oxidized sulphide to form ferric hydroxide. At this stage the potential of the remaining free pyrite surfaces to be coated by iron hydroxides is high, preventing pyrite oxidation on subsequent additions. This is not to say that multi-addition method is not good, rather it is fast and cost-effective way of qualitatively determining the acid generating potential of samples without relying so much on numbers.

It is important to understand that acid generation from sulphides goes beyond sulphide oxidation (which in my opinion is captured by NAG tests) to ferric oxidation. It is at this point that a lot of H^+ are released into solution due to the presence of ferric ions acting as strong oxidant and the progression of acid generation is at its peak. Sulphide oxidation is only an initiator. This was observed during the NAG test and acid base titration. There were days the samples were not able to be heated after the 2-Hour reaction time stated in literature (Parbhakar-Fox, et al., 2018; Smart, et al., 2002). The pH of these samples prior to the next day was higher than the pH measured when the reaction time was extended to 24hrs. There were times the samples were left over the weekend. These samples during the titration consumed a lot of NaOH and gave dark green precipitate when the pH went beyond 4.5. This indicates the presence of Fe^{3+} which then precipitate as $Fe(OH)_3$. Sometimes the liquor from such tests took a long time to arrive at neutrality during titration which was completely different for samples that had been

heated right after the 2-hour reaction time. An indication that time is a crucial factor of acid mine drainage, giving opportunity to released ferric ions to exponentiate the acid generation after ferrous oxidation.

The two Acid Base Accounting classification schemes used shows that Thalanga mine waste and waste rock are acid generating Figure 36 after Weber, et al., (2006) and Smart, et al., (2002). When the classification results is compared to the initial compositional map showing where samples have been taken from, it is reasonable for samples from such locations to be classified as the scheme did. All cells of the tailings dam gave NAG capacity greater than 0 kg H_2SO_4/t except the samples from the fresh tailings (i.e. the THLG samples in cell 9). MLA data of samples from cell 9 brought to Liège was not received from Australia so further analysis could not be done on those samples, but there is the assumption that tailings in cell 9 might have appreciable neutralising minerals looking at the NAG pH and NAG capacity of the few samples that were analysed.

It is important to disclose that the initial tailings in cell 9 are reprocessed tailings from cell 1/7 which had come from Highway Reward. However, since auger drill was used on cell 9 and could not reach the bottom of the cell, it is possible those materials were not accessed but only the tails from Vomacka were accessed. The high sphalerite and chalcopyrite content found in some waste rock could have been misclassification during the mining operation, but most importantly, it could also be that the cut-off grade for those ores were high as already discussed above with grades, it could also be that complex mineral matrix and interlocking nature of ore made processing of some ores difficult despite their good grade and so ended up in the waste rock.

5.2 Critical Element Occurrence

The mineral phases of bismuth identified by the bright phase search and SEM spot mode analysis cannot be said with certainty as the number bismuth mineral grains analysed were too few to confidently name a mineral. However, per the stoichiometry and comparison to over 4700+ minerals, these minerals of bismuth may be present in Thalanga waste; Native bismuth, Ximengite, Bismite, Sillenite, Arsenobismite, Beyerite, Neyite, Muckeite, etc. (Refer to Table 12, Table 13, and in Appendix B).

Tellurium was below the detection limit of the technology and could not be studied further although ICP-MS indicated a concentration over 1000 times its average crustal abundance. This is possible to occur if tellurium exists as trace element in other minerals that are abundant in

Thalanga for example a lot of lead in the tailings and tellurium could exist in traces in the phase of Altaite. However, Tellurium was not identified by the SEM at all.

Antimony and Arsenic existed in tetrahedrite and arsenopyrite respectively, and in tetrahedrite-tennantite series where they substitute for each other. Some elements which were identified and could be of future research interest on Thalanga tails is Tungsten in the form of scheelite and Tin in the form of Cassiterite. Images shown in Figure 62 Appendix B.

Element Deportment

It was impossible to do element deportment because the number of grains analysed were too few to give robust results for element deportment. Also, almost all elements of the various phases of the minerals example Bi have been shared with two or more mineral phases which makes it very difficult to be done manually. The SEM analysis indicated the presence of these critical elements but due to the above shortcoming, deportment could not be made.

Relationship between the critical element and the deposit geology

Pb-Cu-Zn-Ag-Au are typical polymetallic sulphides associated with volcanogenic massive sulphide (VHMS) deposits. These deposits normally form on or near the seafloor in association with volcanic activity, mostly at back-arc basins and island arcs in relation to seafloor roll back and subduction (Betts, Stewart, & Armit, 2012; Berry, et al., 1992); Ridley, 2013; Henderson R. A., 1986). VHMS deposits are characteristic of complex mineralogy often including sulphides and sulfosalts of metals. The complexity of mineralisation of Thalanga deposit is analogous to the Kuroko type VHMS. It is syngenetic and had formed during or shortly after magmatic crystallisation. The critical element occur in secondary minerals that often accompany the hydrothermal deposition of pyrite, galena, chalcopyite, and sphalerite in local geochemical environment. The form and associations of bismuth especially native bismuth indicates mineral formation in late stage of hydrothermal processes. The results of which is usually deposition of bismuth and other minerals during late stage hydrothermal fluid remobilisation and metamorphic alteration. The mineralisation could have been controlled by the temperature range and prevailing pressure of the hydrothermal flow with mineral deposition typicaly occuring between 200-450 ^{o}C. This confirms literatures assertion of metamorphic facies from greenschist facies to amphibolite facies. Indicating a low grade to high grade metamorphic environment during the mineralisation of the Seventy Mile Range VHMS. The tennantite and tetrahedrite sulfosalts are mineral series that are common in hydrothermal veins and massive sulphides occuring alongside the base metals mined in Thalanga. These sometimes can result in foramtion of solid solutions between antimony, arsenic and other metals which is

similar to the solid solution of antimony observed in this sample. In general, the critical element mineralisation shows multi-stage hydrothermal fluid flow through conduits (forming veins) that remobilized these critical element resulting in a complex mineralisation process, variety of geochemical and fluid compositions reflecting the VHMS polymetallic deposit in Seventy Mile Range Group.

Chapter Six Conclusion and Recommendations

This thesis work provides a comprehensive evaluation of the potential of using Thalanga Pb-Cu-Pb-Ag-Au mine waste as a secondary source of critical elements without touching on possible extraction or processing techniques. It further assessed the Acid Metalliferous Drainage potential of the mine waste as an associated environmental risk of mine operations. Through a detailed sampling, laboratory work encompassing geochemical and mineralogical analysis, and static acid base accounting tests, reasonable environmental risk classification has been made for Thalanga mine waste. Interesting findings have emerged in terms of mineralogy and critical element endowment.

First, the study has identified in concentrations much higher than crustal abundance, critical elements including Bi, Sb, As, and Te. This indicates only elevated concentrations and cannot be solely used as basis to declare Thalanga mine waste as economically viable secondary source of these critical elements.

It discusses the potential mineralogical hosts of the critical metals, revealing their association with other minerals within the mine waste and within the primary environment of formation. This mineralogical and geochemical understanding is crucial for developing effective recovery processes and predict their metallurgical behaviour as well as their environmental behaviour under different conditions.

The Acid Base Accounting tests indicates that Thalanga tailings and waste rock are significant acid generating materials, driven essentially by the high concentration of pyrite. Current cover system provides some mitigation by limiting the exposure of atmospheric conditions and thus oxidation of pyrite. However, the presence of unoxidized sulphide mineral content remains a long-term liability for Acid Mine Drainage; thus, necessitating constant, continuous monitoring and maintenance of the cover system to prevent environmental pollution. For reliable and rapid tailings classification, the NAG method can deliver good results. Whereas the modified NAG method promotes safety by reducing violent reactions during tests with samples containing >0.3% S, it tends not to deliver the best results. Therefore, the modified NAG is to be used for samples with <0.3% S and sequential NAG method should be used for samples with >0.3% S as already stated by most literature.

The findings highlighted two important information potential to contribute to environmental management and potentially added economic benefit of the mine waste. If further research proves economically viable CRM, this will create avenue for not only the reduction in the environmental footprint of Thalanga mine but also the establishment of new revenue stream

through recovering Bi, As, and Sb which is currently controlled by China. This is achievable by developing suitable mineral processing technologies which also opens bright avenues for future research and industrial applications in Australia.

6.2 Recommendations for Future Work

The work presented in this thesis only form part of the stream one of the Geological Survey of Queensland's (GSQ) New Economy Minerals Initiative (NEMI) project. It is necessary to advance the study on Thalanga mine waste to the next stage where research will focus on robust resource estimation and proper quantification techniques for the critical elements (Bi, Sb, As) in the waste. There is also the need for exploring on advanced mineral processing technologies capable of extracting these metals in a cost-effective way as well as enhancing AMD prevention and mitigation strategies. Application of the methodologies in this study especially the NAG test on other mine waste from different places (notably Europe) could provide valuable data to improve the test method to support sustainable and efficient mine practices on the larger scale when assessing AMD prior, during and after mine operations.

In conclusion, this thesis underscores the relevance of a geometallurgical approach in assessing and predicting both the economic and environmental risks of mine waste. The study contributes to existing methodologies and ideas related to AMD assessment and critical element potential of mine wastes through integrated mineralogical and geochemical characterisation and laboratory testing to tell the environmental risk state of waste and the specific CRM's available for potential recovery. The results from Thalanga mine waste serves as a compelling case study, which will be able to enlighten similar efforts worldwide contributing to more sustainable and economically feasible mining practices.

6.3 Limitations

It is imperative to acknowledge the limitations of this research which could affect the results and interpretations presented herein.

1. Sample size and representation: This research work only started with 58 samples from the paste pH and later reduced to 38 for the rest of the experiment and analysis. The extent to which the samples represent the whole Thalanga waste could be questionable. The overall idea was to look at the variability of the worst-case scenario of AMD across the tailings dam and waste rocks which influenced the selection of samples. Therefore, samples were specifically selected from drill holes that registered high Fe% and S% content according to the ICP-MS assay results.

2. Time and Resource Constraints: Within six months both internship and research work were done. Methods that could have improved understanding and provided more information on the research results (such as LIBS, XRD, ICP-MS on leachates) could not be done.
3. Assumptions: Assumption that all sulphur are from pyrite or pyrrhotite may be wrong. Sulphide may have come from sulphate sulphur and not only sulphide sulphur. Again, this is related to the time and resources constraint of not being able to do LECO analysis for total carbon and total sulphur content.
4. Sample nature and preparation: The samples looked well pulverised, but most had numerous agglomerations. This has the tendency to impact the degree of oxidation of sulphides as hydrogen peroxide may not fully react with liberated but engulfed sulphides.

By clearly defining the scope, objectives and acknowledging these limitations, the research outcome will be handled without compromising on the potential impact of these limitations.

Europe's decision to get back fully into primary mining has been a matter of discussion in the European Parliament for years. Recent meetings of the European Union in Brussels hints that Europe is on course to open mines (both brown and greenfield), calling for a collaboration between Europe and Australia. The move is geared toward sustainable supply of critical raw minerals, especially battery metals, rare earths, and other industry-driven metals for the green transition. The revised EU critical raw material act (CRM, 2023) clearly states that the Union aims to at least; extract 10%, process 40%, and recycle 15% of its annual CRM consumption by 2030. In the revised CRM list, nickel, copper, arsenic, helium, feldspar, manganese, lithium, phosphorous, and coking coal have been added. Europe acknowledges the fact that, mine waste reprocessing can contribute only a handful of the raw material demand, yet it is important to augment primary production with secondary sources such as waste re-processing and recycling. This also ensures an efficient circular economy and proper environmental management.

Thalanga mine waste is a waste deposit from complex, different ore bodies within the Seventy-Mile Range Group in Queensland region-Australia. It comprises of waste (tailings and waste rock) from Thalanga Cu-Pb-Zn-Au-Ag deposit, Highway Reward Cu-Au deposit, and Balcooma Cu-Pb deposit. Antimony, Arsenic, and Lead were discarded as penalty elements. These were associated with pyrite, arsenopyrite, galena, etc. which often host refractory metals. Considering that the application of geometallurgy for complete utilisation of resources was limited a century ago, there is a good prospect in assessing old mine tailings and waste for recoverable CRMs with an added opportunity of mitigating prevailing environmental issues.

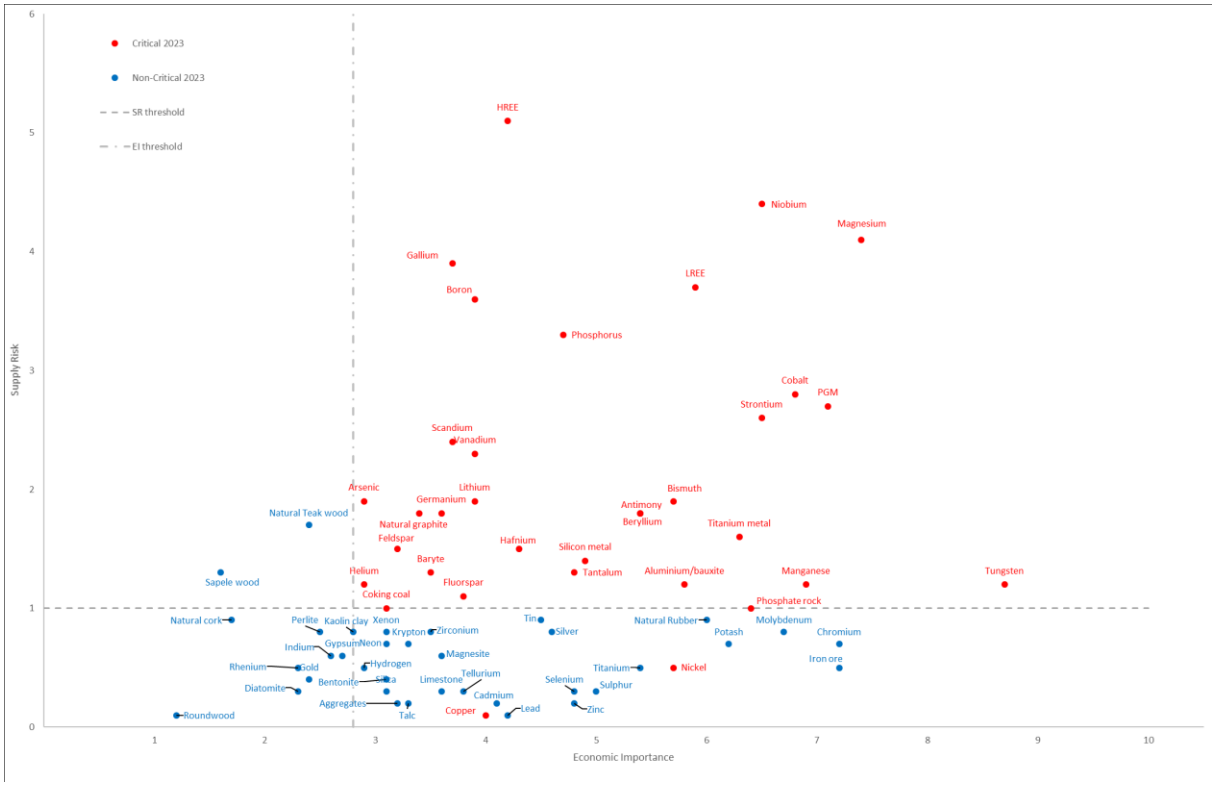

Figure 52: Critical Raw Minerals update 2023 source: (European Commision, Grohol, & Veeh, 2023)

7.2 Geopolitics of Arsenic, Bismuth, and Antimony

From Figure 52 above, arsenic, antimony, and bismuth have been added to the updated European Commission's critical raw materials. Both the EU and Australia considers them as elements with potential supply risk and economic importance. The graphs below are presented to show Belgium's (EU) contribution to As, Bi, and Sb supply to the USA economy. As at the end of 2023, Peru, China, Morocco were the leading As producers in the global market. All forms of As imports by the USA from 2019-2022 are shown in Figure 53 (Just to show Belgium's or (Europe's) contribution to the global supply through recycling and refinery of imported concentrates). Arsenic is used to produce gallium-arsenide, indium-arsenide, indium-gallium-arsenide semi-conductors for biomedical, communication, computer, electronics, and photovoltaic applications.

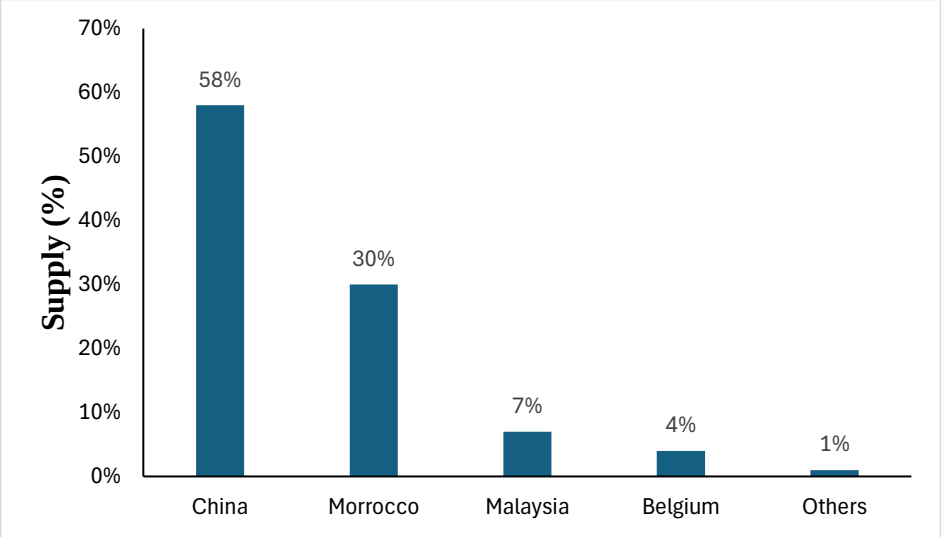

Figure 53: USA arsenic import sources from 2019-2022. Source: (U. S. Geological Survey, 2024)

Bismuth has substitutes in the pharmaceutical industry and electrical and electronics industry. For instance, bismuth can be substituted by cadmium, indium, lead, and tin in low-temperature solders. It can also be replaced by lead, selenium, or tellurium as an alloy in triggering devices for fire sprinklers. However, its environmental friendliness and availability as compared to the substitutes puts it in a position to remain sought after.

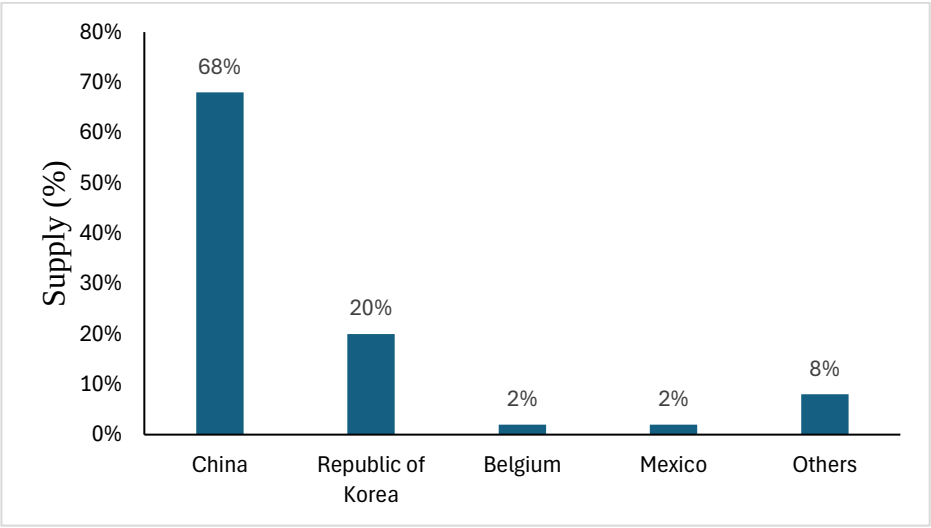

Figure 54: USA bismuth import sources from 2019-2022. Source (U S Geological Survey, 2024)

China's antimony mine production has fallen over the years, yet it was the leading global antimony producer in 2023 and accounted for 48% of global mine production Figure 55. The import source of antimony by USA from 2019-2022 is shown in Figure 56. There are numerous substitutes to antimony for instance, hydrated aluminium oxide can replace it as a flame retardant. In terms of enamels, paints and pigments, zinc, titanium, tin, chromium, and zirconium can substitute for antimony.

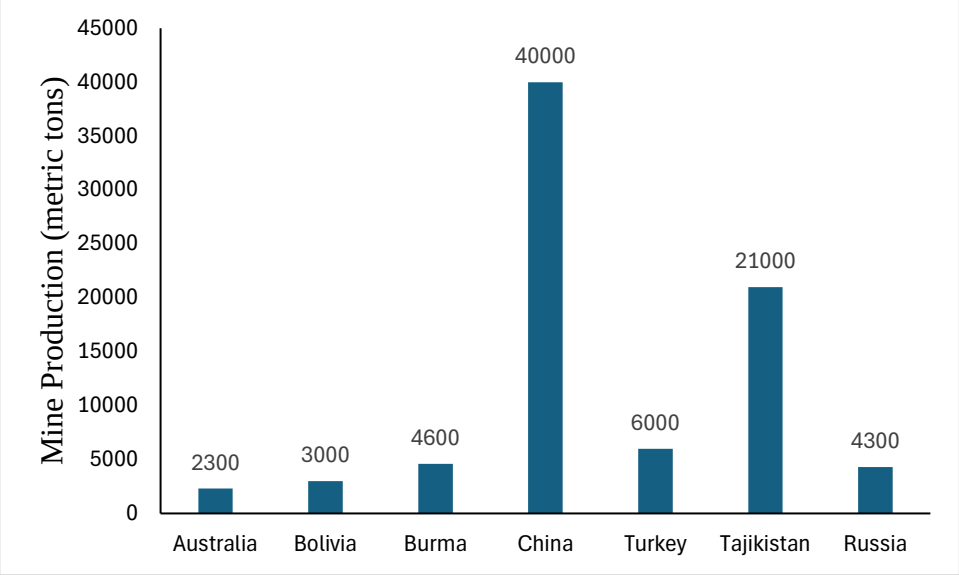

Figure 55: Mine production of antimony by country in 2023 (only production above 1000 metric tons). Source (U S Geological Survey, 2024)

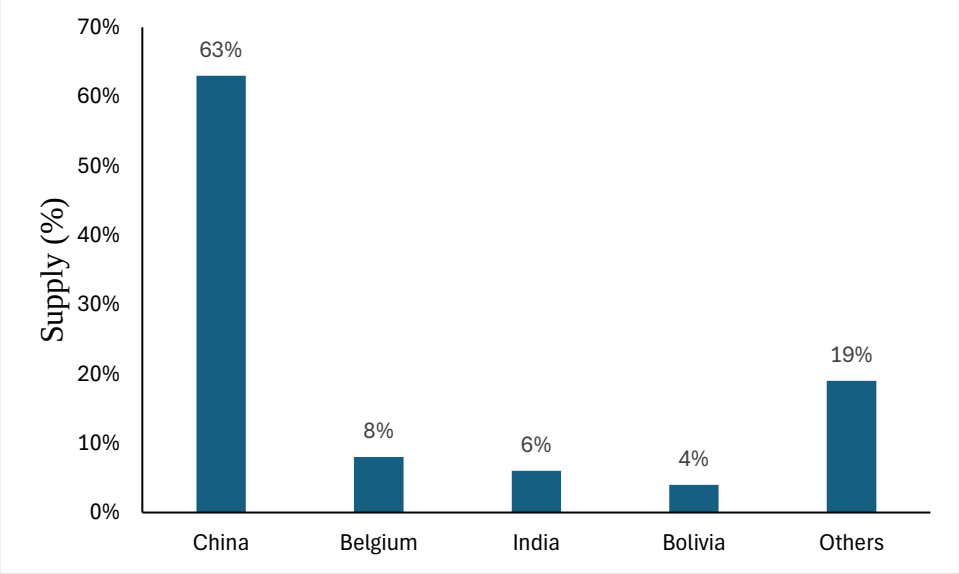

Figure 56: USA antimony imports sources from 2019-2022. (U S Geological Survey, 2024)

From the above information, China controls both the production of raw materials and final products(refined) of As, Sb, and Bi. These critical elements are mostly recovered as by-

products of base and precious metal processing (lead, copper, zinc, gold). An exception is a Chinese mine and Tasna mine in Bolivia (inactive since 1996) which are the only mines where bismuth has been produced as the primary ore. Reserves of bismuth are generally not reported at a mine or country level and are difficult to quantify(USGS). Whereas Australia does not export any of these products to USA, Belgium does contribute to USA's imports of these critical elements. Although there are no mines in Belgium or Europe that primarily produce these metalloids, they are chiefly sourced from processing of imported concentrate and processing of end-of-life of materials by companies like Umicore, Trafigura Group, ArcelorMittal (USGS, 2023). China's monopoly in critical metals and rare earths poses geopolitical tensions on certain metals as any attempt to hoard these products will put pressure on other parts of the world. Australia on the other hand has all it takes to join the global competition of production and refining of these critical metals to limit China's dominance as well as supply risk through its numerous mines and mine wastes. Instead of exporting concentrates to China, Australia can capitalize on adding up refineries to its current processing industries to process their concentrates while benefiting from ownership of the valuable by-products. It boils down to being ready to accept the environmental consequences of this downstream process and find appropriate ways to counter the menaces. Likewise, as Europe prepares to embark on reopening of new and old mines it is important to consider closing the mining value chain loop by building more value-added downstream processes.

The study and search for secondary prospectivity of mine waste and AMD assessment as done for Thalanga mine is an important aspect of the circular economy Europe can adopt from Australia. Europe has a lot of legacy mines in many places for instance the Libiola copper mine which operated between 1864-1962, legacy mines in Sardinia and Tucsony region in Italy. Most of old mines had high cut-off grades during the time of operation. These are potential sources of newly added strategic metals of the EU like copper and nickel, critical metals like antimony, indium, and arsenic. Australia has a lot of legacy mines and have worked extensively on this type of research through the establishment of government arms looking specifically into secondary prospectivity of mine waste and implementation of proper waste management system for both old and new waste.

It is important to understand that the physical properties and to some extent the chemistry of mine wastes especially tailings, may change over time due to exposure to natural chemical processes. For instance, regrinding tailings becomes inefficient, costly, and waste of energy especially when the material has already undergone oxidation which greatly affects the surface processes in flotation. Phytomining is one of the environmentally friendly waste re-processing

techniques that uses specific species of plants to extract metals from the soil (waste). However, the method takes long time and may not be so efficient. Inasmuch as time and budget did not allow for analysis of best process methods to extract CRMs from mine wastes experimentally, I believe with innovative backing from the EIT Europe can make a lasting impact on its mine waste transformation secondary prospectivity.

Overall, the findings of AMD assessment, the methods of determining acid generating potential, and assessing the secondary prospectivity of mine waste done in this thesis, provides knowledge that can be improved upon and used in the European setting. Most importantly incorporating into new mining projects in Europe right from the projects inception stage through the geometallurgical approach to ensure a sustainable circular economy and green transition Europe.

References

Abdulluh, R., & Rosenbaum, G. (2017, January 2). Orogen-Perpendicular Structures in the Central Tasmanides and Implications for the Paleozoic Tectonic evolution of Eastern Australia. *Tectonophysics*, 444-463. doi:10.1016/j.tecto.2016.11.031

Australia's Critical Minerals List and Strategic Material List. (2023, June 20). (C. M. Office, Producer) Retrieved January 22, 2024, from Australian Government Department of Industry, Scinece and Resources: https://www.industry.gov.au/publications/australias-critical-minerals-list-and-strategic-materials-list

Beams, S. D., Dronseika, E. V., & Doyle, M. G. (1998). The exploration history, geology and geochemistry of the polymetallic Highway-Reward deposit, Mt Windsor Subprovince. *Economic Geology of Northeast Queensland*, 137-153.

Bellenfant, G., D'Hugues, P., Bodenan, F., & Cassard, D. (2013). Reprocessing of Mining Waste: Combining Environmental and Metal Recovery. *Australian Centre for Geomechanics*, 1-12.

Berry, R. F., Huston, D. L., Stolz, A. J., Hill, A. P., Beams, A. D., Kuronen, U., & Taube, A. (1992). Stratigraphy, Structure, and Volcanic-Hosted Mineralization of the Mount Windsor Subprovince, North Queensland, Australia. *Economic Geology*, 739-763.

Berry, R. F., Huston, D. L., Stolz, A. J., Hill, A. P., Beams, S. D., Kuronen, U., & Taube, A. (1999). Stratigraphy, structure, and volcanic-hosted minerlaisation of the mount Windsor Subprovince, Northern Queensland, Australia. *Economic Geology*.

Betts, P. G., Spampinato, G. P., Ailleres, L., & Armit, R. J. (2015). Early tectonic evolution of the thomson Orogen in Queensland inferred from constrained magnetic and gravity data. *Tectonophysics*, 99-120.

Betts, P., Stewart, J., & Armit, R. (2012). *A synthesis of the geological evlution of North Queensland from the Late Neoproterozoic to the present. DEEDIO0107 NQGSM Report.* Queensland: Geological Survey of Queensland.

Bouzahzah, H., Benzaazoua, M., & Bussière, B. (2013). Acid-Generating Potential Calculation Using Mineralogical Static Test: Modification of the Paktunc Equation. *23rd World Mining Congress*, (pp. 92-110). Montreal.

Bouzahzah, H., Benzaazoua, M., Mermillod-Blondin, M., & Pirard, E. (2015). A novel procedure for polished section preparation for automated minerlaogy avoiding internal

particle settlement. *12th International Congress for Applied Minerlaogy (ICAM).* Istanbul Turkey.

Bouzahzah, H., Mafra, C., Stamenov, L., & Gaydardzhiev, S. (2020). Insights on the Effect of Pyrite Liberation Degree upon the Acid Mine Drainage Potential of Sulphide Flotation Tailings. *Applied Geochemistry*, 1-12.

Burt, R. (1999). The Role of Gravity Concentration in Modern Processing Plants. *Elsevier*, 1-10.

Burton, G., & Trigg, S. (2014). Geodynamic Significance of the Boundary Between the Thomson Orogen and The Lachlan Orogen, Northwstern New South Wales and Implications for Tasmanide Tectonics: Discussion. *Australian Journal of Earth Sciences.*, 639-641.

Butcher, A. R., Dehaine, Q., Menzies, A. H., & Michaux, S. P. (2023). Characteristics of Ore Properties for Geometallurgy. *Elements*, 1-7. doi:0.2138/gselements.19.6.352

Butcher, R. A., Dehaine, Q., Menzie, H. A., & Michaux, P. S. (2023, January). Characteriisation of ore properties for geometallurgy. 1-7. doi:10.2138/gselements.19.6.352

Campbell, & Hronsky. (n.d.). The Mineral System Concept: The Key to Exploration Targeting. *Centre for Exploration Targeting and Australian Research Council Centre of Excellence for Core to Crust Fluid Systems,.*

Chernoburova, O., & Chagnes, A. (2023). *Mining and Processing Residues.* Ecole Nationale Superiuer Geologie, Georesource, observatoire terre et environment de lorraine. Nancy: Candice Janco.

Chopard, A., Benzaazoua, M., Bouzahzah, H., & Plante, B. (2017). A Contribution to improve the Calculation of the Net Acid Generating Potential of Mining Waste. *Chemoshere*, 97-107.

Cowan, J., & Beatson, r. (2003). Practical Implicit Geological Modelling. *5th International Mining Geology Conference* (pp. 1-14). Bendigo, Victoria: The Australatian Institute of Mining And Metallurgy.

CRM. (2023). *The European Critical Raw Material Act- Fact Sheet.* Luxembourg: European Union.

Cross, A. J., Purdy, D. J., Champion , D. C., Brown, D. D., Siegel, C., & Armstrong, R. A. (2018). Insights into evolution of the Thomson Orogen from geochronology,geochemistry, and zircon isotopic studies of magmatic rocks. *Australian Journal of Earth of Sciencee*, 987-1008. doi:https://doi.org/10.1080/08120099.2018.1515791

Dowd, P. (2006). The Businees Case for the Prevention of Acid Drainage. *5th Australian Workshop on Acid and Metalliferous Drainage* (pp. 1-10). Kenmore, Australia: Australian Centre for Minerals Extension and Research.

Doyle, M. G. (2001). Volcanic Influences on Hydrothermal and Diagenic Alteration: Evidence from Highway-Reward, Mount Windsor Subprovince, Australia. *Economic Geology*, 1133-1148.

Doyle, M. G., & Huston, D. (1999). The Subsea-Floor Replacement Origin of the Ordovician Higway-Reward Volcanic-Associated Massive Sulphide Deposit, Mount Windsor Subprovince, Australia. *Economic Geology*, 825-844.

Doyle, M. G., & Huston, D. L. (1999). The Subsea-Floor Replacement Origin of the Ordovician Highway-Reward Volcanic-Associated Massive Sulphide Deposit, Mount Windsor Subprovince, Australia. *Economic Geology*, 825-844.

Doyle, M. G., & McPhie, J. (2000). Facies Architecture of a SIlicic Intrusion-Dominated Volcanic Centre at Highway-Reward, Queensland, Australia. *Journal of Volcanology and Geothermal Research*, 79-96.

European Commision, Grohol, M., & Veeh, C. (2023). *Study on the Critical Raw Materials for the EU, Final Report.* Brussels: European Commission.

European Commission, E. (2020). *Critical Raw Materials Resilience: Charting a Path Towards Greater Security and Sustainability.* Brussels: European Commission. Retrieved January 22, 2024

Fergusson, C. L., Henderson, R. A., Lewthwaite, K. J., Philips, D., & Withnall, I. W. (2005). Structure of the Early Palaeozoic Cape River Metamorphics, Tasmides of north Queensland: Evaluation of roles of convergent and extensional tectonics. *Australian Journal of Earth Sciences*, 261-277.

Foucaud, Y., Filippov, L., Dehaine, Q., & Kroll-Rabotin. (2019). Experimental Investigation into the kinetics of Falcon UF Concentration: Implication for fluid-dynamic base modelling. *Separation and Purification Technology*, 1-12.

Glen, R., Saeed, A., Hegarty, R., Parcival, I., Bordokos, S., & Griffin, W. (2010). Preliminary Zircon Data and Tectonic Framework for the Thomson Orogen, Northwestern NSW. *Geological Survey of New South Wales*, GS2010/0379.

Gregory, P. W., Hartley, J. S., & Wills, K. J. (1990). Thalanga Zinc-Lead-Copper-Silver Deposit. *Geology of the Mineral Deposit of Australia and Papua New Guinea*, 1527-1537.

Gregory, P., & Hartley, J. (1982). The Thalanga Zinc-Lead-Copper-Silver Deposit. *Charters Towers Greenvale Area* (pp. 12-22). Queensland: Geological Society of Australia.

Guatame-Garcia, A., Buxton, M., Tinti, F., Kasmaeeyazdi, S., Bodenan, F., & Schick, J. (2023). Residue Sampling and Characterization. In O. Chernoburova, & A. Chagnes, *Mining and Processing Residues: Future's Source of Critical Raw Materials* (pp. 25-45). Amsterdam: Elsevier.

Habashi, F. (2001). Arsenic, Antimony, and Bismuth Production. *Elsevier*, 332-336. doi:10.1016/B0-08-043152-6/00069-3

Harvey, K. J. (1989). *The Geology of the Balcooma Massive Sulphide Deposit, North-East Queensland.* Queensland: James Cook University.

Henderson, R. (1986). Geology of the Mount Windsor Subprovince- a Lower Palaeozoic Volcano-Sedimentary Terrane in the Northern Tasma Orogenic Zone. *Australian Journal of Earth Sciences*, 343-364. doi:10.1080/08120098608729371

Henderson, R. A. (1986). Geology of the Mount Windsor Subprovince- a Lower Palaeozoic Volcano-Sedimentary Terrane in the Northern Tasma Orogenic Zone. *Australian Journal of Earth Sciences*, 343-364. doi:10.1080/08120098608729371

Henderson, R. A. (1986). Geology of the Mt Windsor Subprovince- a Lower Palaeozoic Volcano-sedimentary terrane in the Northern Tasman Orogenic Zone. *Australian Journal of Earth Sciences*, 343-364.

Herrmann, W. (1995). Geochemical Aspects of the Thalanga massive Sulphide Deposit, Mt Windsor Subprovince. In S. D. Beams, *Mineral Deposits of Northeast Queensland: Geology and Geochemistry* (pp. 155-170). National Library of Australia Cataloguing in Publication data.

Herrmann, W., Blake, M., Doyle, M., Huston, D., Kamprad, J., Merry, N., & Pontual, S. (2001). Short Wavelength Infrared (SWIR) Spectral Analysis of Hydrothermal

Alteration Zones Associated with Base Metal Sulphide Deposits at Roseberry and Western Tharsis, Tasmania, and Highway-Reward, Queensland. *Economic Geology*, 939-955.

Hunt, J., Lottermoser , B. G., Parbhaker-Fox, A., Van Veen, E., & Goemann, K. (2016). Precious Metals in Gossanous Waste Rock from Iberian Pyrite Belt. *Minerals Engineering*, 45-53.

Huston, D. L., Bottril, R. S., Crefelman, R. A., Zaw, K., Ramsden, T. R., Rand, S. W., . . . Large, R. R. (1992). Geologic and Geochemical Controls on the Mineralogy and Grain Size of Gold-Bearing Phases, Eastern Australian Volcanic-Hosted Massive Sulphide Deposits. *Economic Geology*, 542-563.

Isaaks, H. E., & Srivastava, R. M. (1989). *Applied Geostatistics.* New York: Oxford University Press.

Jackson, L. M., & Parbhaker-Fox, A. (2016). Mineralogical and Geochemical Cgaracterization of the Old tailings Dam, Australia: Evaluating the Effectiveness of Water Cover for Long-Term AMD Control. *Applied Geochemistry*, 64-78.

Jamieson, H. E. (2011). Geochemistry and Mineralogy of Solid Mine Waste: Essential Knowledge for Predicting Environmental Impact. *Elements*, 381-386.

Johnson, B. D., & Hallberg, B. K. (2004). Acid Mine Remediation options: a review. *Science of the Total Environment*, 3-14.

Kilgariff, B. (2003). Thalango Processing Plant- As Many Lives as a Cat and Just Curious. *The Australasian Institute of Mining and metallurgy* , 129-142.

Klein, C., & Dutrow, B. (2008). *Mineral Science* (The 23rd edition of the manual of mineral science: (after James D. Dana). ed.). India: Wileys.

Klootwijk, C. (2023). Middle-Late Paleozoic Australia-Asia Convergence and Tectonic Extrusion of Australia. *Gondwana Research*, 5-54.

Lamberg, P. (2011). Particles- The Bridge Between Geology and Metallurgy. *Minerals*, (pp. 1-16). Luleå.

Large, R. R. (1992). Australian Volcanic-Hosted Massive Sulphide Deposits: Features, Styles, and Genetic Models. *Economic Geology*, 471-510.

Large, R. R., Gemmell, B. J., Paulick, H., & Huston, D. L. (2001). The Alteration Box Plot: A smple Approach to Understanding the Relationship Between Alteration Mineralogy andLithogeochemistry Associated with Volcanic-Hosted Massive Sulphides. *Economic Geology*, 957-971.

Lindsay, M. B., Moncur, M. C., Bain, J. G., Jambor, J. L., & Ptacek, C. J. (2015). Geochemical and Mineralogical Aspects of Sulphide Mine Tailings. *Applied Geochemistry*, 157-177.

Lottermoser, B. (2010). Characterization, Treatment and Environmental Impacts. In B. Lottermoser, *Mine Wastes Characterization, Treatment and Environmental Impacts* (3 ed., pp. 1-40). London, New York: Springer. doi:10.1007/978-3-642-12419-8

Lottermoser, B. (2017). Environmental Indicators in Metal Mining. In B. Lottermoser, *Environmental Indicators in Metal Mining* (p. 1). Switzerland: Springer. doi:10.1007/978-3-319-42731-7

Lottermoser, B. (2017). Environmental Indicators in Metal Mning. In B. Lottermoser. Springer.

Lottermoser, B. (2017). Predictive Environmental Indicators in Metal Mining. In B. Lottermoser, *Environmental Indicators in Metal Mining* (pp. 3-15). Switzerland: Springer.

Lottermoser, B. G. (2010). *Mine Wastes Characterisation, Treatment, and Environmental Impacts.* Berlin: Springer.

Lottermoser, B., & Parbhaker-Fox, A. (2017). Principles of Sulphide Oxidation and Acid Rock Drainage. In B. Lottermoser, *Environmental Indicators in Metal Mining* (pp. 15-30). Switzerland: Springer. doi:10.1007/978-3-319-42731-7

Louwrens, E. L. (2015). *A Novel Geometallurgical Approach to Tailings Storage Facility Characterisation and Evaluation.* Brisbane: University of Queensland. Retrieved February 2024

Louwrens, E. L. (2015). *A Novel Geometallurgical Approach to Tailings Storage Facility Characterization and Evaluation.* Brisbane: University of Queensland.

Lund, C., & Lamberg, P. (2014). Geometallurgy- A Tool for Better Resource Efficiency. *European Geologist*, 39-42.

Lund, C., Lamberg, P., & Lindberg, T. (2013). Practical Way to Quantify Minerals from Chemical Assays at Malmberget Iron Ore Operations- An important tool fot the Geometallurgical Program. *Minerals Engineering*, 7-16.

Lydon, J. W. (1988). Ore Deposit Models #14. Volcanogenic Massive Sulphide Deposits Part 2: Genetic Models. *Geoscience Canada*, 15(1), 43-65.

Mafra, C., Bouzahzah, H., Stamenov, L., & Gaydardzhiev, S. (2022). An Integrated Management Strategy for Acid Mine Drainage Control of Sulfidic Tailings. *Minerals Engineering*, 185.

Miller, C., Halley, S., Green, G., & Jones, M. (2001). Discovery of the West 454 Volcanic-Hosted Massive Sulphide Deposit Using Oxygen Isotopes and REE Geochemistry. *Economic Geology*, 1227-1237.

Mononen, T., Kivnen, S., Kotilainen, M. J., & Leino, J. (2022). *Social and Environmental Impacts of Mining Activities in the EU.* Brussels.

Noble, T. L., Lottermoser, B. G., & Parbhakar-Fox, A. (2016). Evaluation of pH Testing Methods for Sulfidic Mine Waste. *Mine Water Environ*, 318-331.

NRA, C. (2018). *Cover System Research Program- Thalanga Tailings Storage Facility.* Queensland: NRA Environmental Consultants of Red River Resources.

Ortiz, J. M., Avalos, S., Riquelme, A. I., Leuangthong, O., Madani, N., & Frenzel, M. (2023). Uncertainity and Value: Optimising Geometallurgical Performance Along the Mining Value Chain. *Elements*, 377-383. doi:10.2138/gselements.19.6.377

Parbhakar-Fox, A. K., Edraki, M., Walters, S., & Bradshaw, D. (2011). Development of a Textural Index for the Prediction of Acid Rock Drainage. *Minerals Engineering*, 1277-1287.

Parbhakar-Fox, A., & Baumgartner, R. (2023, January). How Geometallurgy can improve mine waste management across the life-of-mine. 1-6. doi:10.2138/gselements.19.6.371

Parbhakar-Fox, A., & Baumgartner, R. (2023). How Geometallurgy can Improve Mine Waste Management across the Life-of-Mine. *Elements*, 1-6. doi:10.2138/gselements.19.6.371

Parbhakar-Fox, A., Edraki, M., Walters, S., & Bradshaw, D. (2011). Development of Textural Index for the Prediction of Acid Rock Drainage. *Minerals Engineering*, 1277-1287.

Parbhakar-Fox, A., Fox, N., Ferguson, T., Hill, R., & Maynard, B. (2018). Dissection of the NAG pH Test: Tracking the Efficacy Through Examining Reaction Products. *11th ICARD IMWA MWD Conference- Risk to Opportunity*, (pp. 949-955). Pretoria.

Parbhakar-Fox, A., Whitworth, J. A., Forbes, E., Verster, I., Jokovic, V., & Awatey, B. (2022). Review on Advances in Mineral Processing Technologies suitable for Metal Recovery from Mining and Processing Waste. *Cleaner Engineering and Technology*, 1-16. Retrieved January 2024

Parbhaker-Fox, A., & Baumgartner, R. (2023). Action versus Reaction: How Geometallurgy Can Improve Mine Waste Management Across The Life-Of-Mine. *Elements*, 371-376. doi:10.2138/gselements.19.6.371

Parbhaker-Fox, A., & Lottermoser, B. (2015). A Critical Review of Acid Rock Drainage Prediction Methods and Practices. *Minerals Engineering*, 107-124.

Parian, M., Lamberg, P., Möckel, R., & Rosenkranz, J. (2015). Analysis of Mineral Grades for Geometallurgy: Combined Element-To-Mineral Conversion and Quantitative X-Ray Diffraction. *Minerals Engineering*, 25-35.

Paulick, H., & McPhie, J. (1999). Facies Architecture of the Felsic Lava-Dominated Host Sequence to the Thalanga Massive Sulphide Deposit, Lower Ordovician, Northern Queensland. *Australian Journal of Earth Sciences* , 391-405.

Paulick, H., Herrmann, W., & Gemmell, B. (2001). Alteration of Felsic Volcanics Hosting the Thalanga Massive Sulphide Deposit (Northern Queensland, Australia) and Geochemical Proximity Indicators to Ore. *Economic Geology*, 463-490. doi:0.2113/96.5.1175

Payá, P. A., & Paláez, S. S. (2017). *European Achievements in Soil Remwdiation and Brownfield Redevelopment.* Brussels: Joint Research Centre, The European Commission.

Pereira, L., Schach, E., Tolosana-Delgado, R., & Frenzel, M. (2023). All About Particles: Modelling Ore Behaviour in Mineral Processing. *Elements*, 359-364. doi:10.2138/gselements.19.6.359

Pirard, E., & Sardini, P. (2011). Image Analysis for Advanced Characterisation of Industrial Minerals and Geomaterials. In E. Pirard, *Advanced Characterisation of Industrial Mineral* (pp. 1-52). Liege: European Mineralogical Union.

Pownceby, M. I., & Macrae, C. M. (2010). Electron Microbeam Analysis Techniques Used for the Characterisation of Industrial Minerals. In M. I. Pownceby, *Advances in the Characterisation of Industrial Minerals.* (pp. 1-74). London: European Mineralogical Union. doi:https://doi.org/10.1180/EMU-notes.9.7

Richmond, A., & Shaw, W. (2009). Geometallurgical Modelling- Quo Vidas? Seventh International Mining Geology Conference, Perth, WA. Perth, WA.

Ridley, J. (2013). *Ore Deposit Geology.* New York: Cambridge University Press. doi:10.1017/CBO9781139135528

Simate, G. S., & Ndlovu, S. (2014). Acid Mine Drainage: Challenges and Opportunities. *Journal of Environmnetal Chemical Engineering*, 1785-1803.

SLR Consulting Pty Lmtd. (2020). *Thaalanga Environmental Evaluation.* Townsville: SLR Consulting.

Smart, R., Skinner, B., Levay, G., Gerson, A., Thomas, J., Sobieraj, H., . . . Weber, P. (2002). *Project P387A Prediction and Kinetic Control of Acid Mine Drainage.* Auckland: AMIRA.

SRK-Consulting. (2022). *NI 43-101Technical Repoort: Prefeasibility Study of Segovia Project.* Antioquia, Colombia: GCM.

Struers. (2018, April 16). *Struers.com.* Retrieved from MD- Systems: https://www.struers.com

Tamaduk, P. (2018). *Partial Relinquishment Report, EPM 16929.* RVR.

Tinti, F., Kasmaeeyazdi, S., Guatame-Garcia, A., Changnes, A., & Chernoburova, O. (2023). Critical Raw Material-Containing Residues. In O. Chernoburova, & A. Chagnes, *Mining and Processing Residues; Future's Source of Critical Raw Materials* (pp. 1-23). Armsterdam: Elsevier.

U S Geological Survey. (2024). *Mineral Commodity Summaries 2024.* Virginia: U.S. Department of Interior.

Verhoef, E., Gerard, P., & Reuter, M. A. (2004). Process Knowledge, System Dynamics, and Metal Ecology. *Journal of Industrial Ecology*, 23-43.

Walshe, L. J., Heithersay, S. P., & Morrsison, W. G. (1995). Toward Understanding of the Metallogeny of the Tasman Fold Belt System. *Economic Geology*, 1-20.

Weber, P. A., Hughes, J. B., Conner, L. B., Lindsay, P., & Smart, R. S. (2006). Short-Term Acid Rock Drainage CHaracteristics Determined by Paste pH and Kinetic Testing: Cypress Propect, New Zealand. *7th Iternational Conference on Acid Rock Drainage* (pp. 2289-2310). New Zealand: American Society of Mining and Reclamation.

Whateley, M. K., Moon, C. J., & Evans, A. M. (2006). *Introduction to Mineral Exploration.* Australia, Victoria: Blackwell Publishing.

Whitworth, A. J., Forbes, E., Verster, I., Jokovic, V., Awatey, B., & Parbhaker-Fox, A. (2022). Review on Advances in Mineral Processing Technolgies Suitable for Critical Metal Recovery from Mining and Processing Wastes. *Cleaner Engineering And Technology*, 7.

Withnall, I. W. (1982). The Geology of the Greenvale- Balcooma Area. *1982 Field Conference Charters Towers Greenvale Area* (pp. 31-46). Queensland: Geological Survey of Queensland.

Wyborn. (1994). Australian Proterozoic Mineral System; Essential ingredients and mappable criteria. *Austrlian Institute of Mining and Metallurgy Annual conference*, (pp. 109-115). Melbourne.

Appendix A

NAG TEST DATA SHEET

ALS ID	GeMMe ICP-MS/AES ID (Leachate and Residue)	Sample type	Tailing cell allocation	Sample Mass (g)	NAGpH			AVG NAGpH	Molar Con. NaOH (M)	Titre vol of NaOH @ pH 4.5	Titre Vol of NaOH (V) @ pH 7	NAG Capacity @ pH 4.5	NAG Capacity @pH 7 (Kg H2SO4/tonne)	Observation/Comments
THA-T099	KAJ 15/04 010	Tailings	Cell 2	2.5007	2.34	2.34	2.34	2.34	0.0948	28.4	50.6	52.75	93.99	Very low effervescence with small-sized bubbles that form single layer of foam during first addition. No visible bubbling and efferscence after 10mins until 2hrs. Effervescence and bubbling observed to increase during heating. After 10 mins of heating the reaction becomes violent and attempts to spill over with very large bubbles. When the hot plate was turned off and the sample taken off to prevent spill-over the reaction calmed down and went into quiescence completely even after re-heating for 1hr. There was no boiling, no bubbling and no effervescence during this time. Vigorous reaction with effervescence, bubbling, and boiling on second addition of 100ml (H2O2). The reaction is short-lived. Effervescence, bubbling, and boiling ceased completely after 30mins. There was no bubbling, effervescence, and boiling during the second heating. Short-lived but violent effervescence and bubbling on third addition. Sample goes into quiescence after 15mins of adding H2O2. No efferevescence and bubbling during heating. Brick-red precipitate during titration which changes to green after pH reaches 6. pH is highly unstable at around pH 7 due to consumption of NaOH which leads to a drop in pH below 7 after some time.
THA-T100	KAJ 16/04 011	Tailings	Cell 2	2.503	2.31	2.32	2.33	2.32	0.0948	31.25	50	58.00	92.79	There was mild effervescence with small bubbles for 2hrs after first addition. Violent effervescence and large bubbles during first heating. The reaction is short-lived and goes visibly dead after 15 minutes. Violent effervescence and large bubbles on second addition. But reaction is short-lived and dies out. No bubbling or effervescing during heating. Violent but decreases effervescence and bubbling on third addition as compared to the second addition. No effervescence and bubbling during third heating for 2hrs. No discoloration before titration. Brown precipitate during titration.
THA-T102	KAJ 24/04 023	Tailings	Cell 2	2.5005	2.49	2.49	2.49	2.49	0.0948	15.2	42.15	28.24	78.30	No effervescence or bubbling on first addition until after 45 mins when thin layer of tiny bubbles formed. There was no effervescence, bubbling or boiling during the heating stage. Vigorous reaction with effervescence, bubbling, scum and boiling during second addition of peroxide. There was no visible reaction during the heating stage. Reaction is short-lived. The third addition gives similar reaction as the second addition and there was no visible reaction during heating. There was discoloration to pale brown. Brick red precipitate formed during titration
THA-T104	KAJ 15/04 009	Tailings	Cell 2	2.5013	2.75	2.74	2.74	2.74	0.0948	9	24	16.71	44.57	Very low effervescence with small-sized bubbles that form single layer of foam during first addition. No visible bubbling and efferscence after 10mins until 2hrs. Effervescence and bubbling observed to increase during heating. After 10 mins of heating the reaction becomes vigorous and attempts to spill over with very large bubbles. When the hot plate was turned off and the sample taken off to prevent spill-over the reaction calmed down and went into quiescence even after further heating for 1hr- There was no boiling, no bubbling and no effervescence during this time. Vigorous reaction with effervescence, bubbling, and boiling on second addition of 100ml (H2O2). The reaction is short-lived. Effervescence, bubbling, and boiling ceased completely after 30mins. Short-lived but vigorous effervescence and bubbling on third addition. Sample goes into quiescence after 15mins of adding H2O2. No effervescence and bubbling during third heating. Orange precipitate during titration.
THA-T105	KAJ 24/04 024	Tailings	Cell 2	2.5014	2.32	2.32	2.32	2.32	0.0948	22.05	48.2	40.95	89.51	Vigorous reaction with peroxide addition. Effervescence, bubbling scumd observed. But reaction is short-lived. Vigorous reaction with effervescence, bubbling and boiling during second addition of peroxide. There was no visible reaction during the heating stage. Reaction is short-lived. The third addition gives similar reaction as the second addition and there was no visible reaction during heating. Greenish-brown precipitate formed during titration.
THA-T057	KAJ 19/04 018	Tailings	Cell 4	2.5009	2.59	2.59	2.59	2.59	0.0948	14.1	36.7	26.19	68.17	Mild effervescence and small bubbles during first addition. Tiny bubbles forming thin layer of foam after 50mins of addition. Strong effervescence, bubbling and boiling which gradually dies out after 30mins during the second addition. Decreased effervescence, bubbling and boiling during third addition as compared to the second. There was no boiling or effervescence during heating stages. Discoloration to light orange after cooling for overnight. Green precipitate forms during titration. Very unstable pH above 7.
THA-T059	KAJ 22/04 019	Tailings	Cell 4	2.5031	3.64	3.64	3.64	3.64	0.0948	1.35	10.4	2.51	19.30	Mild effervescence and small bubbles during first addition. Tiny bubbles forming thin layer of foam after some time of H2O2 addition. Effervescence and bubbling increases during reaction time until 2hrs. Effervescence, boiling and bubble size increases during heating. This phenomenon is observed throughout the subsequent peroxide addition and heating steps but more gently. There was no discoloration observed during addition and heating. Yellowish-green precipitate observed during titration at pH 7
THA-T060	KAJ 12/04 007	Tailings	Cell 4	2.5016	7.51	7.51	7.52	7.51	0.0948	0	0	0.00	0	Mild reaction and effervescence which increases with time. Scummy bubbles until 1hr. Then the reaction becomes vigorous with large scummy bubbles for 10mins before it dies out. No bubbling and effervescence during heating. Gentle effervescence and bubbling after second addition until 1hr, then effervescence increased for about 30mins before it calmed down. effervescenc continued for 2hrs without stopping. Reaction becomes vigorous with effervescence and large bubbles during heating for about 45mins and stopped. Quiet reaction for the next 1hrs was observed. The third addition gave a gentle reaction and effervescence with small bubbles. Gentle boiling and effervescence with smallbibbles during heating. Effervescing and boiling increases after 20mins of heating. Observation of big bubbles
THA-T061	KAJ 22/04 020	Tailings	Cell 4	2.5022	5.15	5.15	5.15	5.15	0.0948	0	3.6	0.00	6.68	Mild effervescence and small bubbles during first addition. Tiny bubbles forming thin layer of foam after some time of H2O2 addition. Effervescence and bubbling increases during reaction time until 2hrs. Effervescence, boiling and bubble size increases during heating. This phenomenon is observed through out the subsequent peroxide addition and heating steps but more gently. Gelatinous light-blue precipitate that easily dissolves on agitation observed during the titration.
THA-T062	KAJ 23/04 021	Tailings	Cell 4	2.5044	2.48	2.48	2.48	2.48	0.0948	15.8	42.15	29.31	78.18	Violent but short-lived efferverscence upon addition of peroxide. Large bubbles and formation of scum during the first addition. No effervescence or boiling or bubbling during the first heating. Violent but short-lived effervescence and boiling observed during second addition of Peroxide. Yellow-to-green precipitate observed during titration.
THA-T063	KAJ 23/04 022	Tailings	Cell 4	2.5013	2.29	2.29	2.29	2.29	0.0948	32.8	55.25	60.91	102.61	Violent but short-lived efferverscence upon addition of peroxide. Large bubbles and formation of scum during the first addition. No effervescence or boiling or bubbling during the first heating. Violent but short-lived effervescence and boiling observed during second addition of Peroxide. Brown precipitate observed during titration.

Figure 57: NAG test results data sheet

THA-T006	KAJ 17/04 013	Tailings	Cell 6	2.5055	2.25	2.24	2.24	2.24	0.0948	44.25	59.9	82.04	111.05	Mild effervescence with tiny bubbles on first addition for 2hrs. Violent effervescence and large bubbling after 15mins of heating. Attempt to prevent boiling over by taking the flask off the hot plate and taking off the lid results in ceasure of effervescence and bubbling and any visible reaction. The sample goes into quiescence for the rest of the first heating. Vigorous effervescence, bubbling and boiling during second addition. The effervescence and boiling stopped after 15mins except tiny rising bubbles. There was no visible reaction when the second heating started. The third addition gave effervescence, boiling and bubbling but not as vigorous and lasting as during the second addition. The sample goes quiet during third heating. Brick-red precipitate observed during titration
THA-T007	KAJ 11/04 005	Tailings	Cell 6	2.5013	2.49	2.49	2.49	2.49	0.0948	16.95	30.55	31.48	56.73	Initial Mild effervescence with small bubbles on first addition of H2O2. Reaction increases and effervescence more visible after 1hr. Reaction effervescenc continues after 2hrs. Reaction becomes more vigorous and large bubbles observed during first 45mins of heating after which efferescence ceases. Quiet and mild effervescence during second addition and heating. No effervescence observed after 1hr of heating. Mild effervescence on third addition. Effervescence decreases with time until it is no more after 1hr. No effervescence during heating. Slight Discoloration to orange. Orange precipitate during titration after pH reaches 4.5
THA-T008	KAJ 17/04 014	Tailings	Cell 6	2.5066	2.33	2.33	2.33	2.33	0.0948	33.8	51.8	62.64	96.00	Mild effervescence with tiny bubbles on first addition for 2hrs. Violent effervescence and large bubbling after 15mins of heating. Attempt to prevent boiling over by taking the flask off the hot plate and taking off the lid results in termination of effervescence, bubbling and any visible reaction. The sample goes into quiescence for the rest of the first heating. Vigorous effervescence, bubbling and boiling during second addition. The effervescence and boiling stopped after 15mins except tiny rising bubbles. There was no visible reaction when the second heating started. The third addition gave effervescence, boiling and bubbling but not as vigorous and lasting as during the second addition. The sample goes quiet during third heating.
THA-T140	KAJ 26/03 001	Tailings	Cell 7	2.5	1.69	1.68	1.7	1.69	0.489	21.55	24.7	206.54	236.73	Violent but short-lived efferverscence upon addition of peroxide (signal of readily released carbonates and/or high amount of pyrite). Large bubbles and formation of scum during the first addition and heating. Observed an unstable pH aroung pH7 during titration. Discoloration from orange to deep green precipitate during titration.
THA-T143	KAJ /18/04 015	Tailings	Cell 7	2.5022	1.97	1.97	1.97	1.97	0.489	16.5	23.2	158.00	222.16	Highly violent reaction with effervescence, boiling and large bubbles that forms scum during first addition. The reactio occurs within a short time frame, up to 10 mins then it becomes quiet. The sample remains quiet without bubbling and efferescence througout reaction time and heating time. Violent reaction with effervescence, boiling, and bubbling during the second addition- except that reactio was less violent and produced no scum. The reaction is short-lived and remains quiet during reation time and second heating. The reaction after the third addition is similar to the observations made on the second addition.
THA-T145	KAJ 18/04 016	Tailings	Cell 7	2.5006	1.99	1.99	1.99	1.99	0.489	16.5	22.9	158.10	219.43	Highly violent reaction with effervescence, boiling and large bubbles that forms scum during first addition. The reactio occurs within a short time frame, up to 10 mins then it becomes quiet. The sample remains quiet without bubbling and efferescence througout reaction time and heating time. Violent reaction with effervescence, boiling, and bubbling during the second addition- except that reactio was less violent and produced no scum. The reaction is short-lived and remains quiet during reation time and second heating. he reaction after the third addition is similar to the observations made on the second addition.
THA-T148	KAJ 19/04 017	Tailings	Cell 7	2.5019	2.56	2.56	2.56	2.56	0.0948	14.6	39.65	27.11	73.62	Mild effervescence and small bubbles during first addition. Tiny bubbles forming thin layer of foam after 50mins of addition. Strong effervescence, bubbling and boiling which gradually dies out after 30mins during the second addition. Decreased effervescence, bubbling and boiling during third addition as compared to the second. There was no boiling or effervescence during heating stages. Discoloration to light orange after cooling for overnight. Green precipitate forms during titration. Very unstable pH above 7.
THA-T150	KAJ 11/04 006	Tailings	Cell 7	2.5009	2.82	2.82	2.81	2.82	0.0948	15.75	34.5	29.25	64.08	Initial Mild effervescence with small bubbles on first addition of H2O2. Reaction increases and effervescence more visible after 1hr. Reaction effervescenc continues after 2hrs. Reaction becomes more vigorous and large bubbles observed during first 45mins of heating after which efferescence ceases. Quiet and mild effervescence during second addition and heating. No effervescence after 1hr of heating. Mild effervescence on third addition. Effervescence decreases with time until it is no more after 1hr. No effervescence during heating. No discoloration after standing for overnight. Orange precipitate observed during titration after pH reaches 6
THA-T175	KAJ 25/04 025	Tailings	Cell 8	2.5018	1.94	1.94	1.94	1.94	0.489	22	29.15	210.71	279.18	The first addition of H2O2 gave a violent reaction with bubbling, effervescence and boiling. But the reaction is short-lived. Second addition was also viloent with large bubbles and efferverscence which lasts longer than during the first addition. No visible reaction during heating. Discoloration to brick red during the second heating. The reaction after third addition is the same as during the second addition. No effervescence or boiling or bubbling during the heating stage. Discoloration observed to dark green during titration. Brown precipitate forms. Unstable pH observed around pH of 7 Titration residue taken for SEM analysis.
THA-T177	KAJ 25/04 026	Tailings	Cell 8	2.5005	2.15	2.15	2.15	2.15	0.0948	72.5	100	134.68	185.77	The first addition of H2O2 gave a violent reaction with bubbling, effervescence and boiling. But the reaction is short-lived. Second addition was also viloent with large bubbles and efferverscence which lasts longer than during the first addition. No visible reaction during heating. Discoloration to brick red during the second heating. The reaction after third addition is the same as during the second addition. No effervescence or boiling or bubbling during the heating stage. Discoloration to brick red during titration. Brown precipitate forms. Titration residue taken for SEM analysis
THA-T179	KAJ 26/04 027	Tailings	Cell 8	2.5008	2.05	2.05	2.05	2.05	0.0948	94	131.05	174.60	243.42	Violent reaction on addition of H2O2 with effeverscence, bubbling, boiling and scumming. But the reaction is short-lived. Discoloration observed after first heating. There was no effervescence or bubbling or boiling during the heating stage. Violent reaction accompanied with effervescence, bubbling with scums and boiling on second addition of H2O2. Reaction is short-lived. No visible reacton during the heatimg stage. Effervescence and bubbling with boiling during the third addition but no scum formation. No visible reaction during heating. Discoloration to pale brown. Discoloriation to dark green during titration. Brown precipitate forms after pH reaches 7. Very unstable pH around as NaOH is consumed after minutes to bring pH down to below 7. Titration residue taken for SEM analysis
THA-T182	KAJ 26/04 028	Tailings	Cell 8	2.5006	2.13	2.13	2.13	2.13	0.0948	60.05	88.4	111.55	164.21	Violent reaction on addition of H2O2 with effeverscence, bubbling, boiling and scumming. But the reaction is short-lived. Discoloration observed after first heating. There was no effervescence or bubbling or boiling during the heating stage. Violent reaction accompanied with effervescence, bubbling with scums and boiling on second addition of H2O2. Reaction is short-lived. No visible reacton during the heatimg stage. Effervescence and bubbling with boiling during the third addition but no scum formation. No visible reaction during heating. Discoloration of solution into light blue. Discoloriation to dark green during titration. Brown precipitate forms after pH reaches 7. Very unstable pH around pH 7 as NaOH is consumed after minutes to bring pH down to below 7. Titration residue taken for SEM analysis
THLG_05	KAJ 26/04 029	Tailings	Cell 9	2.5018	5.08	5.08	5.08	5.08	0.0948	0	1.5	0.00	2.785	Almost no effervescence but tiny bubbles forming a thin layer of foam on the surface of the mixture. Gentle Boiling and effervescence which increases with time during heating. Vigorous effervescence and bubbling 40min into heating. There was gentle reaction with effervescence and boiling during the second addition. The Heating stageis accompanied by violent effervescence, bubbling and boiling which increases with time in all stages. However the third stage heating had a more gentle reaction than the first two. No discoloration observed. White precipitate observed during titration.
THLG_06	KAJ 10/04 004	Tailings	Cell 9	2.5001	7.77	7.78	7.79	7.78	0.0948	0	0	0.00	0	Calm reaction with H2O2, small bubbles and less effervescence until after 45mins. Efferverscence increases with increased bubble sizes. There was still Effervescence after two hours of reaction with H2O2. Second and third addition had no initial effervescence, but had effervescence during heating. Mild effervescence during the last heating until about 1hr.30min. No discoloration observed. No titration done since pH was already above 7

THLG_07	KAJ 26/04 030	Tailings	Cell 9	2.5016	7	7	7	7	0.0948	0	0	0.00	0	Almost no effervescence but tiny bubbles forming a thin layer of foam on the surface of the mixture. Gentle Boiling and effervescence which increases with time during heating. Vigorous effervescence and bubbling 40min into heating. There was gentle reaction with effervescence and boiling during the second addition. The Heating stage is accompanied by violent effervescence, bubbling and boiling which increases with time in all stages. However the third stage heating had a more gentle reaction than the first two. No discoloration observed. pH already 7 so no titration performed.
THLG_09_2	KAJ 07/05 031	Tailings	Cell 9	2.5029	7.9	7.9	7.9	7.9	0.0948	0	0	0.00	0.00	On first addition of H2O2, sample reacts very gently and producing effervescnece and tiny bubbles with gentle boiling. No effervescence after 2hrs. Reaction gets violent for 15 mins during heating. Large bubbles and effervescence observed during this first heating after which the sample enters into complete quiescence. Very gentle boiling , bubbling, and effervescing after 15mins of second addition of H2O2. Reatcion conitnues after 2hrs. Effervescnence and bubbling gets violent with time during heating. The reaction calms down and dies out completly after 1.45mins of heating. No visible reaction on the third addition. No effervescence or bubbling observed. Gentle effervescing and bubbling during the last heating. No titration since leachate had pH above 7
THA-10	KAJ 26/03 002	Waste Rock	Waste dump	2.5014	2.83	2.83	2.83	2.83	0.0948	4.45	10.55	8.26	19.59	Gentle reaction with efferverscence at initial stage but increases the effervescence and bubbling after 30mins for the first H2O2 addition. Gentle reaction on second addition but no reaction on the third addition. Discoloration of from light orange to green precipitate during titration
THA-020	KAJ 10/04 003	Waste Rock	Waste dump	2.5035	2.31	2.33	2.31	2.32	0.0948	25.6	38.7	47.50	71.81	Calm reaction with H2O2, small bubbles and less effervescence until after 45mins. Efferverscence increases appreciably. There was still Effervescence after two hours of reaction with H2O2. Mild effervescence during second and third addition and vigorous effervescence during heating. No efferscence during the last heating. Discoloration to orange appeared during the second addition and heating. Orange precipitate observed during titration after pH reaches 5
THA-09	KAJ 12/04 008	Waste Rock	Waste dump	2.5014	2.56	2.57	2.58	2.57	0.0948	0	22.1	0.00	41.04	Mild reaction with increasing efferverscence and bubble size with time. No scummy bubbles observed. Reaction becomes vigorous giving off large bubbles and effervescence after 30 mins and lasts for about 20mins until it dies out completely. There was no effervescence and bubbling during heating. Gentle effervescence and bubbling after second addition until 1hr, then effervescence increased for about 30mins before it calmed down. Reaction continued for 1hr with gentle effervescence for additional 1hr. Discolaration from dark brown to **light blue** during heating for 2hours. No effervescence during heating. There was gentle reaction with small bubbles and boiling upon third addition. Discoloration from **light blue** to dark brown upon third addition. Gentle boiling and effervescence with small bubbles during heating. Sample stops boiling and effervescing after 30mins even at 150 degree celsius. mixture changes colour from dark brown to **light blue again.** Sample forms white precipitate at pH of 6.5 during titration which makes it look milky.
THA-002	KAJ 16/04 012	Waste Rock	Waste dump	2.504	3.02	3.02	3.02	3.02	0.0948	4.65	125.85	8.63	233.47	There was no visible effervescence and bubbling during first addition but gentle boiling after 2hrs. Violent effervescence and large size bubbling during heating. Reaction is short-lived and goes visibly dead after 15 minutes. No visble reaction or effeverscence and bubbling on second addition. Sample immediately start boiling, effervescing and bubbling during heating until 1hr. Then it became quiet. No visible reaction and effervescence on third addition until after 30 mins when the sample begins effervescing and bubbling. No effervescence or bubbling during the third heating for 2hrs. White precipitate forms during titration. A lot of NaOH consumed to reach a pH of 7. Clear part of the mixture still below pH 7 when precipitate settles.
THA-011	KAJ 07/05 032	Waste Rock	Waste dump	2.5025	4.6	4.6	4.6	4.6	0.0948	0	2.25	0	4.18	No visible reaction until after 15mins where sample begins to boil very gently and generate tiny numbered bubbles on first addition. Sample still effervercing and producing bubbles after 2hrs. Reaction gets violent for 15 mins during heating. Large bubbles and effervescence observed during this first heating after which the sample enters into complete quiescence. Very gentle boiling , bubbling, and effervescing after 15mins of second addition of H2O2. reaction continues for 1hr and dies out. Gentle effervescence and bubbling which increases with time during heating. Effervescing and bubbling stops after 1hr.30min of heating and sample goes into complete quietness. No visible reaction on the third addition. No effervescence or bubbling observed. Gentle effervescing and bubbling during the last heating. Decoloration of leachate to red. Orange precipitate forms during titration.
THA-013	KAJ 07/05 033	Waste Rock	Waste dump	2.5025	2.04	2.05	2.05	2.05	0.489	10.85	14.1	103.89	135.01	Violent reaction immediately on first addition of H2O2 accompanied by effervescence, bubbling, and boiling. The reaction is exothermic, lasts very few minutes and return to quiet state. No visible reaction during heating. Sample remains quiet throughout for 2hrs. Immediate reaction with H2O2 with bubbles and effeverscence on second addition. Reaction is short-lived. Mixture decolorises to light greenish-blue. No reaction during heating. Gentle effervescence, bubbling and boiling immediately after H2O2 addition. Effervescence and bubbling stoppes after 45mins. Sample remains calm and quiet throughout third heating. Sample decolarises to brick-red after last heating. Brown gossanous precipitate forms during the titration
THA-014	KAJ 07/05 034	Waste Rock	Waste dump	2.5038	1.94	1.94	1.93	1.94	0.489	20.95	22.85	200.49	218.67	Violent reaction on first addition of H2O2 accompanied by effervescence, bubbling, and boiling. The reaction is exothermic, lasts very few minutes and return to quiet state. No visible reaction during heating. Sample remains quiet throughout for 2hrs. Delayed reaction with H2O2 on second addition. Effervescence and bubbling after 10mins of adding H2O2. Decolorised solution to milky colour. Effervescence, bubbling and boiling does not start immediately but increases with time when it starts and lasts for 2hrs reducing to tiny rising bubbles after 45 mins. Sample remains calm and quiet during last heating. Sample decolorises to brick red after last heating. Brown gossanous precipitate forms diring titration.
THA-05	KAJ 09/05 035	Waste Rock	Waste dump	2.5008	1.88	1.88	1.88	1.88	0.489	19	25	182.05	239.53	Immediate violent reaction with H2O2 producing large bubbles, scum, with effervescence and boiling. Reaction is short-lived. No visible reaction during heating. Sample remains quiet throughout first heating. Immediate effervescence, bubbling and boiling observed after second addition of H2O2. Formation of scum around the walls of erlenmeyer flask observed. Violent reaction is short-lived (5-10mins). Sample remains quiet during second heating/ Effervescence, bubbling and boiling on third addition of H2O2. Reaction is short-lived. Sample remains quiet throughout the third heating. Brown precipitate forms during titration
THA-03	KAJ 09/05 036	Waste Rock	Waste dump	2.5002	2.02	2.02	2.02	2.02	0.489	10.95	21.2	104.94	203.17	Immediate violent reaction with H2O2 producing large bubbles, scum, with effervescence and boiling. Reaction is short-lived. No visible reaction during heating. Sample remains quiet throughout first heating. Immediate effervescence, bubbling and boiling observed after second addition of H2O2. Formation of scum around the walls of erlenmeyer flask observed. Violent reaction is short-lived (5-10mins). Sample remains quiet during second heating/ Effervescence, bubbling, scumming and boiling on third addition of H2O2. Reaction is short-lived. Sample remains quiet throughout the third heating. Deep green precipitate forms during titration
THA-029	KAJ 09/05 037	Waste Rock	Waste dump	2.502	8.02	8.04	8.05	8.04	0	0	0	0	0	Very gentle effervescence, small sized bubbling, and low boiling at the initial stages of first H2O2 addition. Effervescence, bubbling and boiling increased with time and became violent with large sized bubbles and scum around the walls of the eulemeyer flask. Reaction lasts for 15mins and dies out. Sample remains quiet during first heating. Gentle effervescence, bubbling and boiling which increases with time. Effervescing and bubbling intensifies during heating for about 30mins before going back to quientness. Very gentle effervescence, boiling, and small sized bubbles on the third addition.
THA-033	KAJ 09/05 038	Waste Rock	Waste dump	2.5026	3.01	3.01	3.01	3.01	0.0948	4.5	26	8.35	48.26	Very gentle effervescence, small sized bubbling, and low boiling at the initial stages of first H2O2 addition. Effervescence, bubbling and boiling increased with time and became violent with large sized bubbles and scum around the walls of the eulemeyer flask. Reaction lasts for 15mins and dies out. Sample remains quiet during first heating. Sample remains quiet after second addition until 30mins when it starts generating gentle but tiny bubbles for the next 1hr.30. Effervescing and bubbling intensifies during heating for about 30mins before going back to quientness. Very gentle effervescence, boiling, and small sized bubbles on the third addition. Orange precipitate forms during titration.

Table 6: Sequential NAG test Results

Stage	NAG pH	NAG Capacity	comment
1	1.68	24..59	Sample is very reactive immediately upon first addition of H2O2. Large bubbles coupled with boiling and effervescence for a short while. Solution decolorises to orange. Temperature of reaction reaches 80 degrees Celsius. Dark green precipitate forms during titration. Obsevation is same for second stage except that precipitate during titration was brick red.
2	1.67	299.04	Obsevation is same for second stage except that precipitate during titration was brick red. Dark brown precipitate forms immediately during titration and intensifies at pH 7.
3	1.87	164.69	Sample gradually increased in reaction generating effervescence, bubbling and boiling until it turned violent after 30 mins. Sample decolorises during heating. Sample turns brick-red at pH 4.5 during titration. Few drops of NaOH changed the pH of the liquor to 7 after having reached pH of 4.5. This was the opposite in the first and second stages of the Test
4	2.17	61.24	Sample takes appreciably long time to react and give effervescence, bubbling and boiling which also lasts longer. Sample turns brick red after pH reaches 4.5. Then the pH reaches 7 on few added drops of NaOH. NaOH consumption after pH reaches 4.5 reduces drastically. This could be because of less Fe (III) in solution to be reduced.
5	2.9	5.59	Tiny gentle bubbles seen without any effervescence or boiling during the reaction time. Sample begins to boil and bubble during heating even after 2hrs. No precipitate forms during titration. Less NaOH consumed
6	4.02	5.33	Tiny gentle bubbles seen without any effervescence or boiling during the reaction time. Sample begins to boil and bubble during heating even after 2hrs. No precipitate forms during titration. Less NaOH consumed

Table 7: MPA calculation according to Sobek

ALS ID	Type of material	Paste pH	NAG pH	NAG @V4.5	NAG @V7	S_%	Fe_%_ME-MS61	Sobek AP	Diff. (Sobek-NAG)
THA-T175	Tailings	3.50	1.94	210.71	279.18	32.80	36.00	1025.00	745.82
THA-T140	Tailings	3.46	1.69	206.54	236.73	32.10	36.30	1003.13	766.40
THA-T105	Tailings	4.43	2.32	40.95	89.51	24.60	22.40	768.75	679.24
THA-T063	Tailings	5.06	2.29	60.91	102.61	15.85	15.30	495.31	392.70
THA-T062	Tailings	4.88	2.48	29.31	78.18	24.20	19.85	756.25	678.07
THA-T061	Tailings	7.77	5.15		6.68	13.60	12.00	425.00	418.32
THA_33	Waste rock	7.29	3.01	8.35	48.26	28.50	29.40	890.63	842.37
THA_29	Waste rock	8.01	8.04			29.40	20.30	918.75	918.75
THA_11	Waste rock	4.87	4.60		4.18	0.96	6.64	30.00	25.82
THA_09	Waste rock	6.60	2.57	22.10	41.04	21.30	2.39	665.63	624.59
THA_03	Waste rock	3.38	2.02	104.94	203.17	35.50	28.80	1109.38	906.21
THA_02	Waste rock	6.04	3.02	125.85	233.47	28.20	10.55	881.25	647.78

Table 8: MLA Data for analysed samples

Column1	THA-T140	THA-T175	THA-T105	THA-T063	THA-T062	THA-T061	THA-02	THA-03	THA-09	THA-011	THA-029	THA-033
Pyrite	62.28	67.74	44.51	20.89	32.92	20.22	13.42	62.65	4.08	0.10	18.76	13.52
Pyrrhotite	2.60	2.17	0.97	2.16	2.77	1.66	0.04	0.19	0.02	0.01	0.02	0.13
Fe sulphides	64.88	69.91	45.48	23.05	35.69	21.88	13.46	62.84	4.10	0.11	18.78	13.65
Chalcopyrite	0.24	0.36	0.81	0.24	1.17	1.92	0.44	0.91	6.07	0.04	25.90	63.14
Sphalerite	0.14	0.04	1.31	0.48	3.07	2.24	44.30	3.82	18.45	0.04	34.86	2.87
Galena	0.00	0.02	0.16	0.10	0.21	0.51	9.91	0.45	3.62	0.01	4.81	0.21
Other Cu-minerals							0.29	0.18	25.58	0.01	0.30	1.17
Arsenopyrite	0.01		0.01	0.02	0.02	0.02		0.02				
Enargite	0.00		0.19	0.03	0.21	0.22						
Chalcocite/covellite	0.00		2.11	0.06	2.31	1.08						
Bornite			0.08		0.14	0.03						
Tetrahedrite			0.05	0.02	0.08	0.10						
Molybdentite							0.22	1.16	0.03		0.05	0.05
Cobaltite												
Other sulphides	0.01		2.44	0.13	2.76	1.45	0.22	1.18	0.03		0.05	0.05
Chlorite	6.87	5.31	1.40	4.95	5.01	8.34	10.15	1.34	1.00	2.63	3.18	1.34

Plagioclase	3.38	3.08	4.85	11.47	5.25	7.36	1.36	1.23	0.60	0.65	0.46	0.32
K_Feldspar	0.36	0.12	3.11	6.46	2.85	3.21						
Orthoclase							0.08	0.06	0.01	0.12		
Neutralizing silicates	10.60	8.51	9.36	22.88	13.11	18.91	11.59	2.63	1.61	3.40	3.64	1.66
Augite	0.13	0.11	0.69	1.70	1.27	5.19	4.73	0.08	3.43	0.12	1.38	1.36
Muscovite_illite							0.27	10.92	0.23	3.80	0.05	0.03
Kaolinite_pyrophyllite							0.04	0.12	0.10	2.36	0.18	
Clay							0.19	0.29	0.01	0.82	0.58	1.11
Biotite	2.01	2.10	0.83	5.70	2.72	5.73	2.03	0.55	0.45	0.32	0.33	0.10
Muscovite	1.40	0.64	4.21	10.16	11.10	7.83						
Garnet	0.02		0.36	0.76	0.48	1.11	0.07	0.04		0.01	0.23	3.37
Talc	0.05	0.04	0.13	0.09	0.13	0.53	0.03	0.01	0.03		0.28	0.14
Titanite	0.00		0.03	0.11	0.03	0.34	0.02	0.01	0.01			
Other Silicates	3.61	2.89	6.25	18.52	15.73	20.73	7.38	12.02	4.26	7.43	3.03	6.11
Quartz	10.45	8.30	23.78	25.42	20.13	19.61	0.65	6.62	2.12	70.11	0.97	3.29
Siderite	0.15	0.26	0.10	0.43	0.22	0.17						
Calcite	0.02	0.03	0.03	0.27	0.08	4.64		0.01	2.95	0.05		0.04
Dolomite	0.00		0.02	0.10	0.05	1.91			2.10	0.02		
Ankerite									0.09	0.12		0.01
Mn-Calcite												

Carbonates	0.16	0.29	0.15	0.80	0.35	6.72		0.01	5.14	0.19		0.05
Fe-sulphate	0.63	0.38	0.02	0.02	0.02	0.02						
Jarosite	1.35	0.73	1.43	0.60	0.61	0.49	0.04	1.00	0.06	2.56	0.59	0.67
Gypsum	0.09	0.05	0.12	0.26	0.63	0.66		0.01	0.05			0.17
Alunite (KAl3(SO4)2(OH)6)	0.05	0.01	1.05	1.13	2.21	0.60	0.26	0.64	0.11	0.77	0.20	0.01
Anglesite	0.00		0.49	0.07	0.15	0.42						
Schwertmannite							0.01	0.34	0.04	1.03	0.31	1.26
Barite	0.01	0.01	4.92	4.81	2.97	2.85	6.02	5.91	5.03	0.40	3.61	0.08
Brochantite (Cu4(SO4)(OH)6)							0.01		17.19	0.04		0.03
Sulfates	2.13	1.18	8.03	6.89	6.59	5.04	6.34	7.90	22.48	4.80	4.71	2.22
Magnetite	7.57	8.21	1.58	1.02	0.63	0.50						
Chromite												
Ilmenite	0.06	0.12	0.01	0.01	0.02	0.03				0.01		
Titano-magnetite	0.04	0.10	0.01			0.01						
Rutile	0.01	0.02	0.04	0.04	0.04	0.02						
FeOxide							0.03	0.03	0.03	12.86	0.73	5.20
Goethite								0.01		0.49	0.04	0.11

Steel	0.02	0.01										
Fe-Ti oxides	7.71	8.46	1.64	1.07	0.69	0.56	0.03	0.04	0.03	13.36	0.77	5.31
Gahnite (ZnAl2O4)	0.02	0.01	0.01	0.02	0.01							
ZnFe-Oxide?			0.20	0.21	0.37	0.06						
Smithsonite			0.24		0.01							
Zn-silicate			0.01		0.01	0.01						
ZnMg-silicate			0.07	0.03	0.03	0.06						
AuAg-minerals												0.02
Apatite	0.02	0.04	0.01	0.13	0.05	0.22	0.03	0.02	0.12	0.01	0.20	
Monazite	0.01		0.03	0.02	0.02	0.06						
Zircon	0.01	0.01	0.01			0.04				0.01		
Fluorite									0.04	0.01		
Halite												
SbTiFEOxide												
MgFeCarbonate												
Celsian							0.33	0.42	0.01	0.01	1.19	0.01
PbCuSOxide							1.33	0.05	3.93		0.21	0.05
Unknown							0.23	0.17	0.17	0.08	0.10	0.08
Other							3.46	0.73	2.24	0.37	0.46	
Other trace minerals	0.06	0.06	0.58	0.41	0.50	0.45	5.38	1.39	6.51	0.49	2.16	0.16

Appendix B

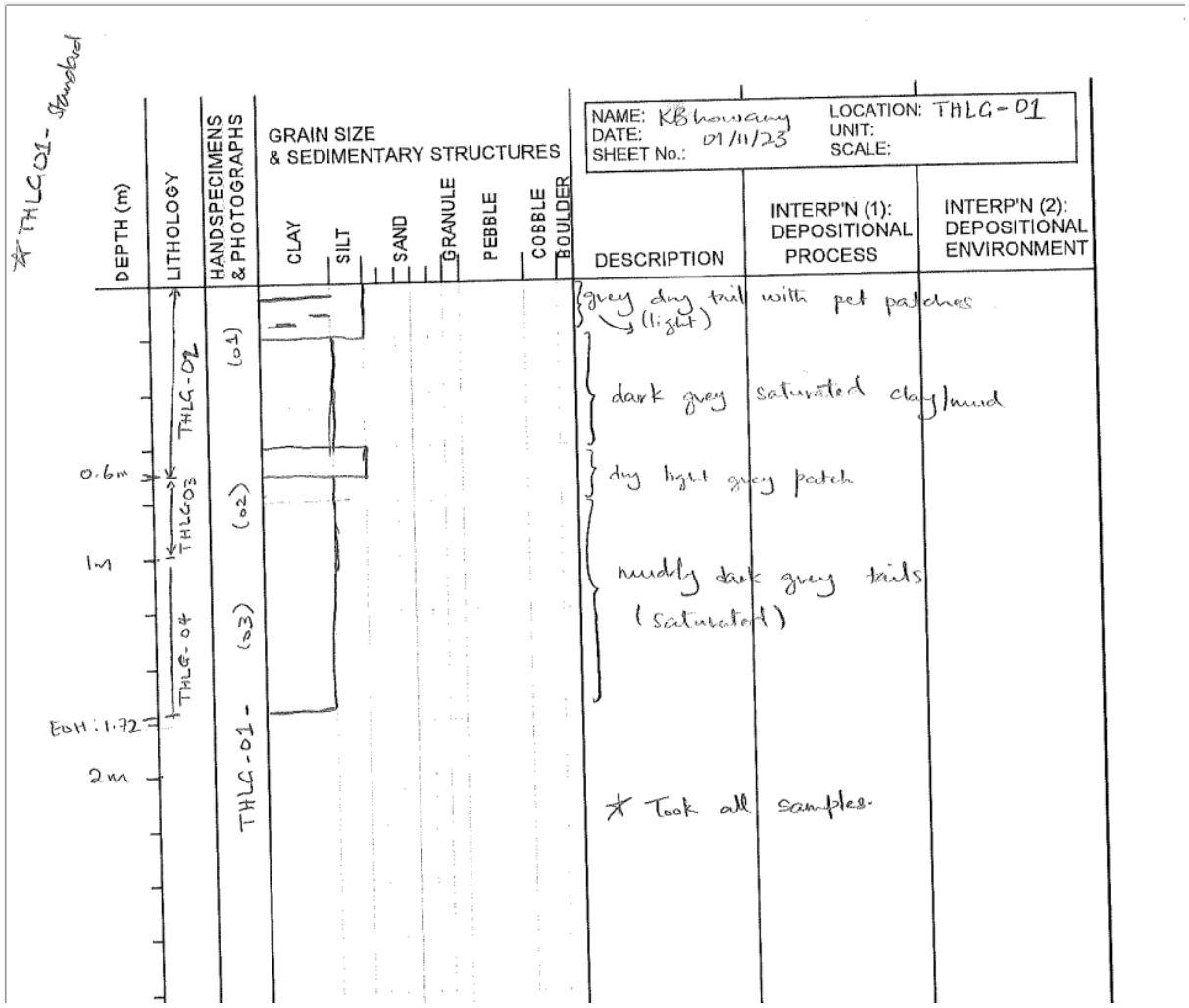

Figure 58: Sample Log sheet

Figure 59: A retrieved sonic drill core.

Table 9: Spectra of Bismuth minerals

a	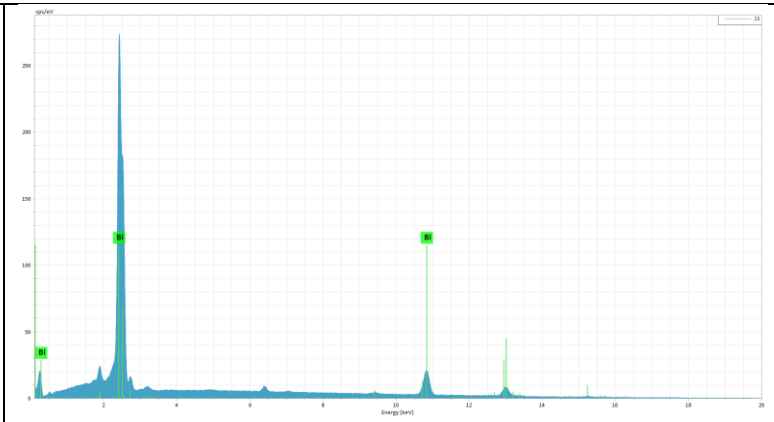
b	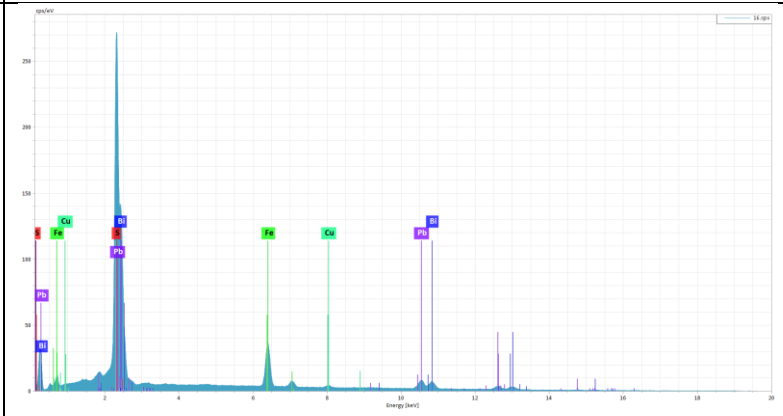

d	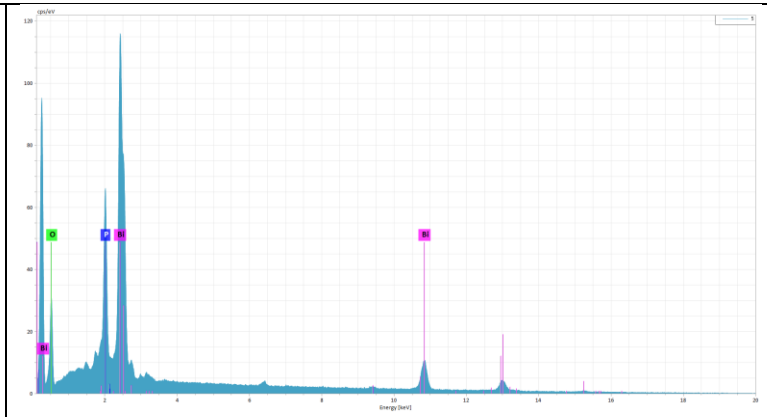 cps/eV O P Bi Bi Bi Energy [keV]
e	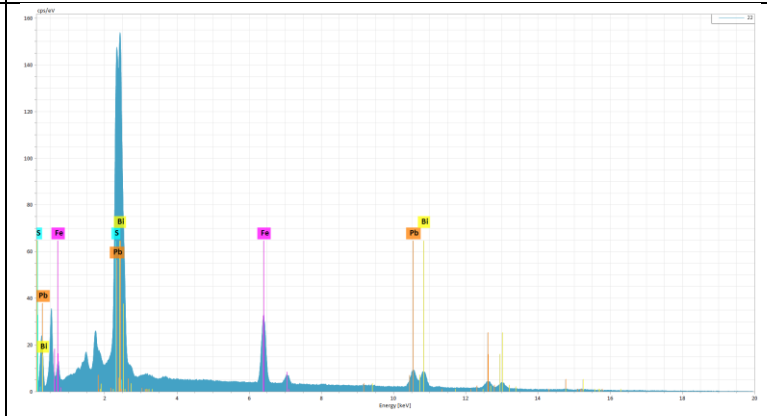 cps/eV S Fe Bi S Pb Fe Bi Pb Pb Bi Energy [keV]

f	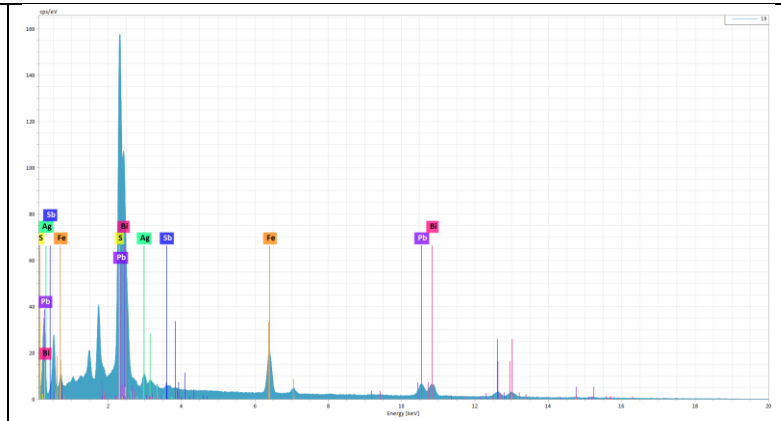

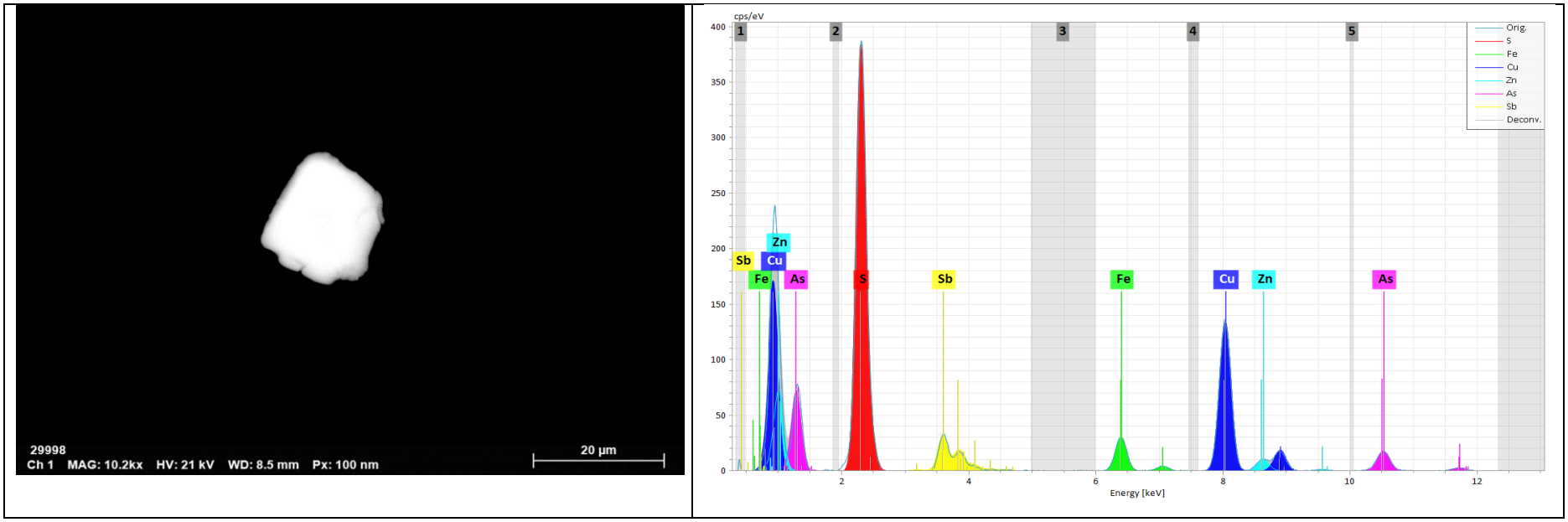

Figure 60: Spectrum of tennantite

Table 10: Stoichiometry of tennantite

Element	S	Fe	Cu	Zn	As	Sb
Stoichiometry	24.77	5.81	42.76	3.83	15.12	7.72

Table 11: Stoichiometry of tetrahedrite

Element	S	Fe	Cu	Zn	Sb
Stoichiometry	23.77	4.1	40.8	5.71	25.62

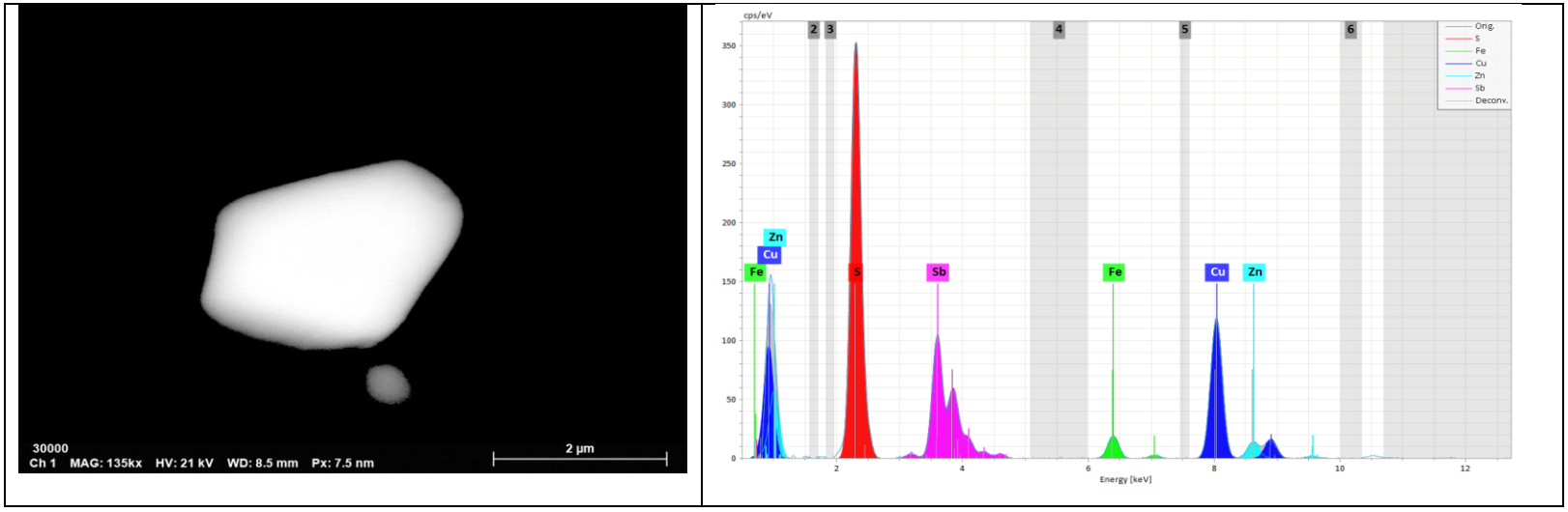

Figure 61: Spectrum of tetrahedrite

Table 12: Possible minerals of Bismuth suggested by Mineral database according to stoichiometry in sample THA-T175

Element	S	Fe	Cu	Pb	Bi	Possible Mineral
Grain 1-1	30.13	26.97	1.32	19.18	22.4	Unknown
Grain 1-2	25.36	16.02	1.4	28.4	28.83	Unknown
Grain 2-1	9.12	16.45		10.42	64.01	Unknown
Grain 2-2	25.75	18.1		42.22	13.92	Unknown
Grain 2-3	40.04	52.74		4.22	3	Bartonite (93,8%) Greigite (92,3%) Pyrrhotite (84,6%) Rasvumite (83,4%) Troilite (83,0%)
Grain 2-4	8.06	15.02		36.53	40.39	Unknown
Grain 3-1	7.88	14.53			77.59	Garavellite (8,9%)
Grain 3-2	2.75	5.75			91.5	Sphaerobismoite (98,5%) Bismite (98,0%) Sillenite (95,8%) Chrombismite (95,3%) Zavaritskite (93,2%)

Table 13: Possible minerals of Bismuth suggested by Mineral database according to stoichiometry in sample THA-T63

Element	O	P	S	Fe	Cu	Pb	Bi	Possible mineral
Grain 5-1			2.47			7.92	89.61	Beyerite (60,2%) Urvantsevite (40,0%) Crerarite (27,4%) Jonassonite (25,5%) Polarite (19,9%)
Grain 6-1	16.61	8.8					74.59	Petitjeanite (79,3%) Ximengite (78,9%) Smrkovecite (44,9%)
Grain 6-2	17.79	7.15					75.06	Petitjeanite (94,5%) Smrkovecite (74,0%) Ximengite (70,2%)
Grain 6-3	18.1	5.86					76.04	Smrkovecite (96,7%) Eulytite (95,2%) Hechtsbergite (93,3%) Arsenobismite (89,4%) Dukeite (88,6%)
Grain 6-4	21.56	6.81					71.63	Petitjeanite (85,5%) Smrkovecite (77,4%) Ximengite (66,8%) Waylandite (0,5%)
Grain 7-1			16.39	6.59	4.28	17.99	54.76	Unknown

Table 14: Possible minerals of Bismuth suggested by Mineral database according to stoichiometry in sample THA-133

Element	S	Cu	Bi	Possible Mineral
Grain 1	30.79	15.12	54.09	Muckeite (63,2%) IMA2005-036 (58,4%) Malyshevite (47,9%) Kupcikite (45,2%) Pizgrischite (39,8%)

Scheelite (O=25.04%, Ca=13.83%, W=61.13%)	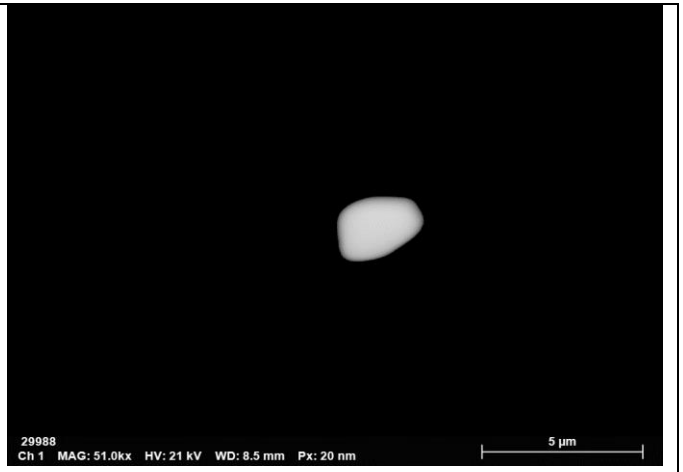

Cassiterite (O=20.61%, Sn=79.39%)	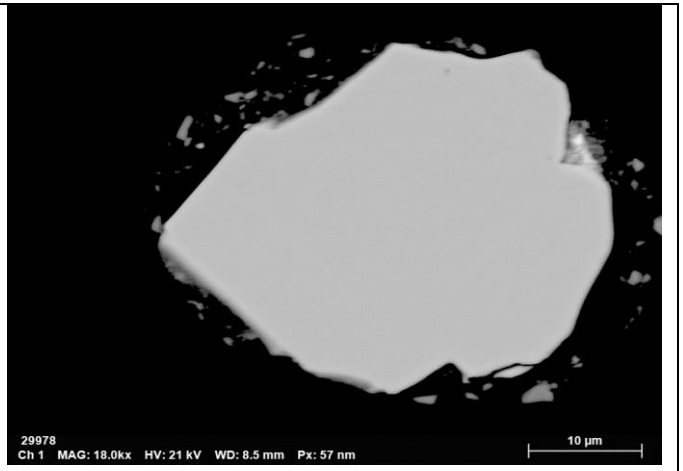

Figure 62: Scheelite and Cassiterite grains